



HAL
open science

Theory of quantum phase slips in disordered one-dimensional superconductors

Aleksandr Svetogorov

► **To cite this version:**

Aleksandr Svetogorov. Theory of quantum phase slips in disordered one-dimensional superconductors. Superconductivity [cond-mat.supr-con]. Université Grenoble Alpes, 2019. English. NNT : 2019GREAY036 . tel-02491344

HAL Id: tel-02491344

<https://theses.hal.science/tel-02491344>

Submitted on 26 Feb 2020

HAL is a multi-disciplinary open access archive for the deposit and dissemination of scientific research documents, whether they are published or not. The documents may come from teaching and research institutions in France or abroad, or from public or private research centers.

L'archive ouverte pluridisciplinaire **HAL**, est destinée au dépôt et à la diffusion de documents scientifiques de niveau recherche, publiés ou non, émanant des établissements d'enseignement et de recherche français ou étrangers, des laboratoires publics ou privés.

THÈSE

Pour obtenir le grade de

DOCTEUR DE LA COMMUNAUTE UNIVERSITE GRENOBLE ALPES

Spécialité : Physique de la Matière Condensée et du Rayonnement

Arrêté ministériel : 25 mai 2016

Présentée par

Aleksandr SVETOGOROV

Thèse dirigée par **Denis BASKO**, CNRS

préparée au sein du **Laboratoire Laboratoire de Physique et de
Modélisation des Milieux Condensés**
dans l'**École Doctorale Physique**

**Théorie de sauts de phase quantiques dans
des supraconducteurs uni-dimensionnels
désordonnés.**

**Theory of quantum phase slips in disordered
one-dimensional superconductors.**

Thèse soutenue publiquement le **2 octobre 2019**,
devant le jury composé de :

Monsieur Denis BASKO

Directeur de Recherche, CNRS, Directeur de thèse

Monsieur Yuli Nazarov

Professeur des Universités, Technische Universiteit Delft, Rapporteur

Monsieur Benoît Douçot

Directeur de Recherche, CNRS, Rapporteur

Monsieur Philippe Joyez

Ingénieur de Recherche, CEA, Examineur

Monsieur Manuel Houzet

Ingénieur de Recherche, CEA, Examineur

Madame Léonie Canet

Professeur des Universités, Univ. Grenoble Alpes, Présidente du jury



Contents

1	Introduction	1
1.1	One-dimensional superconductivity: superconducting nanowires and Josephson junction chains	1
1.2	Phase slips	3
1.3	Superconductor-insulator transition	5
1.4	Structure of the thesis	6
2	Quantum phase slips in an underdamped Josephson junction	8
2.1	Coherent QPS and Bloch oscillations	8
2.2	Incoherent QPS and resonant Zener breakdown: Lindblad master equation	12
2.3	Voltage peaks due to incoherent QPS	15
2.3.1	Effective two-level case	15
2.3.2	Several levels in one minimum	18
2.4	Possibility of experimental observation	21
3	Coherent quantum phase slips in Josephson junction chains (general relations)	23
3.1	Action for coherent QPS in a JJ chain	23
3.1.1	Euclidean action for a closed ring	23
3.1.2	Classical phase configurations	26
3.1.3	The QPS action on a classical trajectory	30
3.1.4	Normal modes, chain impedance	32
3.2	QPS amplitude for a homogeneous chain	35
3.2.1	Classical trajectory	35
3.2.2	Pre-exponent	39
3.3	Weak junction limit (fluxonium)	41
3.4	Open chain	45

3.5	Relation to Kosterlitz-Thouless renormalization group	47
4	QPS in inhomogeneous JJ chains	51
4.1	Linear response to a spatial modulation of the chain parameters . . .	51
4.2	Periodically modulated chain	53
4.2.1	Physical mechanisms for the modulation	53
4.2.2	Junction area modulation	54
4.2.3	Island area modulation	58
4.2.4	SQUID area modulation	58
4.2.5	Combined modulation	59
4.3	Disordered chain	59
4.3.1	Fluctuations of the QPS action	59
4.3.2	QPS amplitude distribution without random induced charges .	63
4.3.3	QPS amplitude distribution in the presence of random induced charges	68
5	QPS in superconducting nanowires	71
6	Conclusions and Outlook	78
A	WKB calculation of the tunneling matrix element in the tilted washboard potential	80

Abstract

In this thesis quantum phase slips in one-dimensional superconductors are studied. One-dimensional superconductors can be represented by two physical systems: a superconducting wire and a Josephson junction chain. A superconducting wire can be considered one-dimensional, if its transverse dimensions are smaller than the superconducting coherence length. In one-dimensional systems fluctuations strongly influence the system properties. The quantum phase slips correspond to quantum tunneling between different phase configurations along the superconductor. They can be of two types. Coherent quantum phase slips do not involve dissipation and only shift energy levels of the system. Incoherent quantum phase slips lead to a dissipative relaxation in the system.

We start with studying an incoherent phase-slip process in a single underdamped current-biased Josephson junction. This process corresponds to dissipative tunneling between weakly broadened levels in neighboring minima of the tilted washboard potential. We derive an expression for the voltage peaks near the resonant values of the external current, which correspond to matching energies of the lowest level in one minimum and an excited level in the lower neighboring minimum. This process is analogous to resonant Zener breakdown known for electrons in a superlattice subject to a strong electric field.

We continue with studying coherent quantum phase slips in a Josephson junction chain. First, we determine the amplitude of a coherent quantum phase slip in a homogeneous chain. It has already been shown that the amplitude is determined by the imaginary-time instanton action, which can be divided into the local (corresponding to phase winding by 2π on one junction) and environmental (corresponding to phase readjustment in the rest of the chain, which is determined by gapless Mooij-Schön modes) parts. We derive a numerical correction to the environmental part of the action, going beyond logarithmic precision. Second, we study the effect of spatial periodic modulations of the chain parameters on the coherent quantum phase slip process. We calculate the corrections both to the local and environmental part of the coherent quantum phase slip action and show that both of them can be significant, depending on the chain and modulations parameters. Then, we study the effect of two types of quenched disorder: random spatial modulation of the junction areas and random induced background charges. The main result is that the dominant

contribution to the coherent quantum phase slip action is local. We also study the statistics of the mesoscopic fluctuations of the quantum phase slips amplitude and show that it can be non-Gaussian for chains which are not sufficiently long.

Finally, we consider one-dimensional superconducting wires. There is no microscopic theory available for the fast phase winding in the phase-slip core, where the order parameter is suppressed. However, the slow phase readjustment process, determined by the Mooij-Schön modes with frequencies lower than 2Δ , is analogous to that in Josephson junction chains, so the resulting environmental part of the coherent quantum phase slip action takes the same form. Therefore, we discuss how our results, obtained for Josephson junction chains, can be applied to inhomogeneous superconducting wires.

My publications related to the thesis

1. A. E. Svetogorov, M. Taguchi, Y. Tokura, D. M. Basko, and F. W. J. Hekking. Theory of coherent quantum phase slips in Josephson junction chains with periodic spatial modulations. *Phys. Rev. B* **97**, 104514 (2018).
2. A. E. Svetogorov and D. M. Basko. Effect of disorder on coherent quantum phase slips in Josephson junction chains. *Phys. Rev. B* **98**, 054513 (2018).

Résumé

Dans cette thèse, j'étudie les sauts de phase quantiques dans des supraconducteurs unidimensionnels. Les supraconducteurs unidimensionnels peuvent être représentés par deux systèmes physiques: un fil supraconducteur ou une chaîne de jonctions de Josephson. Un fil supraconducteur peut être considéré unidimensionnel si ses dimensions transversales sont inférieures à la longueur de cohérence supraconductrice. Dans les systèmes unidimensionnels, les fluctuations ont une grande influence sur les propriétés du système. Les sauts de phase quantiques correspondent au tunnel quantique entre différentes configurations de phase le long du supraconducteur. Ils peuvent être de deux types. Les sauts de phase quantiques cohérents n'impliquent pas de dissipation et ne font que déplacer les niveaux d'énergie du système. Les sauts de phase quantiques incohérents entraînent une relaxation dissipative dans le système.

Nous commençons par étudier un processus incohérent de saut de phase dans une jonction de Josephson sous-atténuée et soumise à un courant externe. Ce processus correspond à un processus tunnel dissipatif entre des niveaux faiblement élargis dans les minima voisins du potentiel de planche à laver incliné. J'obtiens une expression pour les pics de tension proches des valeurs de résonance du courant externe, qui correspondent à l'énergies du niveau le plus bas dans un minimum et celle d'un niveau excité dans le minimum voisin étant proches. Ce processus est analogue à la rupture résonante de Zener connue pour les électrons dans un super-réseau soumis à un champ électrique fort.

Nous continuons à étudier les sauts de phase quantiques cohérents dans une chaîne de jonctions de Josephson. Tout d'abord, nous déterminons l'amplitude d'un saut de phase quantique cohérent dans une chaîne homogène. Il a déjà été montré que l'amplitude est déterminée par l'action de l'instanton dans un temps imaginaire, qui peut être divisée en deux parties: l'action locale (correspondant à un enroulement de la phase par 2π sur une jonction) et l'environnement (correspondant à un réajustement de la phase dans le reste de la chaîne, qui est déterminée par des parties de Mooij-Schön sans gap). Nous obtenons une correction numérique de la partie environnementale de l'action, allant au-delà de la précision logarithmique. Deuxièmement, nous étudions l'effet de la modulation périodique spatiale des paramètres de la chaîne sur la phase quantique cohérente. Nous calculons les corrections aux parties locale et environnementale de l'action du sauts de phase quantique cohérent et montrons que les deux peuvent être significatives, en fonction des paramètres de la chaîne et des modulations. Puis nous étudions l'effet des deux

types de désordre : modulation spatiale aléatoire des surfaces des jonctions et des charges de fond induites de manière aléatoire. Le résultat principal est que la contribution dominante à l'action cohérente du saut de phase quantique est locale. Nous étudions également la statistique des fluctuations mésoscopiques de l'amplitude des sauts de phase quantiques et montrons qu'elle peut être non Gaussienne pour des chaînes qui ne sont pas suffisamment longues.

Enfin, nous considérons des fils supraconducteurs unidimensionnels. Il n'y a pas de théorie microscopique disponible pour l'enroulement de phase rapide dans le noyau du saut de phase, où le paramètre d'ordre est supprimé. Cependant, le processus lent de réajustement de la phase, déterminé par les modes de Mooij-Schön avec des fréquences inférieures à 2Δ , est analogue à celui des chaînes de jonction de Josephson, de sorte que la partie environnementale résultante de l'action du saut de phase quantique cohérent prend la même forme. Par conséquent, nous discutons de la façon dont nos résultats, obtenus pour les chaînes de jonction Josephson, peuvent être appliqués à des fils supraconducteurs inhomogènes.

Mes publications liées à la thèse

1. A. E. Svetogorov, M. Taguchi, Y. Tokura, D. M. Basko, and F. W. J. Hekking. Theory of coherent quantum phase slips in Josephson junction chains with periodic spatial modulations. *Phys. Rev. B* **97**, 104514 (2018).
2. A. E. Svetogorov and D. M. Basko. Effect of disorder on coherent quantum phase slips in Josephson junction chains. *Phys. Rev. B* **98**, 054513 (2018).

Chapter 1

Introduction

1.1 One-dimensional superconductivity: superconducting nanowires and Josephson junction chains

The phenomenon of superconductivity has taken a significant place in condensed matter physics since its discovery in 1911 by Kamerlingh Onnes [1]. The most interesting feature of the phenomenon is the vanishing resistance of some metals below a critical temperature T_c . Superconductivity is determined by coherent pairs of electrons (Cooper pairs). These coherent Cooper pairs form a Bose-Einstein condensate, whose wave function can be expressed by a complex order parameter Δ , which at the same time determines the energy gap in the spectrum of quasiparticle excitations. As a result, the state of a superconductor can be described by the Cooper-pair condensate and quasiparticle excitations above the energy gap $|\Delta|$. In a bulk superconductor, collective excitations (Goldstone modes) are also gapped by virtue of the Anderson-Higgs mechanism, the gap corresponds to the plasma frequency of the electrons in the metal. However, the picture changes if the system dimensionality is reduced. In this case the collective excitations are no longer gapped, the fluctuations of the order parameter are strong, which can influence the system properties dramatically.

Superconductivity in one-dimensional systems has been studied both theoretically and experimentally since long ago [2, 3, 4, 5, 6]. One-dimensional superconductors are structures in which the order parameter of the Cooper-pair condensate is almost constant across the superconductor and can vary only along the system. Therefore, the properties of the system can be described by the order parameter profile along the superconductor. Presently, one-dimensional superconductivity can

be realized in Josephson junction (JJ) chains or thin metallic wires (see Refs. [7] and [8] for respective reviews). Such structures are of great interest as they have a variety of different applications. These applications range from photon detectors used in astronomy [9] to the proposed realization of a fundamental current standard in quantum metrology [10, 11, 12]. Moreover, one-dimensional superconductivity is a fundamental issue as it corresponds to the case of strong quantum fluctuations resulting in a superconductor-insulator quantum phase transition. A quantum one-dimensional system can be mapped on a two-dimensional classical system, which allows to connect this quantum phase transition to the Berezinskii-Kosterlitz-Thouless transition [13].

Superconducting nanowires can be considered one-dimensional from the condensate perspective, if their thickness w is much smaller than the superconducting coherence length, $w \ll \xi$. Then the superconducting order parameter $\Delta = |\Delta|e^{i\phi}$ varies only along the wire and, in case the absolute value $|\Delta|$ is not suppressed, it is just the phase ϕ configuration along the wire, which determines the system properties. Still, from the fermionic quasiparticle excitation perspective, all realistic wires are three-dimensional, as typical Fermi wavelength is of the order of a few angstroms, while the thinnest existing wires have the transverse size of the order of 10 nm. At low temperatures the dominant excitations are not quasiparticles but collective gapless plasma modes (Mooij-Schön modes [14]) corresponding to small oscillations of phase ϕ . And if the absolute value of the order parameter is suppressed in some region of the wire, allowing the phase to flip by 2π , those modes determine phase readjustment in the rest of the core (for details see Sec. 1.2 and Chapter 5).

A Josephson junction consists of two superconducting electrodes connected by a weak link or a tunnel barrier. It was predicted [15] and then observed [16] that at zero voltage there is a supercurrent I through the junction, which depends on the superconducting phase difference $\Delta\phi$ on the electrodes, $I = I_c \sin \Delta\phi$, where $I_c = 2eE_J$ is the critical current supported by the junction (E_J is the Josephson coupling energy, the electron charge is $-e$ and we put $\hbar = 1$ throughout the thesis). Moreover, for nonzero voltage V along the junction the phase difference evolves as $d\Delta\phi/dt = 2eV$. A JJ chain consists of many superconducting islands, connected by Josephson junctions. The properties of such a system are determined both by the junction parameters, namely critical currents I_c , and effective capacitances C (corresponding to electrostatic interactions between the neighboring islands), as well as superconducting islands' capacitances to the ground C_g (corresponding to elec-

trostatic interactions between the islands and the substrate) schematically shown on Fig. 1.1. The continuous interest in JJ chains is due to their use as elements of various superconducting circuits [17]. As JJ chains can be fabricated with a good degree of control, they are used to create electromagnetic environments with special properties, for example, to suppress charge fluctuations in the system [18, 19, 20]. Moreover, new coherent devices, such as topologically protected qubits [21, 22], were proposed. And finally JJ chains are supposed to be useful in realization of the fundamental current standard [10, 11, 12] dual to the Josephson voltage standard [23].

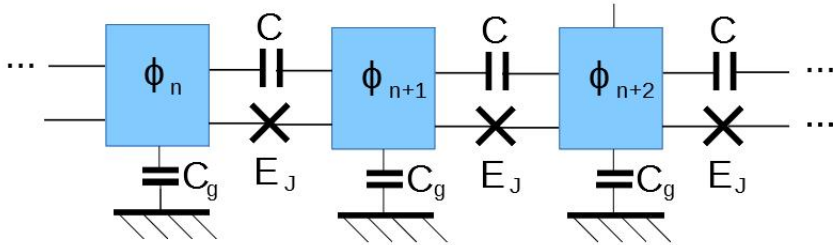


Figure 1.1: A schematic representation of a Josephson junction chain.

There are three main energy scales in a JJ chain. We have already introduced Josephson coupling energy E_J , which determines the energy of the supercurrent flowing through the junction. The Coulomb electrostatic energy associated with Cooper-pair tunneling is determined by the energy scales corresponding to two capacitances, $E_c = e^2/(2C)$ and $E_g = e^2/(2C_g)$. Here we are interested in JJ chains with E_J being the largest energy scale. Then the wave function of the system of N junctions $\Psi(\phi_0, \phi_1, \dots, \phi_N)$ is peaked near some phase values ϕ_n , and a phase-coherent Cooper-pair current can flow through the chain without any external voltage.

1.2 Phase slips

During the studies of one-dimensional superconductivity an important role played by phase slips has been realized [24]. Phase slips can be thermally activated [25, 26] near the critical temperature T_c or caused by quantum tunneling at lower temperatures. A thermally activated phase slip is a nontrivial thermal fluctuation of the complex order parameter Δ , corresponding to a temporal suppression of $|\Delta|$ in a

short region of the system, which allows the phase to jump by 2π . A quantum phase slip (QPS) is a sudden change of the superconducting phase difference along a one-dimensional superconductor by 2π via quantum-mechanical tunneling. In a good superconductor phase slips are rare events, but they can give rise to qualitatively new effects, such as small but finite dc resistance of the superconductor at temperatures lower than the critical temperature T_c [27, 28, 29, 30, 31], or system coupling to external charges [32, 33, 34, 35, 36]. If these phase slips become frequent enough, they can turn the system into an insulator [13, 37, 38, 39], which is superconductor-insulator phase transition. There are two types of QPS: incoherent QPS, which are accompanied by energy dissipation, and coherent QPS, which only shift the system energy levels. Both incoherent [27, 29, 30, 31, 40, 41, 42, 43] and coherent [19, 35, 44, 45] QPSs have been observed experimentally. The simplest system to observe the phase slips is a single Josephson junction. In case of low dissipation and no induced current, the coherent QPSs result in band structure of the system spectrum instead of discrete low-energy levels (discussed in more detail in Sec. 2.1 of the present thesis), while dissipation in combination with induced current can lead to incoherent QPSs, resulting in voltage peaks at resonant values of the current (see Sec. 2.2).

We are mainly interested in coherent QPSs in the regime when phase tunneling can be described quasiclassically. Then the amplitude of a single coherent QPS is proportional to $e^{-S_{\text{QPS}}}$, where $S_{\text{QPS}} \gg 1$ is the action on the classical imaginary-time (instanton) trajectory $\phi_{cl}(x, \tau)$ corresponding to the coherent QPS. This trajectory consists of a fast phase winding by almost 2π in a small region of the superconductor (a core region of the length $\ell_{core} \sim 1$ junction in a JJ chain or $\ell_{core} \sim \xi$ in a superconducting wire) and slow phase readjustment in the rest of the chain/wire. The readjustment is governed by gapless Mooij-Schön modes [46, 47, 48, 49, 50], which represent small phase oscillations in the system. They can be seen as an environment for the coherent QPS. This environment contribution to the action diverges logarithmically with the system length L and gives rise to the logarithmic interaction between phase-slips in multi-QPS configurations [13, 37, 38]. As a result, the action can be divided into two parts: local and environmental, $S_{\text{QPS}} = S_{loc} + S_{env}$. The latter depends on the system length logarithmically, $S_{env} = g \ln \frac{L}{\ell_{core}}$ [8, 51], where g is the dimensionless admittance of the system in units of superconducting conductance quantum $(2e)^2/(\pi\hbar)$ (we momentarily restore \hbar); for JJ chains it is $g = \sqrt{\frac{\pi^2 E_J}{8E_g}}$ [52]. The local part of the action can be calculated explicitly for a JJ chain, $S_{loc} = \sqrt{8E_J/E_c}$ [33]. However, for superconducting nanowire only an order-

of-magnitude estimate is available for the local part of the action, $S_{loc} \sim \nu\xi\Delta$ [53], where Δ is the superconducting gap, ξ is the superconducting coherence length and ν is the one-dimensional density of states at the Fermi level in the normal state. Indeed, as the order parameter Δ is suppressed in the core region of the length ξ , the phase action is not valid in this region, and fluctuations of the absolute value of the order parameter should be taken into account as well as quasiparticle excitations over $2|\Delta|$. A more precise result can be obtained in the weak link limit [53]. Therefore, further we derive quantitative theory for JJ chains, which then allows us to do estimations for the superconducting nanowires.

1.3 Superconductor-insulator transition

As we have already mentioned, proliferation of quantum phase slips gives rise to the superconductor-insulator transition. This is a correct statement for infinite chains. For finite chains the system is rather in superconducting or insulating regime depending on the phase-slip frequency (amplitude for coherent QPS), as phase slips suppress the supercurrent, however, there is rather a crossover than a sharp phase transition.

In their breakthrough work [54] Kosterlitz and Thouless described a new type of phase transition, Berezinskii-Kosterlitz-Thouless (BKT) transition, which can occur in a two-dimensional XY model or in neutral superfluids. The transition is caused by the process of vortex-antivortex unbinding. It is known that a one-dimensional quantum system can be mapped on a two dimensional classical system: the first dimension corresponds to the coordinate x along the JJ chain, $0 < x < L$, while the second dimension is the imaginary time τ , $0 < \tau < \beta \equiv 1/T$, the inverse temperature. It was shown that the JJ chain can be mapped on a classical XY model [13, 38], where the role of the spin orientation angle is played by the superconductor order parameter phase ϕ on each island. As a result, the superconductor-insulator transition in an infinite JJ chain at zero temperature can be seen as an analogy of the BKT phase transition in a classical XY model. A phase slip in a JJ chain corresponds to a vortex in the (x, τ) plane. The phase slips interact logarithmically, the strength of interaction is controlled by g . As a result, the pre-logarithm factor g in the action S_{env} determines the phase transition: if it is larger than the critical value g_c , the vortices are bound in vortex-antivortex pairs; otherwise, free vortices destroy the phase coherence and push the system into an insulating state. Therefore, g plays the same role as the inverse temperature $\beta = 1/T$ in the BKT transition for

the classical XY model. If we consider realistic finite-length systems, there is no real phase transition, however, the BKT theory still can be useful to determine the QPS amplitude scaling with the system size [55]. The scaling shows that there is a crossover from superconducting to insulating regime in the region of g close to the critical value g_c , defined for our infinite system.

1.4 Structure of the thesis

In this thesis we study the QPS process, which corresponds to quantum tunneling between phase configurations, representing classically degenerate states. We start with the simplest system possible – a single Josephson junction, discussed in Chapter 2. First, we review how in case of zero dissipation and no external currents coherent QPSs between infinite number of the potential minima result in a band structure of the system spectrum due to the Bloch theorem. Then we study the effect of dissipation, modelled as an external resistance, which is inevitable in a real experimental setup, on current-biased Josephson junction. We show that due to incoherent quantum phase slips at certain resonant values of induced current there are voltage peaks, and derive the form of these peaks.

In Chapter 3 we study coherent QPS in JJ chains. Starting from the case of homogeneous chain, we study a single coherent QPS process, which can be divided into two parts: fast phase winding by 2π on one junction, and slow phase readjustment in the rest of the chain (which plays the role of the environment for a phase slip). We have been able to improve the result for the QPS action which was previously known only with logarithmic precision [56].

We continue by studying the effects of disorder on the coherent QPS process in Chapter 4. First, we consider an artificial case of spatially periodic modulations (such as weak modulation of the junctions' areas). The Mooij-Schön modes are sensitive to spatial variations of the chain parameters. Indeed, in this case the environment contribution to the QPS action can be significantly modified, both the correction to the local part of the action (determined by the QPS core) and environmental part can be dominant, depending on the chain and modulation parameters. This study was published in [56]. Then we analyze the effect of disorder on both the local and environmental contributions to the QPS action, published in [57]. We consider two types of disorder: random spatial variation of the chain (i.e., junction area variation) and random induced charges (which can arise from random gate voltages or electronic density modulations). The former is known to induce Mooij-Schön

modes localization. However, we find that the effect of disorder on the environment contribution to the QPS action is weak, and that the localization of the Mooij-Schön modes does not significantly affect the coherent QPS amplitude. The coherent QPS amplitude in a disordered chain is a random quantity, determined as a sum of all the partial phase-slip amplitudes on different junctions (each is determined by classical action S_n and, in case of induced charges, by a random phase θ_n)

$$W = \sum_{n=0}^{N-1} W_n = \sum_{n=0}^{N-1} \Omega_n e^{-S_n - i\theta_n}, \quad (1.1)$$

whose statistics is determined by the fluctuations of the local term in the QPS action. We study this statistics and show that it can be non-Gaussian if the chain is not sufficiently long.

In the last chapter we apply the results obtained for Josephson junction chains to superconducting nanowires. We show that the systems have similar low-frequency properties, determined by Mooij-Schön modes, therefore, we can calculate the environmental part of the QPS action in a nanowire. However, for the local part we have only an order-of-magnitude estimate, as the phase action cannot be written on the length scales smaller than superconducting coherence length ξ , which is the typical size of a phase-slip core. Nevertheless, we can show that qualitatively the effects of disorder on QPS amplitude in wires are similar to the ones in Josephson junction chains.

Chapter 2

Quantum phase slips in an underdamped Josephson junction

2.1 Coherent QPS and Bloch oscillations

The simplest system to consider phase slips is a single Josephson junction. We start with the junction with capacitance C formed by the two junction electrodes and Josephson energy $E_J = I_c/(2e)$, where I_c is the critical current supported by the junction. Then the Hamiltonian of the system is

$$H = \frac{Q^2}{2C} - E_J \cos \phi, \quad (2.1)$$

where Q is the electric charge of the capacitance C , while ϕ is the phase difference between the two electrodes of the junction. These variables are conjugate: $[\phi, Q] = 2ei$.

If we consider a Josephson junction disconnected from any other source of charges, the charge on the electrodes is quantized, $Q = 2en$, where n is integer. Then the basis functions of the system have the form $\Psi \sim \exp(-i\frac{Q\phi}{2e}) \sim \exp(-in\phi)$, which is 2π -periodic in ϕ . Phases ϕ and $\phi + 2\pi$ represent the same physical state. Therefore, ϕ is a compact variable. As a result, the system is analogous to a quantum pendulum with angular momentum $Q/(2e)$, angular deflection ϕ and moment of inertia $C/(2e)^2$. The spectrum consists of discrete energy levels.

In experimental setups the junction is usually connected to other circuit elements, the charge on the capacitance is not quantized (as now it is impossible to separate the electron state in the island and in the connected electrodes). Phases ϕ and $\phi + 2\pi$ represent two distinct physical states, the phase ϕ is not compact, and

the wave function is not necessarily 2π periodic. Then the system is equivalent to a particle of mass $C/(2e)^2$ with momentum $Q/(2e)$ moving in a one-dimensional periodic potential $-E_J \cos \phi$, where ϕ is a coordinate. We can rewrite the Hamiltonian as

$$H = -\frac{(2e)^2}{2C} \frac{\partial^2}{\partial \phi^2} - E_J \cos \phi. \quad (2.2)$$

The first term of the Hamiltonian corresponds to the kinetic energy, while the Josephson term is the potential energy. We consider the case, when the potential term dominates, $E_J \gg E_c \equiv \frac{e^2}{2C}$. If we neglect tunneling, we have equivalent sets of energy levels in all minima of the cosine potential. However, if we include quantum tunneling between the minima, the degeneracy between the levels is lifted and, as the tunneling is possible between the infinite number of classically degenerate levels, the resulting spectrum consists of energy bands rather than discrete levels. This tunneling process is a coherent quantum phase slip (as there is no dissipation). Its amplitude can be described by an instanton in the imaginary time.

As the system has a periodic potential, the Bloch theorem can be applied. The eigenfunctions are Bloch waves:

$$\psi_k^{(n)}(\phi) = u_k^{(n)}(\phi) e^{ik\phi}, \quad u_k^{(n)}(\phi + 2\pi) = u_k^{(n)}(\phi). \quad (2.3)$$

Here $q = 2ek$ can be seen as a quasicharge in analogy with quasimomentum. And as the energy is periodic in k within each band, $E^{(n)}(k+1) = E^{(n)}(k)$, we can restrict the quasicharge to the first Brillouin zone, $-1/2 < k < 1/2$. We can substitute eigenfunctions (2.3) into the Schrödinger equation with Hamiltonian (2.2). As we work in the limit $E_J \gg E_c$, for low energy levels, $n \ll \sqrt{E_J/E_c}$, we can apply tight-binding approximation and find:

$$u_k^{(n)}(\phi) = \sum_{l=-\infty}^{\infty} W^{(n)}(\phi - 2\pi l) e^{-i(\phi - 2\pi l)k}, \quad (2.4)$$

where $W^{(n)}(\phi)$ is just the n -th eigenfunction of the harmonic oscillator with frequency $\omega_p = \sqrt{8E_J E_c}$. Then the corresponding lowest energy bands are [58] (see schematic representation of all energy bands in Fig. 2.1)

$$E^{(n)}(\phi) = \omega_p \left(n + \frac{1}{2} \right) + \frac{1}{2} (-1)^{n+1} \delta^{(n)} \cos(2\pi k), \quad (2.5)$$

where $\delta^{(n)}/4$ is the exponentially small tunneling amplitude

$$\delta^{(n)} \approx \sqrt{2/\pi} E_c \left(\frac{E_J}{2E_c} \right)^{n/2+3/4} \frac{2^{4n+5}}{n!} \exp(-8E_J/\omega_p). \quad (2.6)$$

The lowest energy bands are narrow (the bandwidth is $\delta^{(n)}$) and located close to the

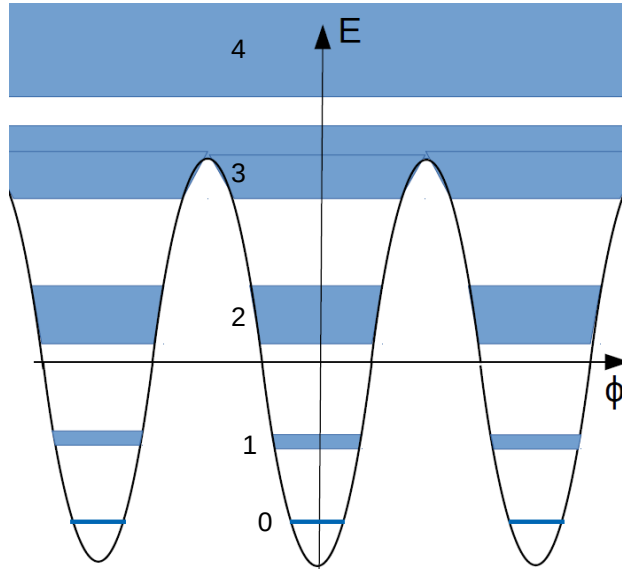


Figure 2.1: A schematic representation of the energy bands in a single Josephson junction

energy levels of the plasma-frequency harmonic oscillator. Here we have illustrated how the coherent quantum phase slips result in a band structure of the spectrum of a single Josephson junction.

If the junction is connected to an external dc current source, the term $-I\phi/(2e)$ should be added to the potential. This can be easily seen from the Heisenberg equation of motion, corresponding to charge conservation, $\partial Q/\partial t = I_{tot} = -I_c \sin \phi + I$, which is correct only if we introduce a term in Hamiltonian, proportional to the induced current and linear in ϕ . If this current is not too large, so that we can neglect the inter-band transitions, the spectrum consists of equally spaced localized levels (Wannier-Stark ladder) [59]. Now, if some dissipation is included in consideration, these Wannier-Stark levels acquire a finite life-time, the phase slowly drifts along the tilted potential and the voltage arises $V = \frac{1}{2e} \frac{d\phi}{dt}$.

At low temperatures quasiparticles are absent, so the dissipation is usually due to the external circuit (i.e. the resistance of the wires, connected to the junction). It can be modelled as an external resistance R (see Fig. 2.3). There are two important

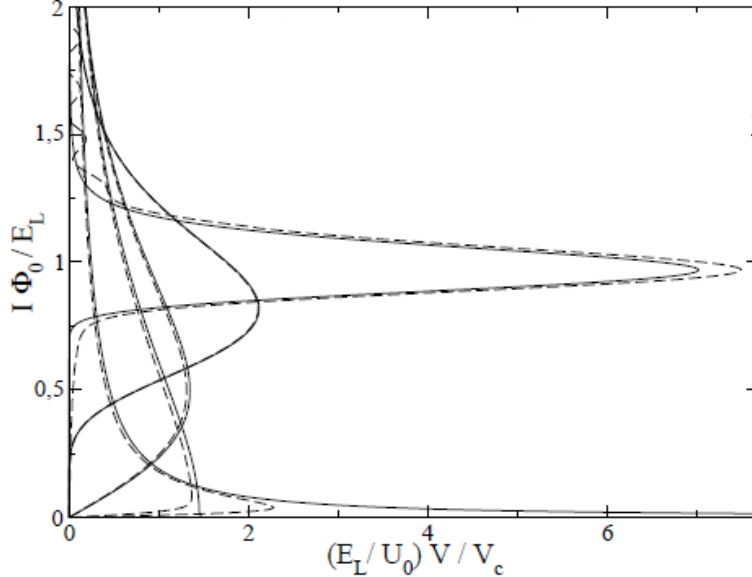


Figure 2.2: $I - V$ characteristics from [60] at $T = 0$ for $\omega_0 = 100\delta^{(0)}$. From top to bottom, solid lines correspond to $R_Q/R = 100, 5, 1, 0.5$ and 0.1 . Dashed lines correspond to finite temperature $T = \omega_0/50$. $\Phi_0 = 2\pi/(2e)$ is a flux quantum, $E_L = \Phi_0^2/(2L)$ is the inductive energy, $\delta^{(0)}$ is the Bloch bandwidth, $V_c = \pi\delta^{(0)}/e$ is the maximal (critical) voltage the junction can sustain. The y -axis corresponds to the current through the junction only, and not to the total external current, which flows both through the junction and the resistance.

limits: an overdamped junction, when this resistance is much smaller than resistance quantum $R \ll R_Q = 2\pi/(2e)^2$, and the opposite limit, which corresponds to an underdamped junction $R \gg R_Q$. In the first limit the supercurrent peak at zero voltage acquires a finite width [60, 61]. Increasing the external resistance R shifts the supercurrent peak to higher voltages, and at $R > R_Q$ the system becomes an insulator: the $I - V$ curve develops a branch with zero current through the junction, but finite voltage [60, 61]. This is often called Shmid phase transition, however, is still debated [62]. In the limit $R \gg R_Q$ of an underdamped junction the $I - V$ characteristics resembles the one for an overdamped junction but with the role of voltage and current interchanged [60]. The voltage peak at zero current is the so-called Bloch nose [63, 58]. The $I - V$ characteristics for a current-biased junction

derived in different regimes in [60] are shown in Fig. 2.2. In the next section we study the $I - V$ characteristics for higher induced currents.

Another important aspect of the underdamped limit is that in the classical RCSJ model the $I - V$ curve is hysteretic, as at $I > I_h = \frac{8e\omega_0}{R(2e)^2}$ there are two possible states: one with zero voltage, corresponding to phase localized inside one minimum of the potential, and the running state, corresponding to a finite voltage, when the phase is sliding down the tilted potential, as the difference of the potential energy between the neighboring potential maxima is larger than energy dissipated, while moving between these maxima. In case of classical thermal noise it was shown [64, 65] that the system is switching from the zero-voltage state to a finite voltage state at some current $I > I_h$. Quantum fluctuations should lead to a crossover between the zero voltage and the finite voltage state at some current $I < I_c$ due to possibility of tunneling through the barrier into the continuous spectrum. To the best of my knowledge, the effect has not been studied yet quantitatively. In the rest of this chapter we study a precursor to this effect – resonant tunneling into weakly broadened excited levels in the neighboring minimum.

2.2 Incoherent QPS and resonant Zener breakdown: Lindblad master equation

In this section we study an underdamped junction $R \gg R_Q$ in the regime of higher induced currents, when the energy difference between the neighboring minima of the potential tilted by the induced current, $-E_J \cos \phi - I\phi/(2e)$, is comparable to the level spacing inside a single minimum and we can no longer neglect transitions between different Bloch bands (here we suppose that we have several energy levels inside each minimum). As a result, at certain current values the energy of the lowest level in one minimum matches the energy of an excited state in the neighboring minimum and, therefore, we have resonant tunneling between them (see Fig. 2.4). Then from the excited state in the lower minimum the system can relax to the ground state and tunnel to the next lower minimum. In the Bloch band representation, this process is the equivalent of resonant Zener tunneling [66] of electron in the presence of strong electric field. Such a process was experimentally observed in superlattices [67, 68, 69]. The tunneling process between the neighboring local minima is dissipative and corresponds to an incoherent quantum phase slip. We assume the dissipation to be weak, so that relaxation rate Γ inside one minimum is much smaller than level spacing. This tunneling results in voltage peaks as a

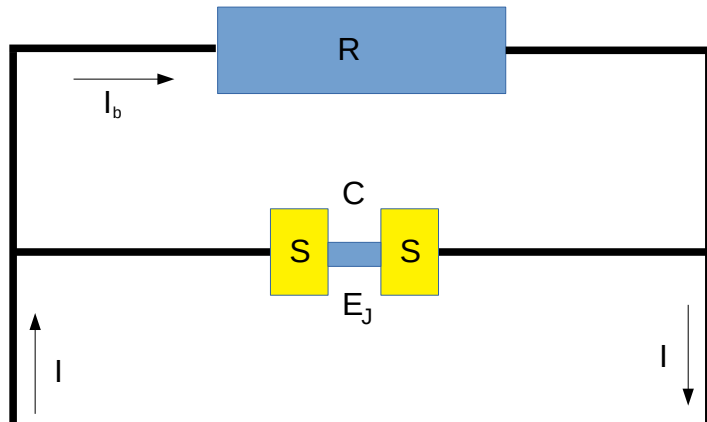


Figure 2.3: A schematic representation of a single dissipative junction with Josephson energy E_J , capacitance C , induced current I and current I_b through external resistance R .

function of current. The opposite case of strongly broadened levels was studied in [37].

The model consists of a single JJ, with external current I , shunted by a resistance R , modelled as a bath of harmonic oscillators [61], (see Fig. 2.3). The Hamiltonian is

$$H = \frac{Q^2}{2C} - E_J \cos \phi - \frac{I}{2e} \phi + \frac{I_b}{2e} \phi + H_b, \quad (2.7)$$

where $I_b = \sum_n 2eg_n (b_n^\dagger + b_n)$ is the current through resistor, $H_b = \sum_n \omega_n b_n^\dagger b_n$ is the bath Hamiltonian, corresponding to dissipation in the resistor, ω_n are frequencies of the harmonic bath modes, b_n and b_n^\dagger are annihilation and creation operators for the bath modes, g_n are coupling constants. The Hamiltonian can be divided into three parts, $H_0 = \frac{Q^2}{2C} - E_J \cos \phi - \frac{I}{2e} \phi$, corresponding to the junction without dissipation, $H_{int} = \frac{I_b}{2e} \phi$, which is the interaction with the thermal bath, and the remaining part H_b is the Hamiltonian of the bath itself.

Let us consider the states of the system in one of the local potential minima of Hamiltonian H_0 , $\phi_{min}^l = \arcsin \frac{I}{2eE_J} + 2\pi l$, where l labels the minima. To have local minima of the potential we need the current to be lower than the critical value $I < I_{crit} = 2eE_J$. For $I \ll I_{crit}$ we can approximate the states inside a minimum as the states of a harmonic oscillator with momentum Q , coordinate ϕ ,

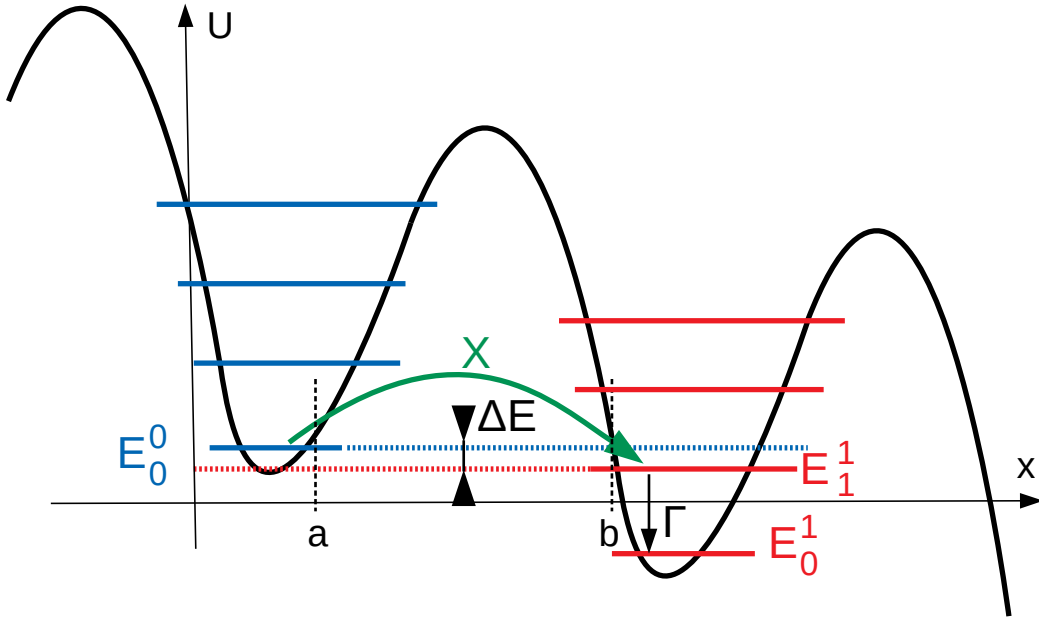


Figure 2.4: The tunneling X from the lowest classical state in the minima to the first excited state in the lower neighboring local minima and further relaxation Γ to the lower state.

mass $m = C / (2e)^2$ and frequency $\omega_0^2 = \omega_p^2 \cos \phi_{min}^l \approx \omega_p^2$:

$$H_0 = \frac{Q^2}{2C} - E_J \cos \phi - \frac{I}{2e} \phi \approx -\frac{(2e)^2}{2C} \frac{\partial^2}{\partial \phi^2} + \frac{1}{2} E_J \cos \phi_{min}^l (\phi - \phi_{min}^l)^2 + const. \quad (2.8)$$

As a result, we have approximate energy levels

$$E_n^l = \omega_0 \left(n + \frac{1}{2} \right) - E_J - \frac{I}{2e} \left(\arcsin \frac{I}{2eE_J} + 2\pi l \right). \quad (2.9)$$

We can write the Lindblad master equation for the reduced density matrix of the system $\hat{\rho}$ (the total density matrix is $\hat{\rho}_{tot} = \hat{\rho} \times \hat{\rho}_b$, where $\hat{\rho}_b$ corresponds to the bath density matrix), using the standard approach (tracing out the bath degrees of freedom) [58]

$$\frac{d}{dt} \hat{\rho}(t) = -i [\hat{H}_0, \hat{\rho}] + \frac{\Gamma}{2} \sum_l \left(2\hat{a}_l \hat{\rho}(t) \hat{a}_l^\dagger - \{ \hat{\rho}(t), \hat{a}_l^\dagger \hat{a}_l \} \right). \quad (2.10)$$

Here \hat{a}_l and \hat{a}_l^\dagger are lowering and raising operators between the harmonic oscillator

levels within each minimum, Γ stands for the relaxation rate inside this minimum,

$$\Gamma \propto \text{Re} \int_0^t \frac{dt'}{(2e)^2} \langle I_b(t) I_b(t') e^{-i\omega_0 t'} + I_b(t') I_b(t) e^{i\omega_0 t'} \rangle. \quad (2.11)$$

To relate Γ to the resistance R , let us neglect tunneling and multiply Eq. (2.10) by $\hat{\phi}$ and take the trace over $\hat{\rho}$. Then we obtain an equation, corresponding to phase evolution inside one minimum

$$\frac{d}{dt} \langle \phi - \phi_{min} \rangle = \omega_0 \frac{\langle Q \rangle}{2e} \left(\frac{8E_c}{E_J} \right)^{1/2} - \frac{\Gamma}{2} \langle \phi - \phi_{min} \rangle. \quad (2.12)$$

Taking time derivative and relating $\frac{d}{dt} \langle Q \rangle$ to $\langle \phi - \phi_{min} \rangle$ through the Heisenberg equation of motion results in

$$\frac{d^2}{dt^2} \langle \phi \rangle + \omega_0^2 \langle \phi \rangle + \frac{\Gamma}{2} \frac{d}{dt} \langle \phi \rangle = \frac{8E_c I}{2e}. \quad (2.13)$$

In linear approximation (so that we can put $\sin \phi \approx \phi$) our system can be seen as an *LCR*-contour, then the Kirchhoff equation is

$$\frac{C}{2e} \ddot{\phi} + \frac{\phi}{2eL} + \frac{\dot{\phi}}{2eR} = I. \quad (2.14)$$

We can compare it to Eq. (2.13) and express relaxation rate Γ through the contour parameters

$$\Gamma = \frac{2}{RC} = \frac{2\omega_0 \sqrt{8E_c/E_J}}{(2e)^2 R}. \quad (2.15)$$

We assume the relaxation rate to be much smaller than the oscillator level spacing, $\Gamma \ll \omega_0$, then we need $R/R_Q \gg \sqrt{E_c/E_J}$. Since we assume $E_J \gg E_c$, this is a weaker condition than $R \gg R_Q$, so this limit is often referred to as moderately damped limit.

2.3 Voltage peaks due to incoherent QPS

2.3.1 Effective two-level case

Let me start with the simplest case, when the lowest level in each minimum matches the first excited level in the neighboring minimum; in this case, only two levels per minimum need to be considered. We are interested in the tunneling between levels

E_1^1 and E_0^0 , which are schematically depicted in Fig. 2.4, then we can rewrite the system Hamiltonian \hat{H}_0 in the multiorbital tight-binding form:

$$\langle ln | \hat{H}_0 | l'n' \rangle = \delta_{ll'} \delta_{nn'} E_n^l + (\delta_{l',l+1} \delta_{n'1} \delta_{n0} + \delta_{l',l-1} \delta_{n'0} \delta_{n1}) X, \quad (2.16)$$

where indices l and l' label minima of the potential, $n, n' = 0, 1$ are the level indices inside one minimum, X stands for the matrix element of tunneling between levels $|l, 0\rangle$ and $|l+1, 1\rangle$ (tunneling between the excited state in the first minimum and ground state in the neighboring). It is calculated in Appendix A.

Since we are interested in the stationary situation, when all minima are equivalent, the density matrix must be periodic in the minimum index:

$$\langle ln | \hat{\rho} | l'n' \rangle = \langle l+k, n | \hat{\rho} | l'+k, n' \rangle. \quad (2.17)$$

We keep the coherence only between the neighboring minima. Then we have an effective two-level system. The non-zero density matrix elements are

$$\begin{aligned} \langle l0 | \hat{\rho} | l0 \rangle &= \sigma_{00}, & \langle l1 | \hat{\rho} | l1 \rangle &= \sigma_{11}, \\ \langle l0 | \hat{\rho} | l+1, 1 \rangle &= \sigma_{01}, & \langle l1 | \hat{\rho} | l-1, 0 \rangle &= \sigma_{10}, \end{aligned} \quad (2.18)$$

all the others are zero.

Now we can write down the equation for the stationary state, including the effects of dissipation, by setting $d\hat{\rho}/dt = 0$ in Eq. (2.10):

$$\begin{cases} 0 = -i(X(\sigma_{00} - \sigma_{11}) - \Delta E \sigma_{10}) - \frac{1}{2}\Gamma \sigma_{10}, \\ 0 = -i(X(\sigma_{11} - \sigma_{00}) + \Delta E \sigma_{01}) - \frac{1}{2}\Gamma \sigma_{01}, \\ 0 = -i(X(\sigma_{10} - \sigma_{01})) + \Gamma \sigma_{11}, \\ 0 = -i(X(\sigma_{01} - \sigma_{10})) - \Gamma \sigma_{11}. \end{cases} \quad (2.19)$$

Here $\Delta E = \pi I/e - \omega_0$ is the energy difference between E_l^0 and E_{l+1}^1 . Γ stands for the relaxation rate between the classical levels in one minimum, Eq. (2.15). We study the system close to the resonance, $\Delta E \ll \omega_0$. The stationary solution is

$$\sigma_{10} = -\mathcal{N} \frac{i(\Gamma/2 + i\Delta E) X}{2X^2 + \Delta E^2 + \Gamma^2/4}, \quad \sigma_{01} = \mathcal{N} \frac{i(\Gamma/2 - i\Delta E) X}{2X^2 + \Delta E^2 + \Gamma^2/4}, \quad (2.20)$$

$$\sigma_{11} = \mathcal{N} \frac{X^2}{2X^2 + \Delta E^2 + \Gamma^2/4}, \quad \sigma_{00} = \mathcal{N} \frac{X^2 + \Delta E^2 + \Gamma^2/4}{2X^2 + \Delta E^2 + \Gamma^2/4}, \quad (2.21)$$

where \mathcal{N} is the overall normalization constant to have $\text{Tr}\hat{\rho} = 1$. The voltage is proportional to the probability current between neighboring sites of our multiorbital tight-binding model

$$\hat{V} = \frac{2\pi}{2e} iX \sum_l (|l, 0\rangle\langle l+1, 1| - |l+1, 1\rangle\langle l, 0|). \quad (2.22)$$

Then the average voltage can be calculated as

$$\langle \hat{V} \rangle = \text{Tr} \left\{ \hat{V} \hat{\rho} \right\} = \frac{1}{\text{Tr}\hat{\rho}} \frac{2\pi}{2e} iX \text{Tr} \left\{ \begin{pmatrix} 0 & 1 \\ -1 & 0 \end{pmatrix} \hat{\sigma} \right\}, \quad (2.23)$$

resulting in a voltage peak with the Lorentzian form:

$$\langle V \rangle \approx \frac{1}{2e} \frac{2\pi\Gamma X^2}{2X^2 + \Delta E^2 + \Gamma^2/4}. \quad (2.24)$$

The matrix element is (see Appendix A and put $m = 1$):

$$|X| = \frac{3^{3/4}\omega_0}{2e\sqrt{2\pi}} e^{-S_1}, \quad (2.25)$$

with the tunneling action

$$S_1 = \sqrt{\frac{8E_J}{E_c}} - \left(2 + \ln \frac{E_J/E_c}{3^{1/4}} \right) + O\left(\left(E_c/E_J\right)^{1/4}\right). \quad (2.26)$$

One can see from Eq. (2.24) that there is a crossover from incoherent QPS (for $X \ll \Gamma$) to coherent (for $X \gg \Gamma$), if we increase tunneling matrix element X . For large $X \gg \Gamma$ the voltage peak is proportional to relaxation rate Γ . It corresponds to the fact that the state of the system is now a coherent superposition of two states in two neighboring minima of the potential, until it relaxes to the ground state in the lower minimum and becomes a superposition of this ground state and an excited state in the next lower minimum. Therefore, the rate of phase sliding down the tilted potential is determined only by the relaxation rate Γ .

However, in the case $X \gg \Gamma$ the above picture is incomplete. Indeed, in the harmonic approximation the resonance between E_l^0 and E_{l+1}^1 automatically implies the resonance between E_{l+1}^1 and E_{l+2}^2 , and so on. Therefore, one must consider the possibility of coherence between more than two minima. On the other hand, the resonant conditions are affected by the anharmonicity of the cosine potential.

Namely,

$$(E_l^1 - E_l^0) - (E_l^2 - E_l^1) \sim E_c \sim \omega_0 \sqrt{E_c/E_J}. \quad (2.27)$$

At the same time, from Eqs. (2.25), (2.26)

$$X \sim \omega_0 (E_J/E_c) e^{-2\sqrt{8E_J/E_c}} \quad (2.28)$$

is exponentially small in the same parameter $\sqrt{E_J/E_c} \gg 1$. Therefore, the two-minima approximation is valid even when $X \gg \Gamma$, as long as $\Gamma \ll E_c$. In this thesis I restrict myself to the case $X \ll \Gamma$, corresponding to incoherent QPS, which seems to be more realistic due to exponential smallness of X .

2.3.2 Several levels in one minimum

Now we can consider a more general case. The assumption is that the m -th energy level in the right minimum is close to the 0-th level in the left one. The non-zero elements of $\hat{\rho}$, which determine the voltage, are

$$\langle ln|\hat{\rho}|ln\rangle = \sigma_{nn} \text{ for } n \in [0, m], \quad \langle l0|\hat{\rho}|l+1, m\rangle = \sigma_{0m}, \quad \langle lm|\hat{\rho}|l-1, 0\rangle = \sigma_{m0}. \quad (2.29)$$

The Hamiltonian is

$$\langle ln|\hat{H}_0|l'n'\rangle = \delta_{ll'}\delta_{nn'}E_n^l + (\delta_{l',l+1}\delta_{n'm}\delta_{n0} + \delta_{l',l-1}\delta_{n'0}\delta_{nm})X. \quad (2.30)$$

The resulting equations of the stationary state are

$$\begin{cases} 0 = -i(X(\sigma_{00} - \sigma_{mm}) - \Delta E\sigma_{m0}) - \frac{1}{2}m\Gamma\sigma_{m0}, \\ 0 = -i(X(\sigma_{mm} - \sigma_{00}) + \Delta E\sigma_{0m}) - \frac{1}{2}m\Gamma\sigma_{0m}, \\ 0 = -i(X(\sigma_{m0} - \sigma_{0m})) + \Gamma\sigma_{11}, \\ 0 = -i(X(\sigma_{0m} - \sigma_{m0})) - m\Gamma\sigma_{mm}, \\ 0 = \Gamma((k+1)\sigma_{k+1,k+1} - k\sigma_{k,k}), \text{ for } 0 < k < m. \end{cases} \quad (2.31)$$

One can see from the last line in Eq. (2.31) that for the diagonal elements between 0 and m we have: $\rho_{k+1,k+1} = \frac{k}{k+1}\rho_{kk}$, then we can write

$$\rho_{kk} = \frac{m}{k}\sigma, \text{ for } 0 < k < m. \quad (2.32)$$

The first four lines of Eq. (2.31) give

$$\sigma = \frac{i\sigma_{m0}X}{\frac{1}{2}m\Gamma + i\Delta} = \sigma_{mm}. \quad (2.33)$$

As a result, we obtain

$$\sigma_{m0} = \sigma_{0m}^* = -\mathcal{N} \frac{iX(m\Gamma/2 + i\Delta E)}{m^2\Gamma^2/4 + \Delta E^2 + (mH_m + 1)X^2}, \quad (2.34)$$

$$\sigma = \mathcal{N} \frac{X^2}{m^2\Gamma^2/4 + \Delta E^2 + (mH_m + 1)X^2}, \quad (2.35)$$

$$\sigma_{00} = \mathcal{N} \frac{m^2\Gamma^2/4 + \Delta E^2 + X^2}{m^2\Gamma^2/4 + \Delta E^2 + (mH_m + 1)X^2}, \quad (2.36)$$

where $H_m = \sum_{n=1}^m 1/n$ is the harmonic number. We focus on $X \ll \Gamma$, then we have $\sigma_{00} \gg \sigma_{kk}$, for $k > 0$. As a result, we can neglect the tunneling between higher energy levels ($|l, k\rangle \rightarrow |l+1, k+m\rangle$), as their population is parametrically smaller.

Now we can calculate the average voltage $\langle V \rangle = \text{Tr} \{ \hat{V} \hat{\rho} \}$ the same way it was done for the effective two-level case. The voltage operator takes the form

$$\hat{V} = \frac{2\pi}{2e} iX \sum_l (|l, 0\rangle \langle l+1, m| - |l+1, m\rangle \langle l, 0|). \quad (2.37)$$

Then the average voltage forms a peak

$$\langle V \rangle = \frac{1}{2e} \frac{2\pi X^2 m \Gamma}{m^2\Gamma^2/4 + \Delta E^2 + (mH_m + 1)X^2}. \quad (2.38)$$

The resonant values of the current are given by $I(m) = \frac{em}{\pi} \omega_0$ (where m is integer). One can see that Eq. (2.24) gives just the first peak with $m = 1$. Moreover, qualitatively the result is valid even if we cannot use parabolic approximation for the potential (for levels with energy $E_m \sim E_J$), the resonant values of the current are $I(m) = \frac{e}{\pi} (E_m - E_0)$ instead of simple $I(m) = \frac{e}{\pi} m \omega_0$. The quantitative difference is in the tunneling matrix element X . Here we consider only energies $E_m \ll E_J$, corresponding to $m \ll E_J/\omega_0 = \sqrt{E_J/(8E_c)}$, which allows us to use parabolic approximation of the potential in the classically allowed regions to calculate X . The resulting matrix element is (see Appendix A)

$$X = \frac{\omega_0 \left(\sqrt{m+1/2} \right)^{m+1/2} e^{-S_m}}{\sqrt{2\pi m!} 2^{1/4}} e^{-\frac{m+1}{2}}, \quad (2.39)$$

with the tunneling action

$$S_m \approx \sqrt{\frac{8E_J}{E_c}} - \left(m + 1 + \ln \frac{E_J/E_c}{(2m+1)^{1/4}} \right) + O\left(\left(E_c/E_J\right)^{1/4}\right). \quad (2.40)$$

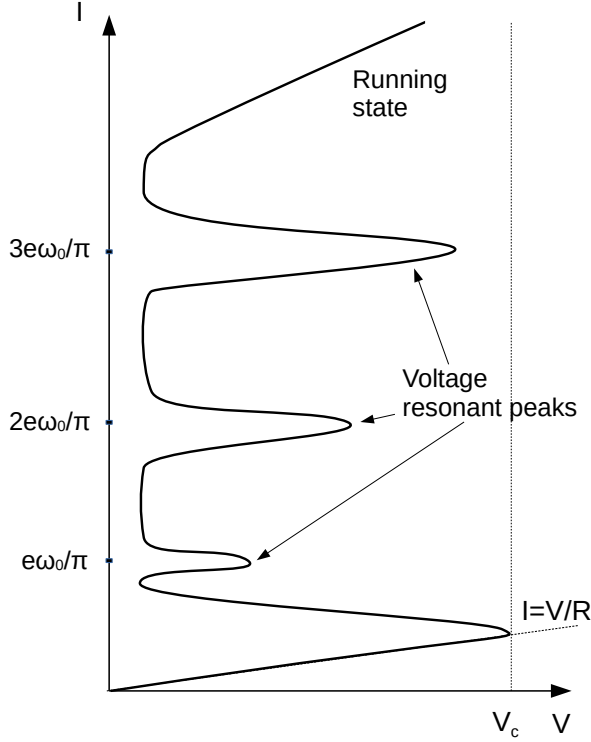


Figure 2.5: A schematic $I - V$ curve for an underdamped junction

One can see that Eq. (2.38) gives a set of Lorentzian peaks for the voltage, corresponding to resonant induced current values. A schematic $I - V$ curve and the form of voltage peaks, derived in harmonic approximation, is depicted in Fig.2.5. The $I - V$ curve consists of a linear part $V = IR$ at low induced currents up to a critical voltage supported by a junction $V_c = \frac{\pi}{e}\delta^{(0)}$, which corresponds to insulating state of the junction when all the current is flowing through the resistor (the so-called Bloch nose) [59, 60], voltage peaks at the resonant current values and running state regime at higher currents.

2.4 Possibility of experimental observation

The voltage peaks corresponding to resonant Zener tunneling in an underdamped Josephson junction have not been measured experimentally yet to the best of my knowledge.

One difficulty is that the underdamped regime of a single Josephson junction requires designing an environment with the impedance much higher than the resistance quantum $R_Q = (2\pi)/(2e)^2 = 6.45 \text{ k}\Omega$ at frequencies ω_0 of the order 10^{10} Hz with low stray capacitance. One of the first successful attempts is described in [70], where the authors used chromium resistors with resistance up to $250 \text{ k}\Omega$ located very close to the junction, which allowed to have impedance sufficiently higher than the resistance quantum at $\omega_0 \approx 5 \times 10^{11}$ Hz as well as low stray capacitance of the electrodes. Another efficient way to design high-impedance environment is with SQUID arrays, where the effective impedance can be controlled by applying a magnetic field perpendicular to the SQUID loops [71, 18], the highest achieved impedance is $50 \text{ M}\Omega$. This approach allowed the scientists to measure the low-current part of $I - V$ characteristics for a single Josephson junction in both overdamped and underdamped regimes, demonstrating charge-phase duality as the regimes resemble each other with the role of I and V interchanged.

The second difficulty is that the voltage, associated with the peaks is exponentially small. Indeed, to have voltage peaks, several energy levels in each potential minimum are required. For example, for one voltage peak there should be at least two energy levels in each minimum, $(3/2)\omega_0 \lesssim 2E_J - \omega_0$ (height of the tilted barrier), which corresponds to $E_J \gtrsim 8E_c$. Note that the voltage of the Bloch nose V_c is proportional to $\delta^{(0)} \propto e^{-\sqrt{8E_J/E_c}}$, while the resonant tunneling peaks are proportional to $X^2 \propto e^{-2\sqrt{8E_J/E_c}}$. For $R/R_Q \sim 10^3$, reported in experiments[18], these peaks are of the order of nanovolts or even smaller. Experimentally, one can detect voltages of the order of hundreds of nanovolts. Therefore, to reach a reliable conclusion about the possibility to observe resonant Zener tunneling peaks experimentally, one has to focus on E_J/E_c not too large and study the system beyond the harmonic approximation.

Chapter summary

In this chapter we studied QPS in a single Josephson junction. First we revisited the simple case of a junction without dissipation, when coherent QPSs result in a

band structure of the system spectrum. Then we discussed the effect of induced current, tilting the cosine potential, with dissipation through external resistance R . Two opposite limits of an overdamped ($R \ll R_Q$) and an underdamped ($R \gg R_Q$) junction are dual, as the $I - V$ characteristics are similar in these limits, but with role of voltage and current interchanged. We studied an underdamped junction with induced current I large enough to shift neighboring minima of the potential by the value, comparable to level spacing inside a minimum $I \gtrsim \frac{e}{\pi} \omega_0$. Near certain resonant values of induced current, $I(m) = \frac{e}{\pi} (E_m - E_0)$, the tunneling between the ground state in one minimum and the m -th excited state in the lower neighboring minimum, which is incoherent QPS, results in voltage peak as a function of current. We derived the form of a few first peaks, $m \ll \sqrt{E_J/(8E_c)}$, when the states inside each minimum can be approximated by the states of a harmonic oscillator with plasma frequency $\omega_p = \sqrt{8E_J E_c}$.

Chapter 3

Coherent quantum phase slips in Josephson junction chains (general relations)

3.1 Action for coherent QPS in a JJ chain

3.1.1 Euclidean action for a closed ring

We consider a chain of N Josephson junctions closed in a ring, pierced by a magnetic flux (Fig. 3.1). The superconducting islands are labelled by an integer n , the dynamical variables are the phases ϕ_n . The island $n = 0$ is identified with the island $n = N$, so that $\phi_0 = \phi_N$. Then the Hamiltonian is

$$H = \frac{1}{2} \sum_{n,m=0}^{N-1} (Q_n - q_n) \hat{C}_{n,m}^{-1} (Q_n - q_n) - \sum_{n=0}^{N-1} E_{J,n} \cos \left(\phi_{n+1} - \phi_n + \frac{\Phi}{N} \right). \quad (3.1)$$

Here Q_n is the excess charge on the island n , q_n is an external induced charge (usually induced by some random gate voltages) on the island n and \hat{C} is the capacitance matrix, defined as $\hat{C}_{nm} = (C_{g,n} + C_m + C_{m-1}) \delta_{n,m} - C_n \delta_{n+1,m} - C_{n-1} \delta_{n-1,m}$. $E_{J,n}$ and C_n are the Josephson energy and the capacitance of the junction between neighbouring islands n and $n+1$ respectively, while $C_{g,n}$ is the capacitance between island n and a nearby ground plane. Φ is the magnetic flux in units of the superconducting flux quantum divided by 2π (one flux quantum piercing the ring corresponds to $\Phi = 2\pi$).

The phases ϕ_n and the excess charges Q_n on the n th island are conjugate variables: $[\phi_n, Q_n] = 2ei$ (the electron charge is $-e$). Moreover, as the chain is closed,

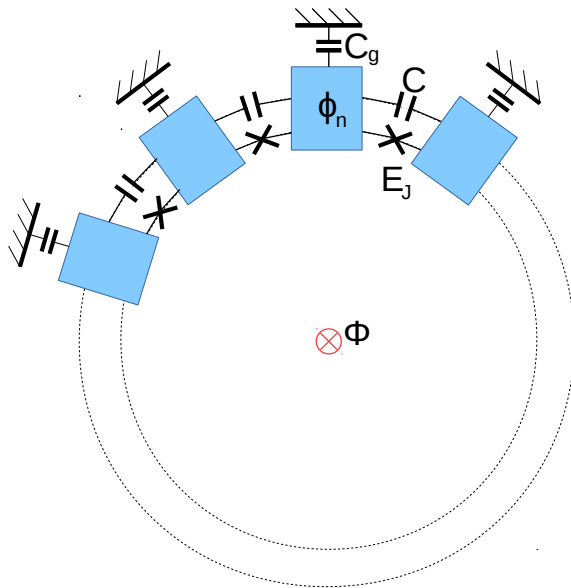


Figure 3.1: A schematic representation of a Josephson junction chain threaded by a magnetic flux Φ and containing N Josephson junctions.

the phases ϕ_n are compact variables. Since we are going to study quantum tunnelling of the superconducting phase ϕ_n in the quasiclassical limit, it is natural to pass to imaginary time τ and describe the system by its zero-temperature Euclidean action, [7]:

$$S = \int \sum_{n=0}^{N-1} \left[\frac{C_{g,n}}{8e^2} \dot{\phi}_n^2 + \frac{C_n}{8e^2} (\dot{\phi}_{n+1} - \dot{\phi}_n)^2 - i \frac{q_n}{2e} \dot{\phi}_n - E_{J,n} \cos \left(\phi_{n+1} - \phi_n + \frac{\Phi}{N} \right) \right] d\tau. \quad (3.2)$$

Here $\dot{\phi}_n \equiv d\phi_n/d\tau$. It is convenient to introduce energy scales corresponding to the capacitances:

$$E_{c,n} = \frac{e^2}{2C_n}, \quad E_{g,n} = \frac{e^2}{2C_{g,n}}. \quad (3.3)$$

Typically in experiments $C_{g,n} \ll C_n$ [50, 72, 73]. We assume that

$$E_J > \frac{32}{\pi^2} E_g \gg E_c, \quad (3.4)$$

which ensures that the phase slips are rare and the chain remains superconducting

for large N [13, 38, 33, 51].

In principle, the phase can slip on any of the N junctions; QPSs at different junctions contribute to the same quantum transition (i. e., with the same initial and final states), so the total QPS amplitude in a ring is a sum over the single QPSs on different chain junctions [32, 33]. Let us choose one of the junctions and study the corresponding amplitude. The term, containing the induced charges q_n , results in a total phase of a single QPS event [for details see Eq. (3.16) and the discussion around it]

$$\theta_n = \sum_{m=0}^n 2\pi \frac{q_m}{2e} + \text{const.} \quad (3.5)$$

Therefore, we can omit the terms containing the induced charges and restore them as the phases in each local QPS amplitude. It is also convenient to number the junctions so that the slipping junction is the one between the islands $n = N$ and $n = 0$, which we will call "boundary". Then, it is convenient to perform a gauge transformation,

$$\phi_n \rightarrow \phi_n - \frac{n}{N} \Phi, \quad (3.6)$$

which corresponds to twisted boundary conditions, $\phi_N = \phi_0 + \Phi$. Then the flux disappears from all cosine terms in Eq. (3.2), except the last one, which becomes $-E_J \cos(\phi_0 - \phi_{N-1} + \Phi)$. As a result, the action is written in the form:

$$S = \int \left(\sum_{n=0}^{N-1} \frac{1}{16} E_{g,n} \dot{\phi}_n^2 + \sum_{n=0}^{N-2} \left[\frac{1}{16} E_{c,n} (\dot{\phi}_{n+1} - \dot{\phi}_n)^2 - E_{J,n} \cos(\phi_{n+1} - \phi_n) \right] + \frac{1}{16} E_{c,N-1} (\dot{\phi}_0 - \dot{\phi}_{N-1})^2 - E_{J,N-1} \cos(\phi_{N-1} - \phi_0 - \Phi) \right) d\tau, \quad (3.7)$$

where the second line corresponds to the boundary junction where the actual tunneling occurs, while the first line contains the rest of the chain, where the phase readjustment takes place.

As we consider the chain to be long, $N \gg 1$, we suppose the phase differences on all the junctions except the slipping one to be small, $\max|\phi_{n+1} - \phi_n| \sim 1/\ell_s$ for $n < N-1$, where $\ell_s = \sqrt{C/C_g}$ is the screening length (typically, $\ell_s \gg 1$), so that we can expand the cosine terms. Then we can go to the continuum limit for the whole chain except the slipping junction. Namely, we take the limit $n \rightarrow x$, $\phi_n \rightarrow \phi(x)$, $\phi_{n+1} - \phi_n \rightarrow \partial\phi/\partial x$, $\sum_n \rightarrow \int dx$, and the action can be written as

$$\begin{aligned}
S = & \int d\tau \int_0^N dx \left[\frac{1}{16E_g(x)} \left(\frac{\partial\phi}{\partial\tau} \right)^2 + \frac{\ell_s^2}{16E_g(x)} \left(\frac{\partial^2\phi}{\partial x \partial\tau} \right)^2 + \frac{E_J(x)}{2} \left(\frac{\partial\phi}{\partial x} \right)^2 \right] + \\
& + \int \frac{d\tau}{16E_c(x)} \left[\frac{\partial\phi(N, \tau)}{\partial\tau} - \frac{\partial\phi(0, \tau)}{\partial\tau} \right]^2 - \int d\tau E_J(x) \cos[\phi(N, \tau) - \phi(0, \tau) - \Phi],
\end{aligned} \tag{3.8}$$

It is convenient to introduce plasma frequency $\omega_p = \sqrt{8E_J E_c}$, plasma velocity $v_p = \omega_p \ell_s = \sqrt{8E_J E_g}$ and dimensionless low-frequency admittance of the chain $g = \pi \sqrt{E_J / (8E_c)}$.

3.1.2 Classical phase configurations

In the quasiclassical limit, for each value of Φ there is a single static classical phase configuration, minimizing the potential energy. The exception is for Φ being an odd multiple of π , when there are two configurations with equal potential energies. Quantum tunnelling between these degenerate configurations is the main subject of our study. As the dependence of action (3.8) on Φ is periodic, we can focus on $\Phi = \pi$ without loss of generality.

Let us find the classical phase configurations taking into account the spatial dependence $E_J(x)$. Minimization of the bulk action leads to the equation

$$\frac{\partial}{\partial x} \frac{\partial \mathcal{L}}{\partial \phi} = \frac{\partial}{\partial x} E_J \frac{\partial \phi}{\partial x} = 0, \tag{3.9}$$

which is nothing but the current conservation. Its solution contains two integration constants, ϕ_0 and ϑ :

$$\phi(x) = \phi_0 + \vartheta \frac{\int_0^x E_J^{-1}(x') dx'}{\int_0^N E_J^{-1}(x') dx'}. \tag{3.10}$$

The constant ϑ should be found by minimizing the total potential energy including the boundary term [52]:

$$\frac{\partial}{\partial \vartheta} \left[\frac{\vartheta^2/2}{\int_0^N E_J^{-1}(x) dx} - E_J \cos(\vartheta - \Phi) \right] = 0. \tag{3.11}$$

For a homogeneous chain it is just [52] (see Fig. (3.4))

$$\frac{\vartheta}{N} + \sin(\vartheta - \Phi) = 0. \tag{3.12}$$

We consider a long chain $N \gg 1$, then $\vartheta \approx \Phi + 2\pi m$ with any integer m gives a local minimum (half-integer values of m give local maxima) with the potential energy $(\Phi + 2\pi m)^2 E_J / (2N)$. If $\Phi = \pi$, then the two configurations with $\vartheta = \pi$ and $\vartheta = -\pi$ have the same energies.

The observable quantities are the flux-dependent ground state energy $\mathcal{E}_0(\Phi)$, or the persistent current $I_0(\Phi) \propto \partial \mathcal{E}_0 / \partial \Phi$. In the zero approximation, one can associate $\mathcal{E}_0(\Phi)$ with the static potential energy, discussed above. Then, $I_0(\Phi)$ has a discontinuous sawtooth-like dependence on Φ , as schematically shown on Fig. 3.2. Quantum tunneling results in energy splitting between the degenerate configurations when Φ is close to an odd multiple of π , which is measurable [35, 44]. Also, the sawtooth in $I_0(\Phi)$ is smoothed. A spatial modulation of the chain parameters modifies the quantum tunneling amplitude, together with the energy splitting and the smoothing of the sawtooth in $I_0(\Phi)$.

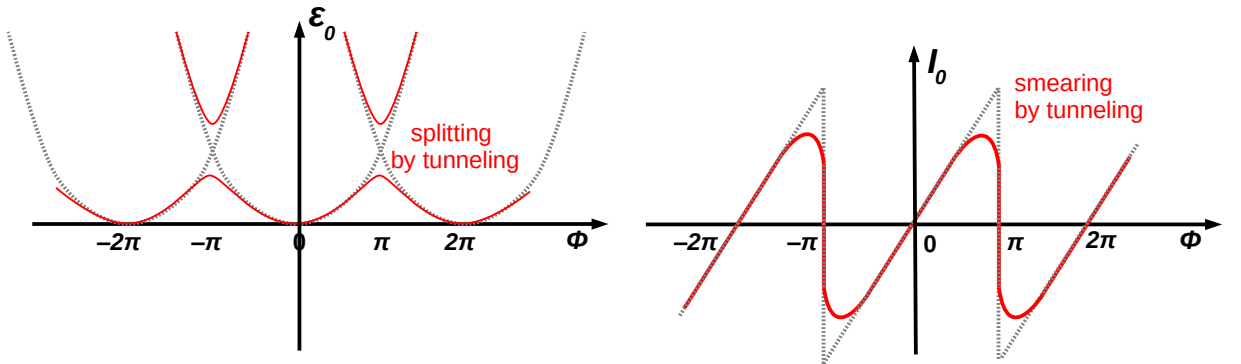


Figure 3.2: Flux dependence of the ground state energy (upper panel) and persistent current (lower panel), shown schematically in the purely classical approximation (grey dashed line) and taking into account quantum tunneling (red solid line).

The second integration constant ϕ_0 in Eq. (3.10) cannot be found from energetic considerations, as the energy does not depend on the global phase. This does not mean, however, that ϕ_0 can be simply dropped from the consideration. Because of the degeneracy with respect to ϕ_0 , each of the found energy minima is a circle rather than a point in the configuration space. The system eigenstates can be classified by the conjugate variable, which is the conserved total charge $\sum_n Q_n$ (the number of Cooper pairs). To estimate the tunnel splitting in the sector with zero excess charge $\sum_n Q_n = 0$, we can assume that the system starts from some point on the $\vartheta = \pi$ circle, which can be taken $\phi_0 = 0$ without loss of generality, and then sum the amplitudes of tunnelling towards different points of the $\vartheta = -\pi$ circle. For a spatially homogeneous chain, symmetry considerations fix the dominant destination

at $\vartheta = -\pi$ to be $\phi_0 = \pi$ [52]. In the inhomogeneous case, it should be determined by the classical trajectory.

As we mentioned before [Eq. (3.5)], the induced charges q_n result in a phase factor for the partial tunneling amplitude corresponding to each QPS trajectory. Consider a trajectory going from the initial phase configuration

$$\phi_n = \phi_i + \pi f_n \quad (3.13)$$

to the final phase configuration

$$\phi_n = \phi_f^{(m)} - \pi f_n + \begin{cases} 0, & n \leq m, \\ 2\pi, & n > m, \end{cases} \quad (3.14)$$

where

$$f_n = \frac{\sum_0^{n-1} E_{J,n'}^{-1}}{\sum_0^{N-1} E_{J,n'}^{-1}} \quad (3.15)$$

is the discrete version of the function appearing in Eq. (3.10), ϕ_i is the arbitrary starting position on the $\vartheta = \pi$ circle, $\phi_f^{(m)}$ is the final position on the $\vartheta = -\pi$ circle (see Fig. 3.3), determined by the classical trajectory involving the phase slip on the junction between islands m and $m + 1$. The phase accumulated on this classical trajectory is given by

$$\text{Im } S_{cl} = \sum_{n=0}^{N-1} \left(\phi_i - \phi_f^{(m)} \right) \frac{q_n}{2e} - 2\pi \sum_{n=0}^{N-1} f_n \frac{q_n}{2e} - 2\pi \sum_{n=0}^{N-1} \frac{q_n}{2e} + 2\pi \sum_{n=0}^m \frac{q_n}{2e}. \quad (3.16)$$

In fact, the first term in this expression should be dropped, since it is an artefact of the quasiclassical approximation. Indeed, a straightforward construction of the WKB wave function on the $\vartheta = -\pi$ circle at the energy of potential minimum would give $\Psi_0(\phi_f) \propto \exp \left[-i\phi_f \sum_{n=0}^{N-1} q_n / (2e) \right]$, since the WKB approximation does not contain the periodic boundary conditions $\Psi(\phi_f) = \Psi(\phi_f + 2\pi)$. That is, the instanton calculation describes tunneling from the initial state $\Psi_0(\phi_i)$ to the final state $\Psi_0(\phi_f)$, and this is the origin of the first term in Eq. (3.16). However, since we focus on the sector with the total charge $\sum_n Q_n = 0$, the wave functions of the initial and the final states are uniformly spread over the corresponding circles (invariant under a constant shift of all ϕ_n). Therefore, ϕ_i and $\phi_f^{(m)}$ do not contribute to the phase factor. Omitting the m -independent terms, we arrive at Eq. (3.5).

The energy splitting due to the tunneling is proportional to the QPS amplitude. The total amplitude for the QPS in the chain is a sum of QPS amplitudes over all

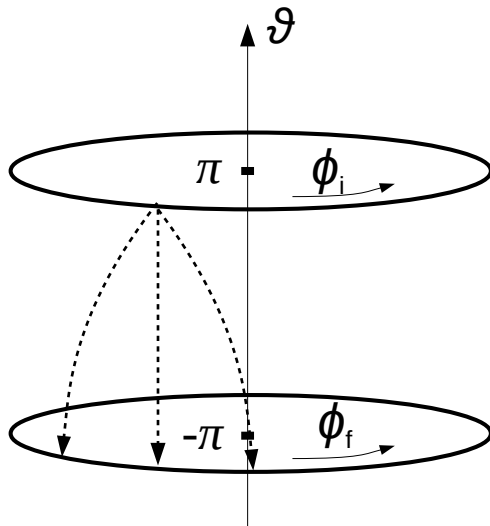


Figure 3.3: Classical trajectories between ϕ_i and $\phi_f^{(m)}$ with different m on $\vartheta = \pi$ and $\vartheta = -\pi$ circles respectively.

chain junctions:

$$W = \sum_{n=0}^{N-1} W_n = \sum_{n=0}^{N-1} \Omega_n e^{-S_n + i\theta_n}. \quad (3.17)$$

Here S_n is the classical action for a phase slip, occurring on a junction n , θ_n is the phase, determined by Eq. (3.5), Ω_n is the pre-exponent, determined by integrating over quadratic fluctuations in the vicinity of the classical trajectory. One can see (Fig. 3.2) that in case of high energy splitting, the lowest energy level is almost constant as a function of magnetic flux, and the persistent current is suppressed, which corresponds to suppression of superconductivity due to QPSs.

Here it is important to mention that in a homogeneous chain due to the fact that the system Hamiltonian is invariant under the circular permutation of the islands, the angular momentum is conserved. Normally we have a zero total charge due to electroneutrality, resulting in zero angular momentum, therefore QPSs are possible as they do not violate this conservation law. However, if the total charge is nonzero (and not $2eNm$, where m is integer), the QPSs do not occur as the classically degenerate states have different angular momenta. This can also be seen

from summing the QPS amplitudes over all the junctions, which will have phase factors due to the nonzero charge, resulting in zero total amplitude [32].

3.1.3 The QPS action on a classical trajectory

The main contribution to the tunnelling amplitude comes from the vicinity of the classical imaginary-time trajectory, connecting the two minima, which satisfies the Lagrange equations of motion in the imaginary time. Following the discussion of Ref. [52] for a spatially homogeneous ring, we schematically show the corresponding configuration space trajectory $\phi(x, \tau)$ in Fig. 3.4.

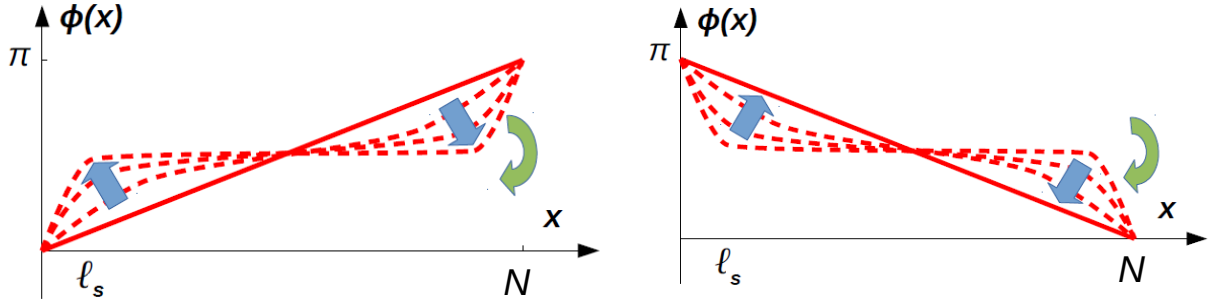


Figure 3.4: A schematic representation of the classical trajectory $\phi(x, \tau)$ going from the static configuration with $\vartheta = \pi$ (solid line on upper panel) to $\vartheta = -\pi$ (solid line on the lower panel) for a spatially homogeneous ring. Straight arrows correspond to the slow adjustment of the phase in the whole ring, the round arrows show the fast flip of the phase in the vicinity of the slipping junction.

The trajectory consists of several stages. (i) Slow flattening of the phase profile in the whole chain on the time scales which are linked to the spatial scales as $\tau \sim x/v_p$, except the vicinity of the boundary junction. This vicinity is characterized by a certain length scale ℓ_* to be determined later. (ii) Flattening of the phase in the vicinity on the time scale $\sim \ell_*/v_p$. (iii) Fast phase flip on the boundary junction, which may occur on the same time scale $\sim \ell_*/v_p$ or a faster one, depending on the parameters. (iv), (v) Phase readjustment in the vicinity and outside to the new classical configuration on the same time scales as (ii) and (i), respectively.

As the phase differences on all the junctions except the slipping one are small, we can expand the cosine terms in the first line of the action (3.7). Then we can

write this harmonic part of the action as

$$S_{harm} = \int \frac{d\omega}{2\pi} \sum_{n,m=0}^{N-1} \frac{|\omega|}{2(2e)^2} \phi_n^*(\omega) Y_{n,m}(i|\omega|) \phi_m(\omega), \quad (3.18)$$

where the admittance matrix of the chain \hat{Y} is defined by the relation

$$\mathbf{I} = \hat{Y}\mathbf{V}. \quad (3.19)$$

Here $\mathbf{V}^T = (V_0, V_1, \dots, V_{N-1})$ and $\mathbf{I}^T = (I_0, I_1, \dots, I_{N-1})$, corresponds to the voltages on the islands $V_n(\omega) = \frac{i\omega}{2e}\phi_n$ and incoming currents, respectively. In the harmonic approximation the non-zero elements of \hat{Y} are

$$Y_{n,n} = \omega C_g + 2\frac{(2e)^2}{\omega} E_J, \quad (3.20)$$

$$Y_{n+1,n} = Y_{n,n+1} = \omega C - 2\frac{(2e)^2}{\omega} E_J. \quad (3.21)$$

Eq. (3.19) represents a linear system of equations, which are nothing else then Kirchhoff's laws for each node n of the circuit. The remaining part can be written as

$$S_{core} = \int \frac{d\omega}{2\pi} \frac{\omega^2}{2(2e)^2} \phi_0(\omega) C \phi_{N-1}(\omega) - \int d\tau E_J \cos(\phi_0(\tau) - \phi_{N-1}(\tau) + \Phi) \quad (3.22)$$

We perform a change of variables, so that we can integrate out $N - 1$ variables in which the action is quadratic:

$$\vartheta = \phi_{N-1} - \phi_0, \quad \varphi_0 = \frac{E_{g,N-1}\phi_{N-1} + E_{g,0}\phi_0}{E_{g,N-1} + E_{g,0}}. \quad (3.23)$$

As a result, we have a variable ϑ , which corresponds to the phase difference on the slipping junction, and φ_0 , which is the average of the phase on this junction and decoupled from ϑ in the action, therefore, can be seen as one of the phases, corresponding to the harmonic modes, along with $\phi_1, \phi_2, \dots, \phi_{N-2}$. To integrate out the harmonic modes we can write the partition function in a path-integral formalism:

$$\mathcal{Z} = \int \prod_{n=0}^{N-1} \mathcal{D}\phi_n e^{-S}. \quad (3.24)$$

As a result, applying the variable change, we can do Gaussian integration over the harmonic modes, whose result contains matrix elements of the impedance matrix,

which is just the inverse of the admittance matrix $\hat{Z} = \hat{Y}^{-1}$

$$\int \prod_{n=1}^{N-2} \mathcal{D}\phi_n \mathcal{D}\varphi_0 \mathcal{D}\vartheta e^{-S} \propto \int \mathcal{D}\vartheta \exp(-S_{eff}[\vartheta]), \quad (3.25)$$

where the effective action takes the form

$$\begin{aligned} S_{eff}[\vartheta] &= \frac{1}{2} \int \frac{d\omega}{2\pi} \left[\frac{|\omega|}{(2e)^2 Z(i|\omega|)} + \frac{\omega^2 C}{(2e)^2} \right] |\vartheta(\omega)|^2 + \int d\tau E_J [1 - \cos(\vartheta(\tau) - \Phi)] \\ &\equiv \frac{1}{2} \int d\tau d\tau' K(\tau - \tau') \vartheta(\tau) \vartheta(\tau') + \int d\tau E_J [1 - \cos(\vartheta(\tau) - \Phi)]. \end{aligned} \quad (3.26)$$

Here $K(\tau - \tau')$ is the Fourier transform of

$$K(\omega) = \frac{|\omega|}{4e^2 Z(i|\omega|)} + \frac{\omega^2}{8E_c}, \quad K(\tau - \tau') = \int \frac{d\omega}{2\pi} K(\omega) e^{-i\omega(\tau - \tau')}. \quad (3.27)$$

The classical imaginary-time trajectory for ϑ satisfies the equation:

$$\int K(\tau - \tau') \vartheta(\tau') d\tau' = E_J \sin \vartheta(\tau). \quad (3.28)$$

3.1.4 Normal modes, chain impedance

To derive the expression for the impedance Z introduced in the previous section, we only need to solve the linear equations of motion, following from Eq. (3.2) in the harmonic approximation. To deal with the dynamics described by the quadratic Lagrangian density of action (3.8),

$$\mathcal{L} = \frac{1}{16E_g} \left(\frac{\partial \phi}{\partial \tau} \right)^2 + \frac{\ell_s^2}{16E_g} \left(\frac{\partial^2 \phi}{\partial x \partial \tau} \right)^2 + \frac{E_J}{2} \left(\frac{\partial \phi}{\partial x} \right)^2, \quad (3.29)$$

it is convenient to decompose the phase field $\phi(x)$ into the normal modes. Namely, we write down the Euler-Lagrange equations of motion and look for the solutions in the form $\phi(x, \tau) = \Psi(x) e^{\pm i\omega\tau}$ (since τ is the imaginary time). This gives the following equation for the normal mode wave functions:

$$\frac{\omega^2}{8E_g} \Psi - \omega^2 \frac{\partial}{\partial x} \frac{\ell_s^2}{8E_g} \frac{\partial \Psi}{\partial x} + \frac{\partial}{\partial x} E_J \frac{\partial \Psi}{\partial x} = 0, \quad (3.30)$$

with the Dirichlet boundary conditions, $\Psi(0) = \Psi(N) = 0$ at $x = 0, N$.

For a spatially homogeneous chain, the solutions are plane waves, $\Psi(x) \propto \sin kx$,

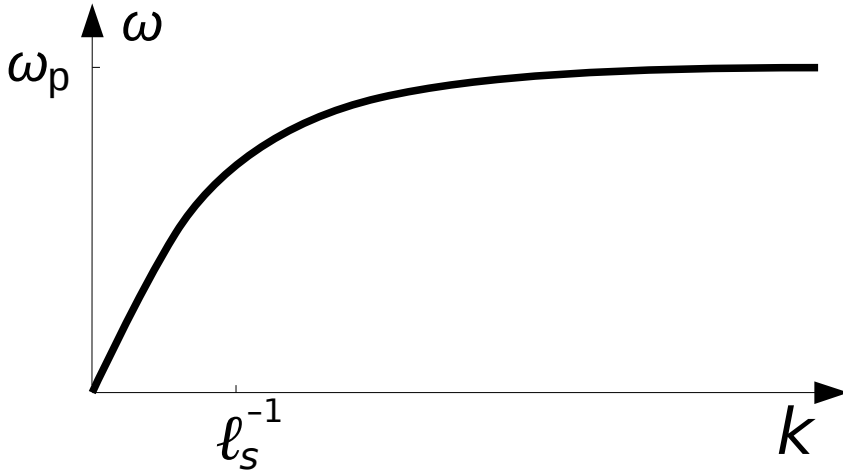


Figure 3.5: The dispersion curve of the phase oscillations (plasmons, Mooij-Schön modes), determined by Eq. (3.31)

for which Eq. (3.30) gives the dispersion relation [49, 50]:

$$\omega(k) = \frac{\omega_p |k| \ell_s}{\sqrt{1 + k^2 \ell_s^2}}. \quad (3.31)$$

The plasma frequency can be expressed through the continuum limit parameters: $\omega_p = v_p / \ell_s$, where $v_p = \sqrt{8E_g E_J}$ is the plasma velocity. At small $|k| \ll 1/\ell_s$ the dispersion is linear, $\omega \approx v_{pl} |k|$. These harmonic modes with linear dispersion are in fact the Goldstone modes, the collective excitations due to spontaneous symmetry breaking.

It is convenient to characterize the chain by its low-frequency impedance in the units of superconducting conductance quantum $(2e)^2/(\pi\hbar)$ (we momentarily restore \hbar), or its inverse, the dimensionless admittance:

$$g \equiv \sqrt{\frac{\pi^2 E_J}{8 E_g}}. \quad (3.32)$$

In the following we assume $g > 2$, otherwise the chain would be in the insulating rather than the superconducting state [13, 37, 38].

Now we need to express the impedance of a general inhomogeneous chain through the normal modes of the chain, determined by wave equation (3.30). The voltage V is related to the phase by $V = i\omega\phi/(2e)$, and the currents injected at the ends

$x = 0, N$, are given by

$$I_0 = 2e \left(\omega^2 \frac{\ell_s^2}{8E_g} - E_J \right) \frac{\partial \phi}{\partial x} \Big|_{x=0}, \quad I_N = -2e \left(\omega^2 \frac{\ell_s^2}{8E_g} - E_J \right) \frac{\partial \phi}{\partial x} \Big|_{x=N} \quad (3.33)$$

Eq. (3.30) defines the scalar product of two arbitrary functions $f_1(x)$ and $f_2(x)$ as

$$\overline{(f_1, f_2)} \equiv \frac{1}{\mathcal{T}_c} \int_0^N \frac{dx}{8E_g(x)} \left[f_1(x)f_2(x) + \ell_s^2 \frac{df_1(x)}{dx} \frac{df_2(x)}{dx} \right], \quad \mathcal{T}_c \equiv \int_0^N \frac{dx}{8E_g(x)}. \quad (3.34)$$

Let us perform a change of variables similarly to Ref. [51]:

$$\phi(x, \tau) = \vartheta(\tau) X(x) + \phi_0(\tau) + \sum_{\alpha=1}^{\infty} \phi_\alpha(\tau) \Psi_\alpha(x), \quad (3.35)$$

where we denoted

$$X(x) \equiv \frac{\int_0^x E_J^{-1}(x') dx'}{\int_0^L E_J^{-1}(x') dx'} - \frac{1}{\mathcal{T}_c} \int_0^N \frac{dx}{8E_g(x)} \frac{\int_0^x E_J^{-1}(x') dx'}{\int_0^L E_J^{-1}(x') dx'}, \quad (3.36)$$

and $\Psi_\alpha(x)$ are the eigenfunctions of Eq. (3.30). Since $\phi_0(\tau)$ and $\vartheta(\tau)$ take care of the uniform phase shift and the phase jump between $x = 0$ and $x = N$, respectively, $\Psi_\alpha(x)$ can be chosen to satisfy the Dirichlet boundary conditions, $\Psi_\alpha(0) = \Psi_\alpha(N) = 0$. They are orthogonal, with the respect to scalar product (3.34)

$$\overline{(\Psi_\alpha, \Psi_\beta)} = \delta_{\alpha\beta}. \quad (3.37)$$

The constant offset in Eq. (3.36) is chosen specifically to yield $\overline{(1, X)} = 0$. Substituting our expression for the phase in terms of normal modes, Eq. (3.35), into the wave equation (3.30), multiplying by $\Psi_{\alpha>0}$, 1 and X , and integrating over x , we obtain

$$\begin{aligned} \omega^2 \overline{(\Psi_\alpha, X)} \vartheta + \omega^2 \overline{(\Psi_\alpha, 1)} \phi_0 + (\omega^2 - \omega_\alpha^2) \phi_\alpha &= 0, \\ \omega^2 \mathcal{T}_c \phi_0 + \omega^2 \mathcal{T}_c \sum_{\alpha=1}^{\infty} \overline{(1, \Psi_\alpha)} \phi_\alpha &= -\frac{I_0 + I_N}{2e}, \\ \omega^2 \mathcal{T}_c \overline{(X, X)} \vartheta + \omega^2 \mathcal{T}_c \overline{(\Psi_\alpha, X)} \phi_\alpha + \frac{X(0) - X(N)}{\int_0^N E_J^{-1}(x') dx'} \vartheta &= -\frac{X(0)I_0 + X(N)I_N}{2e}. \end{aligned} \quad (3.38)$$

Let $I_0 = -I_N = I$, then we eliminate ϕ_0 and ϕ_α from Eqs. (3.38) and find

$$V(0) - V(N) = -\frac{i\omega}{2e}\vartheta \equiv Z(\omega)I, \quad (3.39)$$

resulting in

$$-\frac{i\omega}{(2e)^2}\frac{1}{Z(\omega)} = \omega^2 \left[G_{XX}(\omega) - \frac{G_{X1}(\omega)G_{1X}(\omega)}{G_{11}(\omega)} \right] - \frac{1}{\int_0^N E_J^{-1}(x') dx'}, \quad (3.40)$$

where the Green's functions are defined as

$$G_{f_1 f_2}(\omega) \equiv \mathcal{T}_c \left[\sum_\alpha \frac{\omega_\alpha^2}{\omega^2 + \omega_\alpha^2} \overline{(f_1, \Psi_\alpha)} \overline{(f_2, \Psi_\alpha)} - \sum_\alpha \overline{(f_1, \Psi_\alpha)} \overline{(f_2, \Psi_\alpha)} + \overline{(f_1, f_2)} \right], \quad (3.41)$$

for arbitrary $f_1(x)$, $f_2(x)$. (Note that the last two terms do not necessarily cancel each other: while the functions $\Psi_\alpha(x)$ form a complete set in the space of functions with Dirichlet boundary conditions, both 1 and $X(x)$ do not belong to this space). Eqs. (3.40), (3.41) determine the impedance of an inhomogeneous chain, which enters the effective action, Eq. (3.26).

3.2 QPS amplitude for a homogeneous chain

3.2.1 Classical trajectory

In this section we show how the general calculation scheme, presented above, works for the case of spatially homogeneous chains, for which the results are known [51, 52, 53]. For a spatially homogeneous chain, $K(\omega)$ can be calculated exactly. We have

$$\begin{aligned} \Psi_\alpha(x) &= \sqrt{\frac{2}{1 + k_\alpha^2 \ell_s^2}} \sin k_\alpha x, \quad k_\alpha = \frac{\pi\alpha}{N}, \\ X(x) &= \frac{x}{N} - \frac{1}{2}, \quad \overline{(X, \Psi_\alpha)} = -\sqrt{\frac{2}{1 + k_\alpha^2 \ell_s^2}} \frac{1 + (-1)^\alpha}{2\pi\alpha}, \\ \overline{(X, X)} - \sum_\alpha \overline{(X, \Psi_\alpha)}^2 &= \sum_{n=-\infty}^{\infty} \frac{\ell_s^2/N^2}{1 + (2\pi n \ell_s/N)^2} = \frac{\ell_s}{2N} \coth \frac{N}{2\ell_s}. \end{aligned}$$

Now we evaluate the sum over α in Eq. (3.41) for G_{XX} (G_{1X} vanishes by parity):

$$K(\omega) = \frac{\omega^2}{8E_c} + \frac{\ell_s \omega^2}{16E_g} \sqrt{1 + \frac{\omega_p^2}{\omega^2}} \coth \frac{N}{2\ell_s} \sqrt{\frac{\omega^2}{\omega^2 + \omega_p^2}} - \frac{E_J}{N}. \quad (3.42)$$

We will mostly work with the $N \rightarrow \infty$ limit of this expression [38]

$$K(\omega) = \frac{\omega^2}{8E_c} + \frac{\ell_s \omega^2}{16E_g} \sqrt{1 + \frac{\omega_p^2}{\omega^2}}, \quad (3.43)$$

whose low- and high-frequency asymptotics are

$$K(\omega \ll \omega_K) = \sqrt{\frac{E_J}{8E_g}} \frac{|\omega|}{2}, \quad (3.44a)$$

$$K(\omega \gg \omega_K) = \left(\frac{1}{8E_c} + \frac{\ell_s}{16E_g} \right) \omega^2, \quad (3.44b)$$

$$\omega_K \equiv \frac{\sqrt{8E_J E_g}}{E_g/E_c + \ell_s/2} \approx \frac{\omega_p}{\ell_s}. \quad (3.44c)$$

It is convenient to introduce new length scale $\ell_c \equiv \frac{E_g}{E_c} + \ell_s/2$, which in our limit $\ell_s \gg 1$ tends to $\ell_c \approx \ell_s^2$. We start with the function

$$\vartheta(\tau) = -2 \arctan \sinh \frac{\tau}{\tau_s}, \quad \tau_s \equiv \sqrt{\frac{1}{E_J} \left(\frac{1}{8E_c} + \frac{\ell_s}{16E_g} \right)} \approx \omega_p^{-1}, \quad (3.45)$$

whose Fourier transform is

$$\vartheta(\omega) = \frac{2\pi}{i\omega \cosh(\pi\omega\tau_s/2)}. \quad (3.46)$$

This function is the exact solution of Eq. (3.28) with the kernel (3.44b), which then describes a usual pendulum. The condition $\ell_s \gg 1$ ensures that $1/\tau_s \gg \omega_K$, so expression (3.46) is valid everywhere except the narrow frequency range $|\omega| \lesssim \omega_K$. Indeed, the low-frequency expansion of Eq. (3.46) is

$$\vartheta(\omega) = \frac{2\pi}{i\omega} \left[1 - \frac{\pi^2}{8} \omega^2 \tau_s^2 + O(\omega^4 \tau_s^4) \right], \quad (3.47)$$

while for the low frequencies we expect it to contain a term proportional to $|\omega|$. Therefore, we have to study the low-frequency region in more detail. Indeed, we suppose that there should be $|\omega|$ term corresponding to the fact that the trajectory

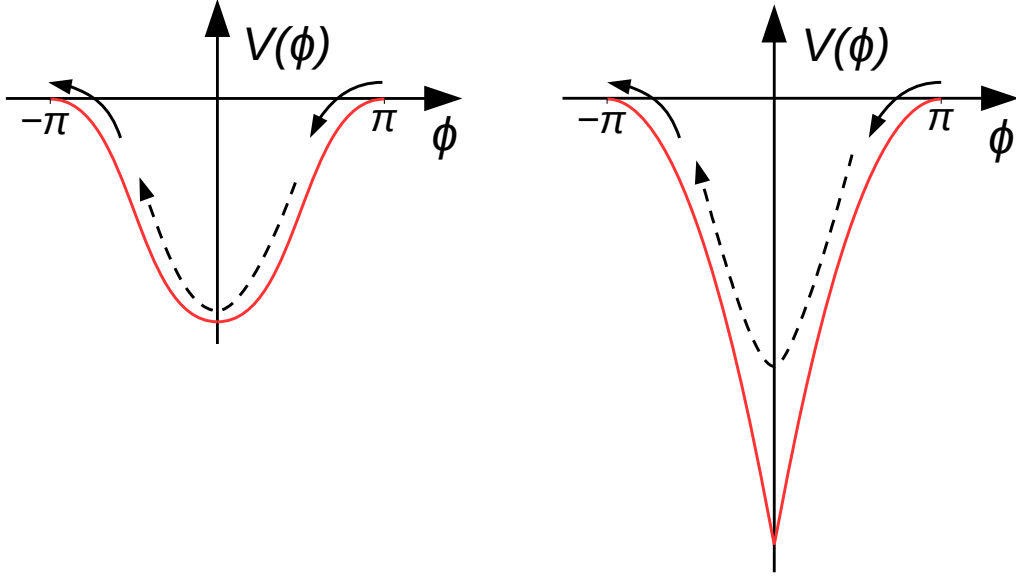


Figure 3.6: The two potentials, $V(\phi) = -E_J(1 + \cos \phi)$ (left panel) and $V(\phi) = -E_J(|\phi| - \pi)^2/2$ (right panel), for which the slow part of the instanton trajectory (solid arrows) should be similar.

$\vartheta(\tau)$ very slowly reaches its limiting values $\pm\pi$, which is due to coupling with the slow Ohmic modes of the chain.

To analyze the slow part of the trajectory $\vartheta(\tau)$, we note that it is mostly determined by the motion near the maxima of the potential at $\vartheta = \pm\pi$. Thus, if one replaces the potential

$$V(\phi) = -E_J(1 + \cos \phi) \quad \rightarrow \quad V(\phi) = -E_J \frac{(|\phi| - \pi)^2}{2},$$

the low-frequency part of the trajectory at $|\omega| \ll 1/\tau_s$ should remain similar. Then we have

$$\int K(\tau - \tau') \vartheta(\tau') d\tau' = E_J [\pi - |\vartheta(\tau)|] \text{sign } \vartheta(\tau). \quad (3.48)$$

This is still a non-linear equation. However, if one introduces a new variable

$$\tilde{\vartheta}(\tau) = \vartheta(\tau) + \pi \text{sign } \tau, \quad (3.49)$$

and uses the fact that $\text{sign } \vartheta(\tau) = -\text{sign } \tau$, it is easy to see that $\tilde{\vartheta}$ satisfies a linear equation which is most easily written in the Fourier space

$$K(\omega) \left[\tilde{\vartheta}(\omega) + \frac{2\pi}{i\omega} \right] = -E_J \tilde{\vartheta}(\omega), \quad (3.50)$$

and gives

$$\vartheta(\omega) = \frac{2\pi}{i\omega} \frac{1}{1 + K(\omega)/E_J}. \quad (3.51)$$

This expression has the required $|\omega|$ term at low frequencies, but if one expands this expression in the powers of $K/E_J \sim \omega^2\tau_s^2 \ll 1$, the $\omega^2\tau_s^2$ term already does not match the expansion of $\cosh(\pi\omega\tau_s/2)$. However, Eq. (3.51) shows that the relative error of the expression (3.46) is $\sim |\omega|\omega_p\ell_s/(8E_JE_g)$, so the relative error in the action evaluated on the trajectory (3.46) will be of the order of $\omega_p\ell_s/(8E_JE_g\tau_s) \sim 1/\ell_s \ll 1$.

To evaluate the action on the trajectory (3.46), we represent $1/\cosh^2 = 1 - \tanh^2$ and notice that in the term with \tanh^2 the limit $N \rightarrow \infty$ can be taken directly:

$$\begin{aligned} S_{\text{cl}} &= \int_{-\infty}^{\infty} \left[\frac{1}{8E_c} + \frac{\ell_s}{16E_g} \sqrt{1 + \frac{\omega_p^2}{\omega^2}} \coth \frac{N}{2\ell_s} \sqrt{\frac{\omega^2}{\omega^2 + \omega_p^2}} - \frac{E_J}{N\omega^2} \right] \frac{\pi d\omega}{\cosh^2(\pi\omega\tau_s/2)} + 4E_J\tau_s \\ &= \int_{-\infty}^{\infty} \left[\frac{\ell_s}{16E_g} \sqrt{1 + \frac{\omega_p^2}{\omega^2}} \coth \frac{N}{2\ell_s} \sqrt{\frac{\omega^2}{\omega^2 + \omega_p^2}} - \frac{\ell_s}{16E_g} \frac{2\ell_s}{N} \frac{\omega_p^2}{\omega^2} - \frac{\ell_s}{16E_g} \right] \frac{\pi d\omega}{\cosh^2(\pi\omega\tau_s/2)} \\ &\quad + 8E_J\tau_s \\ &= g \int_0^{\infty} \left[\sqrt{\frac{4\ell_s^2}{N^2} + \frac{1}{u^2}} \coth u - \frac{1}{u^2} - \frac{2\ell_s}{N} \right] du \\ &\quad - g \int_0^{\infty} \left(\sqrt{1 + \frac{1}{u^2}} - 1 \right) \tanh^2 \frac{\pi\omega_p\tau_s u}{2} du + 8E_J\tau_s. \end{aligned}$$

The first integral converges, as for small u the integrand tends to $1 - 2\ell_s/N + 2\ell_s^2/N^2 + O(u)$, for $1 \ll u \ll N/\ell_s$ it tends to $1/u$, resulting in the logarithm, while for large $u \gg N/\ell_s$ it tends to $(N/(4\ell_s) - 1)/u^2 + O(1/u^4)$. It evaluates to $\ln(N/\ell_s) + c_2 + O(\ell_s/N)$ where the constant $c_2 = -1.567514\dots$. The second integral also converges, for small u the integrand tends to $(\pi\omega_p\tau_s/2)^2 u + O(u^2)$, while for large u it tends to $1/(2u^2) + O(1/u^4)$. Thus, we can write

$$\frac{S_{\text{cl}}}{g} = \frac{8}{\pi} \sqrt{\ell_c} + \ln \frac{N}{\ell_s + \sqrt{\ell_c}} - \Upsilon \left(\frac{\sqrt{\ell_c}}{\ell_s} \right), \quad (3.52a)$$

$$\Upsilon(z) \equiv \int_0^{\infty} \left(\sqrt{1 + \frac{1}{u^2}} - 1 \right) \tanh^2 \frac{\pi z u}{2} du - c_2 - \ln(1 + z). \quad (3.52b)$$

We can define $\Upsilon(z)$ as a monotonic bounded function, as we have extracted $\ln \left(1 + \frac{\sqrt{\ell_c}}{\ell_s} \right)$

from it:

$$1.567514\dots = \Upsilon(0) \leq \Upsilon(z) < \Upsilon(\infty) = 1.922\dots$$

Here one can see that the length $l_* = l_s + \sqrt{\ell_c}$ is determining the vicinity of the slipping junction.

And as we neglect the correction of the order $1/l_s$ we can rewrite the action on the classical trajectory as

$$\frac{S_{\text{cl}}}{g} = \frac{8}{\pi} l_s + \ln \frac{N}{2l_s} - \Upsilon(1) \approx \frac{8}{\pi} l_s + \ln \frac{N}{2l_s} - 1.74126\dots \quad (3.53)$$

The characteristic length scale for the QPS is $l_* \approx 2l_s$.

3.2.2 Pre-exponent

As discussed in Refs. [74, 75], the tunnelling matrix element W between two neighboring minima can be represented as

$$W_n = \sqrt{\frac{\Lambda_{j=0}^{(0)}}{2\pi\tau_*} \prod_{j>0} \frac{\Lambda_j^{(0)}}{\Lambda_j}} e^{-S_{\text{cl}}}, \quad (3.54)$$

where S_{cl} is the action on the classical instanton trajectory $\vartheta_{\text{cl}}(\tau)$, found in the previous subsection, τ_* is defined as

$$\frac{1}{\tau_*} \equiv \int_{-\infty}^{\infty} \left(\frac{d\vartheta_{\text{cl}}}{d\tau} \right)^2 d\tau, \quad (3.55)$$

while Λ_j and $\Lambda_j^{(0)}$ are the eigenvalues of the equation

$$E_J \psi(\tau) + \int K(\tau - \tau') \psi(\tau') d\tau' + V(\tau) \psi(\tau) = \Lambda \psi(\tau), \quad (3.56)$$

for $V(\tau) = -E_J[1 + \cos \vartheta_{\text{cl}}(\tau)]$ and $V(\tau) = 0$, respectively. The infinite product in Eq. (3.54) is over all eigenvalues except the lowest ones, $\Lambda_0 = 0$ and $\Lambda_0^{(0)} = E_J$. We impose the periodic boundary conditions, $\psi(-\beta/2) = \psi(\beta/2)$, where $\beta \rightarrow \infty$ can be viewed as the inverse temperature.

In the limit $l_s \gg 1$, the classical solution (3.45) yields:

$$V(\tau) = -\frac{2E_J}{\cosh^2(\tau/\tau_s)}, \quad \frac{1}{\tau_*} = \frac{8}{\tau_s}. \quad (3.57)$$

Now the high-frequency asymptotics (3.44b) is sufficient, so the eigenvalue equation (3.56) becomes

$$\left(1 - \frac{d^2}{ds^2} - \frac{2}{\cosh^2 s}\right) \psi(s) = \xi \psi(s), \quad s \equiv \frac{\tau}{\tau_s}, \quad \xi = \frac{\Lambda}{E_J}. \quad (3.58)$$

This equation can be solved exactly [76]. It has one discrete eigenvalue $\xi = 0$, corresponding to the zero mode, and the continuous spectrum for $\xi \geq 1$. The reflection coefficient is exactly zero, and the transmission coefficient is a pure phase factor. Namely, the right-travelling solution has the following asymptotics at $s \rightarrow \pm\infty$:

$$\frac{i\sqrt{\xi-1}+1}{i\sqrt{\xi-1}-1} e^{is\sqrt{\xi-1}} \xleftarrow{s \rightarrow -\infty} \psi(s) \xrightarrow{s \rightarrow +\infty} e^{is\sqrt{\xi-1}}.$$

Together with the periodic boundary condition at $\tau = \pm\beta/2$, it determines the quantization of the eigenvalues:

$$\frac{\beta}{\tau_s} \sqrt{\xi-1} + 2 \arctan \frac{1}{\sqrt{\xi-1}} = 2\pi m, \quad m = 1, 2, \dots \quad (3.59)$$

For $V(\tau) = 0$ we have

$$\frac{\beta}{\tau_s} \sqrt{\xi_m^{(0)} - 1} = 2\pi m, \quad m = 1, 2, \dots, \quad (3.60)$$

which results in $\xi_m^{(0)} = \left(\frac{\tau_s}{\beta} 2\pi m\right)^2 + 1$. Expanding Eq. (3.59) in $\delta\xi_m = \xi_m - \xi_m^{(0)}$ we get:

$$\delta\xi_m = -\frac{8\pi m \tau_s^2}{\beta^2} \arctan \frac{\beta}{2\pi m \tau_s}. \quad (3.61)$$

The same set of eigenvalues is obtained for left-travelling solutions. Then the determinants' ratio evaluates to

$$\begin{aligned} \prod_{j>0} \frac{\Lambda_j^{(0)}}{\Lambda_j} &= \exp \left[\sum_{m \neq 0} \ln \frac{\xi_m^{(0)}}{\xi_m} \right]_{\beta \rightarrow \infty} = \exp \left[- \sum_{m \neq 0} \frac{\delta\xi_m}{\xi_m^{(0)}} \right] = \\ &= \exp \left[\frac{4}{\pi} \int_0^\infty \frac{u \arctan 1/u}{u^2 + 1} du \right] = \exp \left[\frac{2}{\pi} \int_0^\infty \frac{\ln(1+u^2)}{1+u^2} du \right] = 4. \end{aligned} \quad (3.62)$$

Collecting all factors, we obtain the amplitude of a single QPS on one of the junctions

$$\begin{aligned}
W_n &= 4\sqrt{\frac{E_J}{\pi\tau_2}} e^{-S_{cl}} = \frac{4E_J}{\sqrt{g}} \sqrt{\frac{1}{\ell_s}} \left[\frac{2\ell_s}{N} e^{\Upsilon - (8/\pi)\ell_s} \right]^g = \\
&= \frac{4}{\sqrt{\pi}} (8E_J^3 E_c)^{1/4} \exp \left(-\sqrt{\frac{8E_J}{E_c}} - \sqrt{\frac{\pi^2 E_J}{8 E_g}} \left[\ln \frac{N}{2\ell_s} - 1.74 + O(1/\ell_s) \right] \right). \quad (3.63)
\end{aligned}$$

To calculate the total QPS amplitude in the chain we have to coherently sum all the QPS amplitudes on chain junctions. As a result we get $W \sim N^{1-g}$, while the height of the potential at the classically degenerate points, corresponding to the odd numbers of π induced by the magnetic flux, is $\Delta E \sim 1/N$ (see Fig. 3.2). Therefore, for $g < 2$ the energy splitting is of the order of potential height, which results in the ground state energy being almost constant as a function of a flux and, as a result, the persistent current is suppressed (and, therefore, the superconductivity). For $g > 2$ the system can be seen as a good superconductor. In the limit of infinite chain there is a sharp superconductor-insulator transition at $g = 2$, which can be seen as a BKT transition (see Sec. 3.5).

3.3 Weak junction limit (fluxonium)

A specific case is when one of the junctions is much smaller than the rest (we can call it weak junction), then the QPS amplitude on this junction dominates over the rest, which can be useful in producing devices such as fluxonium [19, 72, 77, 78]. To describe this situation, we introduce the explicit notations \tilde{C} and \tilde{E}_J for the capacitance and the Josephson energy of the boundary junction between $n = N$ and $n = 0$, the condition for the junction weakness is $\tilde{C} \ll C$, $\tilde{E}_J \ll E_J$. As we consider the rest of the junctions to share the same properties with each other, we can again pass to the continuum limit for the rest of the chain.

As a result, we have the same general expressions for the QPS action (3.26) and the kernel (3.43) with \tilde{E}_J and \tilde{E}_c instead of E_J and E_c for the slipping junction. At this point it is convenient to introduce the length scale $\ell_J \equiv \frac{E_J}{\tilde{E}_J}$. $\ell_J \gg 1$ is the number of chain junctions which has the same Josephson inductance $L_J = [(2e)^2 E_J]^{-1}$ as that corresponding to \tilde{E}_J . Then in the limit

$$\ell_J \equiv \frac{E_J}{\tilde{E}_J} \gg \frac{E_g}{\tilde{E}_c} + \frac{\ell_s}{2} \equiv \ell_c. \quad (3.64)$$

it can be checked directly that the function

$$\vartheta(\tau) = -2 \arctan \frac{\tau}{\tau_1}, \quad \tau_1 \equiv \frac{\sqrt{E_J/(8E_g)}}{2\tilde{E}_J}, \quad (3.65a)$$

with the Fourier transform

$$\vartheta(\omega) = \frac{2\pi}{i\omega} e^{-|\omega|\tau_1}, \quad (3.65b)$$

satisfies Eq. (3.28) with the kernel (3.44a). This approximation is consistent because condition (3.64) ensures that $1/\tau_1 \ll \omega_K$. Then, the instanton action is given by

$$S_{\text{cl}} = \frac{1}{2} \int \frac{d\omega}{2\pi} K(\omega) |\vartheta(\omega)|^2 + \int \tilde{E}_J [1 + \cos \vartheta(\tau)] d\tau. \quad (3.66)$$

The last term equals $\pi\sqrt{E_J/(8E_g)} \equiv g$, while in the first term the integral is logarithmically divergent at $\omega \rightarrow 0$. To handle this divergence, one has to go back to Eq. (3.42). At $\omega \ll \omega_K$ this amounts to replacing Eq. (3.44a) by

$$K(\omega \ll \omega_K) = \frac{E_J}{N} \left[\frac{N}{2\ell_s} \frac{\omega}{\omega_p} \coth \left(\frac{N}{2\ell_s} \frac{\omega}{\omega_p} \right) - 1 \right]. \quad (3.67)$$

Strictly speaking, the solution is no longer given by Eq. (3.65b); however, the $1/\omega$ behaviour at $\omega \rightarrow 0$ is unchanged since it is determined by the overall change of $\vartheta(\tau)$ from $\tau \rightarrow -\infty$ to $\tau \rightarrow \infty$. The resulting action is given by

$$\frac{S_{\text{cl}}}{g} = 1 + \int_0^\infty \frac{du}{u^2} (u \coth u - 1) e^{-(2\ell_J/N)u} = \ln \frac{N}{\ell_J} + c_1 + O(\ell_J/N), \quad (3.68)$$

where the constant $c_1 = -0.837877\dots$ is easily calculated numerically.

While in the opposite limit

$$\ell_J \equiv \frac{E_J}{\tilde{E}_J} \ll \frac{8E_g}{\tilde{E}_c} + \frac{\ell_s}{2} \equiv \ell_c \quad (3.69)$$

the QPS takes the same form as in the homogeneous chain, Eq. (3.52a), just with one more length scale ℓ_J , basically replacing 1, which is the length scale of the junction.

Now we can calculate the pre-exponent for the case of weak junction. Again, for the case of weak junction we have two limiting cases: $\ell_J \equiv \frac{E_J}{\tilde{E}_J} \gg \frac{E_g}{\tilde{E}_c} + \frac{\ell_s}{2} \equiv \ell_c$ and $\ell_J \ll \ell_c$. We start with the case $\ell_J \gg \ell_c$, where the classical solution (3.65a) yields

$$V(\tau) = -2\tilde{E}_J \frac{\tau_1^2}{\tau^2 + \tau_1^2}, \quad \frac{1}{\tau_*} = \frac{2\pi}{\tau_1}. \quad (3.70)$$

It is convenient to pass to the Fourier space, which is discrete, $\omega_m = 2\pi m/\beta$, $m = \dots, -1, 0, 1, \dots$, because of the boundary conditions $\psi(\beta/2) = \psi(-\beta/2)$. Thus, we decompose $\psi(\tau) = \sum_m \psi_m e^{-i\omega_m \tau}$. For $\Lambda \sim \tilde{E}_J \ll \omega_K$ we can use the low-frequency expression (3.44a) for $K(\omega)$, then the eigenvalue equation (3.56) becomes

$$|m| \psi_m - \sum_{m'} e^{-(2\pi\tau_1/\beta)|m-m'|} \psi_{m'} = \frac{\beta}{2\pi\tau_1} \frac{\Lambda - \tilde{E}_J}{\tilde{E}_J} \psi_m. \quad (3.71)$$

Let us define a function

$$\chi_m = -\frac{\delta_{m,0}}{1 - e^{-2\kappa}} + \theta(m + 1/2) e^{-\kappa m}, \quad \kappa \equiv \frac{2\pi\tau_1}{\beta}, \quad (3.72)$$

where $\theta(x)$ is the Heaviside step function, then all eigenvectors and eigenvalues of the problem (3.71) can be written down explicitly:

$$\begin{aligned} \psi_m &= e^{-\kappa|m|}, & \Lambda/\tilde{E}_J &= 1 - \kappa \coth \kappa, \\ \psi_m &= \chi_m, & \Lambda/\tilde{E}_J &= 1, \\ \psi_m &= \chi_{-m}, & \Lambda/\tilde{E}_J &= 1, \\ \psi_m &= \chi_{m-1}, & \Lambda/\tilde{E}_J &= 1 + \kappa, \\ \psi_m &= \chi_{1-m}, & \Lambda/\tilde{E}_J &= 1 + \kappa, \\ \psi_m &= \chi_{m-2}, & \Lambda/\tilde{E}_J &= 1 + 2\kappa, \\ \psi_m &= \chi_{2-m}, & \Lambda/\tilde{E}_J &= 1 + 2\kappa, \\ &\dots & & \end{aligned} \quad (3.73)$$

At the same time, the eigenvalues of (3.71) with $V(\tau) = 0$ are

$$\Lambda^{(0)}/\tilde{E}_J = 1, 1 + \kappa, 1 + \kappa, 1 + 2\kappa, 1 + 2\kappa, \dots, \quad (3.74)$$

that is, $\Lambda_{j>1} = \Lambda_{j-2}^{(0)}$. However, the total number of eigenvalues must be unchanged by the potential, that is we must recover $\Lambda_j = \Lambda_j^{(0)}$ for very large j , otherwise the infinite product in Eq. (3.54) will diverge. Thus, we are obliged to consider high frequencies, where the low-frequency expression (3.44a) is no longer valid and the full frequency dependence (3.43) should be used.

At frequencies $\omega \gg 1/\tau_1$, the potential $V(\tau)$ is a smooth function of τ , so we can use the WKB approximation (note that the domains of validity of the asymptotic expression (3.44a), $\omega \ll \omega_K$, and of the WKB approximation, $\omega \gg 1/\tau_1$, overlap). Note that the solution Eq. (3.65a) for the classical trajectory remains valid even

when the full expression (3.43) for $K(\omega)$ is used. Indeed, in the frequency representation (3.65b) the solution is suppressed at high frequencies $\omega \gg \omega_1$ and thus is insensitive to the kernel deviation from the low-frequency asymptotic expression (3.44a). Therefore, in the WKB approximation we can use the same expression for the potential $V(\tau)$ (3.70). We can write eigenfunctions as $\psi(\tau) = \exp[\pm i \int_0^\tau \omega(\tau') d\tau']$, then $\omega(\tau)$ should be found from the equation

$$\tilde{E}_J + K(\omega(\tau)) + V(\tau) = \Lambda \quad \Rightarrow \quad \omega(\tau) \approx \omega_\Lambda - \frac{V(\tau)}{K'(\omega_\Lambda)}, \quad (3.75)$$

where ω_Λ is the positive solution of the same equation for $V(\tau) = 0$, and $K'(\omega) = dK(\omega)/d\omega$. In the presence of $V(\tau)$, the quantization condition involves the scattering phase,

$$\int_{-\beta/2}^{\beta/2} \omega(\tau) d\tau = \beta\omega_\Lambda + \frac{2\pi\tilde{E}_J\tau_1}{K'(\omega_\Lambda)} = 2\pi m. \quad (3.76)$$

This gives $\Lambda = \tilde{E}_J + K(\omega_m) - \kappa\tilde{E}_J$, where m must run over all integers, positive and negative, except $m = 0$, in order to match Eq. (3.73). Then we can calculate

$$\prod_{j>0} \frac{\Lambda_j^{(0)}}{\Lambda_j} = \prod_{m \neq 0} \frac{\tilde{E}_J + K(\omega_m)}{\tilde{E}_J + K(\omega_m) - \kappa\tilde{E}_J} \stackrel{\beta \rightarrow \infty}{=} \exp \left[\int_{-\infty}^{\infty} \frac{\tilde{E}_J\tau_1 d\omega}{\tilde{E}_J + K(\omega)} \right]. \quad (3.77)$$

The integral can be calculated by choosing some value \bar{u} such that $\ell_s/\ell_J \ll \bar{u} \ll 1$ and writing

$$\begin{aligned} & \int_{-\infty}^{\infty} \frac{du}{2\ell_s/\ell_J + (16E_g/\ell_s\tilde{E}_c)u^2 + u^2\sqrt{1+1/u^2}} \\ & \approx \int_0^{\bar{u}} \frac{2du}{2\ell_s/\ell_J + u} + \int_{\bar{u}}^{\infty} \frac{2du/u^2}{16E_g/\ell_s\tilde{E}_c + \sqrt{1+1/u^2}} \\ & = 2 \ln \frac{\bar{u}\ell_J}{2\ell_s} + \int_0^{1/\bar{u}} \frac{2dy}{16E_g/\ell_s\tilde{E}_c + \sqrt{1+y^2}} \approx 2 \ln \frac{\ell_J}{\ell_s} - \int_{-\infty}^{\infty} \frac{(16E_g/\ell_s\tilde{E}_c) du}{16E_g/\ell_s\tilde{E}_c + \cosh u} \\ & = 2 \ln \frac{\ell_J}{\ell_s} - \frac{\zeta}{2} \ln \frac{\zeta+1}{\zeta-1}, \quad \zeta \equiv \frac{E_g}{\sqrt{E_g^2 - \ell_s^2\tilde{E}_c^2/32}}. \end{aligned}$$

Collecting all factors, we obtain

$$W_n = \sqrt{\frac{2\pi}{g}} \frac{E_J}{\ell_s} \left(\frac{\zeta-1}{\zeta+1} \right)^{\zeta/4} \left(e^{-c_1} \frac{E_J}{\tilde{E}_J N} \right)^g. \quad (3.78)$$

In the opposite limiting case, $\ell_J \ll \ell_c$, we have the same result as for the homogeneous chain (Eq. 3.63), just replacing the typical length scales:

$$W_n = \frac{4\tilde{E}_J}{\sqrt{g}} \left(\frac{\ell_J}{\ell_c}\right)^{1/4} \left[\frac{\ell_s + \sqrt{\ell_J \ell_c}}{N} e^{\Upsilon - (8/\pi)\sqrt{\ell_c/\ell_J}} \right]^g. \quad (3.79)$$

3.4 Open chain

Now let us consider an open JJ chain, which corresponds to a more realistic configuration, when the JJ chain is included into an external circuit. The main formal difference with the closed chain is that now the phases at the ends of the chain are not compact. Therefore, it can be seen as a generalization of the single Josephson junction case discussed in Sec. 2.1 with an N -dimensional potential (where N is the number of junctions in the chain) instead of one-dimensional. The Bloch theorem can be applied and QPS results in a band structure of the spectrum. The Hamiltonian is

$$H = \frac{1}{2} \sum_{n,m=0}^N Q_n \hat{C}_{nm}^{-1} Q_m - E_J \sum_{n=0}^{N-1} \cos(\phi_{n+1} - \phi_n). \quad (3.80)$$

The difference of the phases at the boundary contacts is $\phi_{N+1} - \phi_0 = \theta$. We want to study phase slip between configurations with $\theta = 0$ and $\theta = 2\pi$. We assume that in the final configuration the jump of 2π is on the junction m ($\phi_{m+1}^f - \phi_m^f = 2\pi$); the amplitude should then be summed over m .

For long chains we can use the continuum limit and write the action in the form

$$\begin{aligned} S = & \int d\tau \int_0^m dx \mathcal{L}(\phi, \partial_\tau \phi) + \int d\tau \int_{m+1}^N dx \mathcal{L}(\phi, \partial_\tau \phi) + \\ & + \int \frac{d\tau}{2E_c} \left[\dot{\phi}(m+1, \tau) - \dot{\phi}(m, \tau) \right]^2 - \int d\tau E_J \cos[\phi(m+1, \tau) - \phi(m, \tau)] \end{aligned} \quad (3.81)$$

where \mathcal{L} is the same Lagrangian density as we used in the action for a closed chain [see Eq. (3.29)]. We decompose the phase into modes on both sides of the slipping

junction

$$\begin{aligned} \phi(x, \tau) = & \left(\sum_n \phi_n(\tau) \Psi_n(x) + \nu(\tau) X(x) + \phi_0(\tau) \right) \theta(m-x) + \\ & + \left(\sum_n \varphi_n(\tau) \Phi_n(x) + \varphi_0(\tau) + \eta(\tau) Y(x) \right) \theta(x-m). \end{aligned} \quad (3.82)$$

Here $\Psi_n(x)$ and $\Phi_n(x)$ are eigenfunctions of wave equation for $S = \int dx \mathcal{L}$ with Dirichlet boundary conditions $\Psi_n(0) = \Psi_n(m) = 0 = \Phi_n(m) = \Phi_n(N)$.

Eliminating the variables as in Sec. (3.1.3) we can write the QPS action in the same way as for the closed chain, Eq. (3.26), replacing the kernel with

$$K(\omega) = \frac{|\omega|}{4e^2 [Z_L(i|\omega|) + Z_R(i|\omega|)]} + \frac{\omega^2}{8E_c}, \quad (3.83)$$

where $Z_L(\omega)$ and $Z_R(\omega)$ are the impedances of the left and right side of the chain (with the respect to the slipping junction). One can see that if the phase slip occurs far from the chain ends, the kernel $K(\omega)$ has the same type low- and high-frequency asymptotics [see Eqs. (3.44a and 3.44b)] as in the closed chain, it has a region of linear dependence on frequency, resulting in logarithmic term $S_{env} \sim \ln \frac{\min\{m, N-m\}}{\ell_s}$ in single QPS action. However, if $m \lesssim \ell_s$ or $N-m \lesssim \ell_s$, there is no linear part in the frequency dependence of K , $K \approx \left(\frac{m}{8E_g} + \frac{1}{8E_c} \right) \omega^2$, on all relevant frequencies. Therefore, the QPS amplitude in an open chain is dominated by the phase slips, occurring near the ends of the chain, whose amplitude does not decay with increasing N . The total QPS amplitude can be estimated as

$$\begin{aligned} W & \approx 2 \sum_{m=0}^{\infty} \frac{4}{\sqrt{\pi}} (8E_J^3 E_c)^{1/4} \exp \left(-\sqrt{8E_J/E_c} - \frac{\sqrt{8E_J E_c}}{E_g} m \right) \\ & = \frac{4}{\sqrt{\pi}} \frac{(8E_J^3 E_c)^{1/4}}{1 - \exp \left(-\frac{\sqrt{8E_J E_c}}{E_g} \right)} \exp \left(-\sqrt{8E_J/E_c} \right) \\ & \approx \frac{8}{\sqrt{\pi}} E_g \left(\frac{E_J}{8E_c} \right)^{1/4} \exp \left(-\sqrt{8E_J/E_c} \right). \end{aligned} \quad (3.84)$$

It is independent of the total chain length N , which agrees with the predictions of [55]. The last approximation is valid as usually $\sqrt{E_J E_c}/E_g \ll 1$. The factor 2 is due to the fact that we have to sum QPS amplitudes near both ends of the chain.

3.5 Relation to Kosterlitz-Thouless renormalization group

Here we show that the obtained results for the QPS amplitude are consistent with the standard Kosterlitz-Thouless scaling [54]. As it was mentioned in Introduction, a one-dimensional quantum system can be mapped on a two-dimensional classical system, therefore, superconductor-insulator transition in infinite one-dimensional chain can be seen as an analogy to the Berezinskii-Kosterlitz-Thouless (BKT) transition in the classical XY model [13, 38]. Indeed, the continuous part of the action (3.8) is equivalent to the XY model action at distances $l > \ell_s$, when the second term of the action can be neglected.

The QPSs play the role of vortices in the (x, τ) plane. On an infinite plane at distances $l > \ell_s$ they interact logarithmically, and the strength of the interaction is determined by the the same prefactor g , which stands in front of logarithm $\ln N$ in the QPS action. When g is large, vortex-untivortex pairs remain bounded and the system is a superconductor. For small g vortex-antivortex pairs can unbind, which corresponds to proliferation of QPSs and destruction of the superconductivity, so the system becomes an insulator. Our instanton calculation for finite length chain at zero temperature corresponds to the plane being infinite in the τ direction but finite in the x direction: for a ring, the plane is wrapped into a cylinder, while for an open chain the plane becomes a strip $0 < x < N$. In both cases, interaction between vortices, whose separation in τ exceeds N/v_{pl} , is no longer logarithmic, since the logarithm is cut off on the scale $x \sim N$. Our instanton calculation corresponds to a dilute gas of non-interacting vortices living on a cylinder or a strip and separated by large distance in τ (Fig. 3.7).

Thus, in chains with a finite length the Kosterlitz-Thouless RG flow should be started at $l = \ell_s$ as the shortest scale and integrated up to the longest scale $l \sim N$. As a result, there is no real zero-temperature transition and even at finite but low (compared to T_c) temperatures the chain can be superconducting. However, the RG formalism can still help to predict the QPS amplitude scaling with the system length and, therefore, the superconducting or insulating behaviour. The RG equations are:

$$\frac{dx}{d \ln l} = -y^2, \quad \frac{dy^2}{d \ln l} = -2xy^2, \quad (3.85)$$

where $x \equiv g - 2$, l is running length scale, while y is the QPS fugacity, which is proportional to the QPS amplitude, $y = W \frac{l}{v_{pl}}$. The corresponding flow is shown in

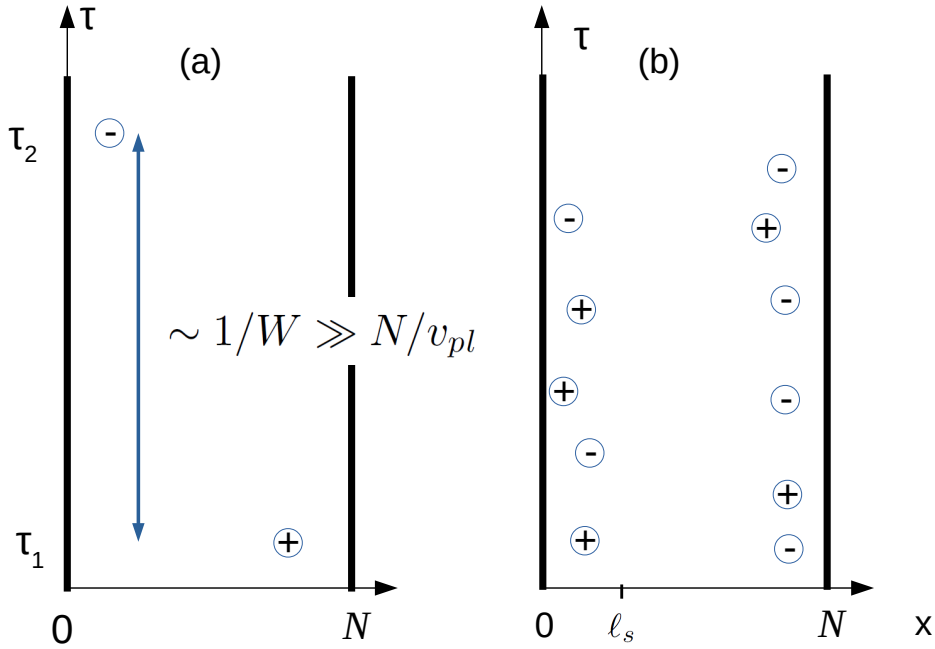


Figure 3.7: A schematic representation of a typical vortex configurations for periodic boundary conditions (a) and open boundary conditions (b).

Fig. 3.8.

As mentioned above, these RG equations should be integrated starting from the scale $l \sim \ell_s$. What are the corresponding initial conditions? For shorter length scales the capacitance C_g does not play a role and the Lagrangian of the chain splits into independent pieces, corresponding to different junctions. There are no interactions between the phase slips. As a result, the parameter g arises only on the scale $l \sim \ell_s$ and its initial value is given by

$$g(\ell_s) = \sqrt{(\pi^2/8)(E_J/E_g)}. \quad (3.86a)$$

In the superconducting regime (not too close to the critical point $g_c = 2$) the initial fugacity is exponentially small for $E_J/E_c \gg 1$,

$$y(\ell_s) = \frac{4}{\sqrt{\pi}} \left(\frac{E_J}{8E_c} \right)^{1/4} \ell_s e^{-\sqrt{8E_J/E_c}} \ll 1. \quad (3.86b)$$

As the system length is increased, for $g > 2$ (so that the system remains in the superconducting regime) y becomes even smaller. Then we can neglect the flow of

x. As a result, we can integrate the second equation (3.85) straightforwardly

$$y(l) = y(\ell_s) e^{-(g-2) \ln \frac{l}{\ell_s}}. \quad (3.87)$$

One can see that $g = 2$ should correspond to the quantum phase transition in case

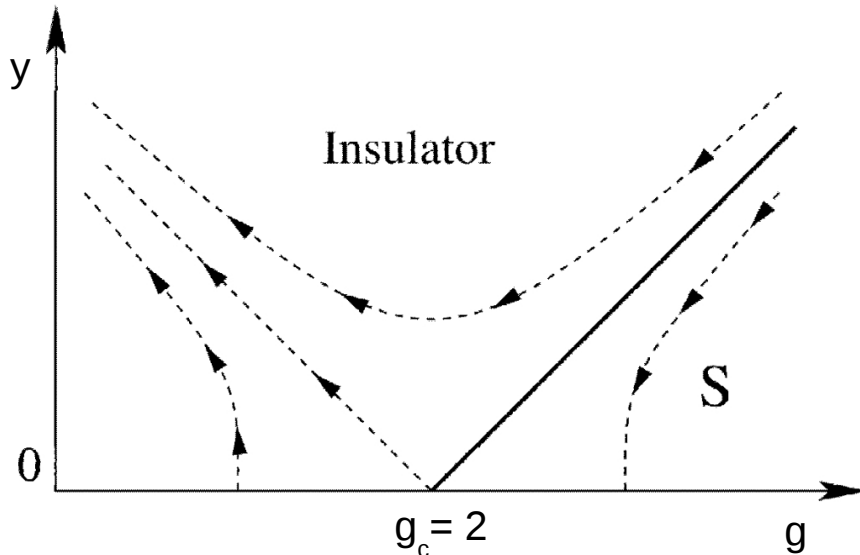


Figure 3.8: Kosterlitz-Thouless RG flows corresponding to Eqs. (3.85): The solid line denotes the transition from insulating to superconducting phase. y is the fugacity of the phase slip. The critical point is $g_c = 2$.

of infinite chain at zero temperature. As we work in the superconducting regime, we consider $g > 2$. For finite length chains at zero temperatures the RG-equation is integrated up to the system length N , which gives

$$W = \frac{v_{pl}}{N} y(N) \sim N^{1-g}. \quad (3.88)$$

This is exactly the same scaling as derived by the instanton calculation, Eq. (3.63). At $g > 2$, the typical distance between the phase slips in imaginary time is the inverse of the CPS amplitude, $\Delta\tau \sim 1/W \gg N/v_{pl}$ (see Fig. 3.7a), so there is no logarithmic interaction between the QPSs (since the logarithm is cut off on the shorter scale $l \sim N$). This justifies the non-interacting instanton gas calculation of the tunneling amplitude.

In an open chain, if a vortex is located near the chain ends, at a distance $m \ll N$, the logarithm in the QPS action is cut off on the scale $l \sim m$. Thus its action

remains finite even for $N \rightarrow \infty$, as we have already seen in Sec. 3.4. This can be interpreted as effect of interaction of the vortex with its mirror image in the picture of two-dimensional Coulomb electrostatics of interacting vortices [55] (see Fig. 3.7b). As a result, the QPS amplitude is determined by a gas of vortices sticking to the boundaries.

Chapter summary

In this chapter we discussed coherent QPS in Josephson junction chains. First, we presented general equations, which determine coherent QPS action in a closed chain. Then we rederived expressions for QPS amplitude for both closed and open homogeneous chains. We also studied a specific weak junction limit, when one of the chain junctions is significantly smaller than the rest. Finally, we discussed scaling of QPS amplitude with the chain length and its relation to Kosterlitz-Thouless renormalization group.

Chapter 4

QPS in inhomogeneous JJ chains

4.1 Linear response to a spatial modulation of the chain parameters

We want to study the effect of a spatial modulation of the junction and island parameters (such as Josephson energies and capacitances) on the QPS amplitude in a JJ chain closed into a ring, as presented in Sec. 3.1. Since modification of these parameters can be useful in controlling the state of the chain, an artificial modulation is worth studying. For example, if the chain is made of SQUIDs, changing the magnetic field in different SQUIDs may lead to a transition between superconducting and insulating states. Studying the effect of a weak random modulations is important as in real experiments it is impossible to produce ideally homogeneous chains, there is always some disorder in the elements' size or uncontrollable random gate voltages.

Here we apply the results of Sec. 3.1. In the following, we will assume the spatial modulation of the chain parameters such as junction capacitance C , Josephson energy E_J and capacitance to the ground C_g to be weak (in Sec. 4.2.1 below we discuss the physical mechanisms for modulations), and focus on the linear correction δS_{cl} to the classical instanton action S_{cl} . The modulation results in a linear correction $\delta K(\tau - \tau')$ to the kernel for a homogeneous JJ chain, which, in turn, produces a correction $\delta \vartheta_{\text{cl}}(\tau)$ to the classical trajectory. Note, however, that the classical trajectory was found from the condition $\delta S / \delta \vartheta = 0$, so the correction to the action can be evaluated on the zero-approximation classical trajectory, which is

most conveniently done in the Fourier space:

$$\delta S_{\text{cl}} = \frac{1}{2} \int \frac{d\omega}{2\pi} \delta K(\omega) |\vartheta_{\text{cl}}(\omega)|^2. \quad (4.1)$$

When calculating the correction $\delta K(\omega)$ to the linear order in the modulations, one can ignore the term containing $\frac{G_{X1}(\omega)G_{1X}(\omega)}{G_{11}(\omega)}$ in Eq. (3.40). Indeed, the homogeneous chain is symmetric with respect to $x \rightarrow N-1-x$, so 1 and $X(x)$ have different parity, and $G_{1X}(\omega) = 0$. A modulation breaking this symmetry will produce $G_{1X}(\omega)$, linear in the modulation, so the term $\sim \frac{G_{X1}(\omega)G_{1X}(\omega)}{G_{11}(\omega)}$ in Eq. (3.40) is quadratic.

The classical trajectory is given by Eq. (3.46)

$$\vartheta_{\text{cl}}(\omega) = \frac{2\pi}{i\omega \cosh(\pi\omega\tau_s/2)}, \quad \tau_s \approx \omega_p^{-1}, \quad (4.2)$$

As $1/\tau_s \sim v_p/\ell_s$, the high-frequency asymptotics of $K(\omega)$ should be taken into account. It is convenient to separate the two contributions as

$$K(\omega) = K_{\text{low}}(\omega) + K_2\omega^2, \quad (4.3)$$

where $K_{\text{low}}(\omega)$ corresponds to the first line in Eq. (3.41) for G_{XX} and remains finite at $\omega \rightarrow \infty$. In the correction to S_{env} from $K_{\text{low}}(\omega)$, the integral converges at frequencies $\omega \sim \omega_p$. Thus, the correction to the logarithmic term in S_{env} can be calculated as

$$S_{\text{env}} + \delta S_{\text{env}} = \pi^2 \mathcal{T}_c \sum_{\alpha} \omega_{\alpha} \left[\overline{(X, \Psi_{\alpha})} \right]^2 \mathcal{F}(\omega_{\alpha}\tau_s), \quad (4.4)$$

where the function $\mathcal{F}(z)$ is defined as

$$\mathcal{F}(z) = \frac{2z}{\pi} \int_0^{\infty} \frac{1}{\cosh^2(\pi u/2)} \frac{du}{z^2 + u^2}. \quad (4.5)$$

The coefficient K_2 in Eq. (4.3) determines the local part of the action S_{loc} ; its general expression is

$$K_2 = \frac{1}{8E_c} + \mathcal{T}_c \left\{ \overline{(X, X)} - \sum_{\alpha} \left[\overline{(X, \Psi_{\alpha})} \right]^2 \right\}. \quad (4.6)$$

Then, $\delta S_{\text{loc}} = 4 \delta K_2 / \tau_s$.

4.2 Periodically modulated chain

4.2.1 Physical mechanisms for the modulation

Here we apply the general scheme, outlined in the previous section, to the simplest case of a weak periodic modulation of the chain parameters. We assume the modulation period, N/m , to be an integer fraction of the chain length N (that is, $m \gg 1$ is integer). This introduces no discontinuity of the JJ chain parameters at the QPS location. Thus, the modulation is assumed to have a profile

$$\mu(x) = 1 - t \cos k_{2m}(x - x_0), \quad (4.7)$$

where $t \ll 1$ is the relative modulation amplitude, $k_{2m} \equiv 2\pi m/N$, and x_0 parametrizes the relative QPS position with respect to the modulation. One can consider different modulations, depending on their physical implementation.

When fabricating JJ chains, one can control the area of each junction. While the Josephson energy E_J and the capacitance C between the islands are both proportional to the junction area, the capacitance of each island to the ground is controlled by the island area. Assuming the junction areas to be modulated and the island areas to remain constant, we arrive at the following spatial pattern of the coefficients in action (3.8):

$$E_g(x) = E_{g0}, \quad \ell_s^2(x) = \ell_{s0}^2 \mu(x), \quad E_J(x) = E_{J0} \mu(x). \quad (4.8a)$$

Another possible way to modulate the parameters is to vary the island areas. In this case, the ground capacitance C_g of each island is modulated, while E_J and C remain constant. This corresponds to

$$E_g(x) = \frac{E_{g0}}{\mu(x)}, \quad \ell_s^2(x) = \frac{\ell_{s0}^2}{\mu(x)}, \quad E_J(x) = E_{J0}. \quad (4.8b)$$

Finally, each Josephson junction can be implemented as a superconducting quantum interference device (SQUID). In a magnetic field, the corresponding Josephson energy of each SQUID is sensitive to the SQUID loop area. This enables one to modulate E_J independently of C ; this may lead to qualitatively different effects from the previous cases [79]. Thus, we consider the profile

$$E_g(x) = E_{g0}, \quad \ell_s^2(x) = \ell_{s0}^2, \quad E_J(x) = e_{10} \mu(x). \quad (4.8c)$$

Below we will analyze these cases separately, closely following the approach of Ref. [80].

4.2.2 Junction area modulation

We start with the case of modulation (4.8a). First, we calculate the correction to the classical configuration:

$$X(x) = \left(\frac{x}{N} - \frac{1}{2} \right) + \frac{t}{k_{2m}N} \sin k_{2m}(x - x_0) + O(t^2). \quad (4.9)$$

Then, we find the normal mode wave functions $\Psi_\alpha(x)$ and frequencies ω_α from the modulated wave equation,

$$\frac{\partial}{\partial x} \mu(x) \frac{\partial \Psi_\alpha}{\partial x} + \kappa^2(\omega_\alpha) \Psi_\alpha = 0, \quad (4.10)$$

where $\kappa(\omega)$ denotes the inverse of the dispersion (3.31):

$$\kappa(\omega) \equiv \frac{\omega}{\sqrt{8E_{J0}E_{g0} - \ell_{s0}^2\omega^2}}. \quad (4.11)$$

For $t = 0$ this gives the homogeneous result $\Psi_\alpha(x) = \sqrt{2/(1 + k^2\ell_{s0}^2)} \sin k_\alpha x$ with $\kappa(\omega_\alpha) = k_\alpha = \pi\alpha/N$.

First, we use perturbation theory in $t \ll 1$, seeking the wave function in the form

$$\begin{aligned} \Psi_\alpha(x) = & \sqrt{\frac{2}{1 + k^2\ell_{s0}^2}} \left(\sin k_\alpha x - \frac{B_+ + B_-}{2} \cos k_\alpha x + \right. \\ & + \frac{B_+}{2} \cos k_{\alpha+2m}x + \frac{B_-}{2} \cos k_{\alpha-2m}x + \\ & \left. + \frac{A_+}{2} \sin k_{\alpha+2m}x + \frac{A_-}{2} \sin k_{\alpha-2m}x \right). \end{aligned} \quad (4.12)$$

The perturbation theory gives

$$A_\pm = -\frac{k_\alpha k_{\alpha\pm 2m}}{k_\alpha^2 - k_{\alpha\pm 2m}^2} t \cos k_{2m}x_0, \quad B_\pm = \pm \frac{k_\alpha k_{\alpha\pm 2m}}{k_\alpha^2 - k_{\alpha\pm 2m}^2} t \sin k_{2m}x_0, \quad (4.13)$$

and the correction to ω_α is $O(t^2)$.

$$\begin{aligned} \overline{(X, \Psi_\alpha)} = & -\frac{1 + (-1)^\alpha}{2} \sqrt{\frac{2}{1 + k_\alpha^2 \ell_{s0}^2}} \frac{1}{k_\alpha N} \left[1 - \frac{t}{4} \cos k_{2m} x_0 \left(\frac{k_\alpha^2}{k_\alpha^2 - k_m^2} + 2\delta_{\alpha, 2m} \right) \right] + \\ & -\frac{1 - (-1)^\alpha}{2} \sqrt{\frac{2}{1 + k_\alpha^2 \ell_{s0}^2}} \frac{2t \sin k_{2m} x_0}{k_\alpha k_{2m} N^2} + O(t^2). \end{aligned} \quad (4.14)$$

However, the perturbative expression (4.12) is not always valid. By a direct check, we see that the corrections are small when two conditions are fulfilled:

$$|\alpha - m| \gg tm, \quad t\alpha \ll m. \quad (4.15)$$

The first condition breaks down in the relatively narrow interval of α , where the gap in the frequency spectrum opens up. The resulting modification of a relatively small number of terms in the α sum in Eq. (4.4), those with $|\alpha - m| \sim tm$, leads to a small correction to the N/m factor inside the logarithm [see Eq. (4.21) below]. This correction is beyond our precision.

For large α , the second condition (4.15) breaks down. Then, instead of doing perturbation theory, one can construct $\Psi_\alpha(x)$ using the WKB approximation:

$$\Psi_\alpha(x) = \sqrt{\frac{2}{1 + \ell_{s0}^2 \kappa^2(\omega_\alpha)}} \frac{\sin s(x)}{[\mu(x)]^{1/4}}, \quad s(x) \equiv \int_0^x \frac{\kappa(\omega_\alpha) dx'}{\sqrt{\mu(x')}}. \quad (4.16)$$

The frequency ω_α is determined by the boundary condition for $\Psi_\alpha(x)$, that is, $s(N) = \pi\alpha$. This results in a small relative correction $O(t^2)$ to the frequency and determines the normalization factor in Eq. (4.16). Although the relative difference between $s(x)$ and its zero-approximation value $k_\alpha x$ is small, the absolute difference may become of the order of one, and then $\sin s(x) - \sin k_\alpha x \sim 1$ as well. This is the reason of the perturbation theory breakdown at large α . Note, however, that the perturbation theory is valid at $\alpha \ll m/t$, while the WKB approximation is valid at $\alpha \gg m$, so their regions of validity overlap.

Now we evaluate the overlap $\overline{(X, \Psi_\alpha)}$ writing it as

$$\overline{(X, \Psi_\alpha)} = \sqrt{\frac{2}{1 + k_\alpha^2 \ell_{s0}^2}} \operatorname{Im} \int_0^N \frac{dx}{N} e^{is(x)} [\mu(x)]^{1/4} \left[\frac{X(x)}{\sqrt{\mu(x)}} + ik_\alpha \ell_{s0}^2 \frac{dX(x)}{dx} \right]. \quad (4.17)$$

Note that $e^{is(x)}$ is fast oscillating, while the rest of the integrand is smooth, due to the condition $k_\alpha \gg k_{2m}$. Thus, we introduce the complex variable z such that

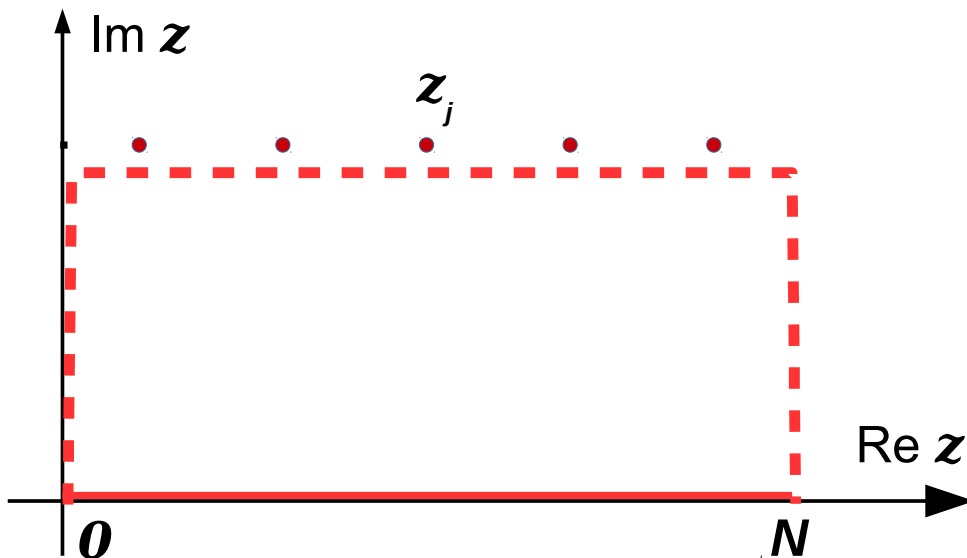


Figure 4.1: (Color online) Deformation of the integration contour in Eq. (4.17) from the real axis (solid red line) into the upper complex half-plane (dashed red line). The dots represent branching points z_j of $s(z)$.

$x = \text{Re } z$, and deform the contour into the upper complex half-plane, as shown in Fig. 4.1. The contour can be moved up to the branching points of $s(z)$, located at

$$z_j = \frac{jN}{m} + x_0 + \frac{i}{k_{2m}} \text{arccosh} \frac{1}{t}.$$

The integral over the horizontal part of the contour near the branching points is suppressed as $t^{\alpha/(2m)}$; the branching points determine the small reflection probability from a weak smooth potential, which in the present case of a periodic modulation leads to opening of small gaps at high frequencies. This effect is beyond our precision, so the contribution of interest comes from the steepest descent in the positive imaginary direction from the points $x = 0$ and $x = N$. To linear order in $1/k_\alpha$ this gives

$$\overline{(X, \Psi_\alpha)} = \sqrt{\frac{2}{1 + k_\alpha^2 \ell_{s0}^2}} \frac{[\mu(0)]^{1/4}}{k_\alpha N} [X(0) - (-1)^\alpha X(N)]. \quad (4.18)$$

This coincides with Eq. (4.14) in the limit $\alpha \gg m$. The reason for this coincidence is that even though the WKB wave function differs significantly from the perturbative one in the bulk of the chain, the overlap integral is dominated by the vicinities of

$x = 0, N$, where the phase accumulated in $s(x)$ is still small on the absolute scale.

Thus, Eq. (4.14) can be used for all α . Substituting it into Eq. (4.4) and neglecting $O(t^2)$ terms, we obtain

$$\frac{\delta S_{\text{env}}}{g} = -\frac{\pi t}{N} \cos k_{2m} x_0 \sum_{\alpha \text{ even}} \frac{k_\alpha}{k_\alpha^2 - k_m^2} \frac{\mathcal{F}(\omega_\alpha \tau_s)}{(1 + k_\alpha^2 \ell_{s0}^2)^{3/2}}. \quad (4.19)$$

\mathcal{F} is defined in Eq. (4.5). The sum can be replaced by the integral which should be understood as the principal value (the contribution of the term with $\alpha = 2m$ has relative smallness $\sim 1/m$). The last factor cuts off the integral at $k_\alpha \sim 1/\ell_s$. At $k_m \ell_s \ll 1$ the integral is logarithmic, where the small k cutoff is determined by the first factor. In this case it is convenient to rewrite it as

$$\frac{\delta S_{\text{env}}}{g} = -\frac{t \cos k_{2m} x_0}{2} \int_0^\infty \frac{\mathcal{F}(\omega(k) \tau_s) dk}{(k + k_m)(k^2 \ell_{s0}^2 + 1)^{3/2}}, \quad (4.20)$$

where we used the fact that the integral of $k/(k^2 - k_m^2) - 1/(k + k_m)$ is identically zero. As a result,

$$\frac{\delta S_{\text{env}}}{g} = -\frac{t}{2} \cos k_{2m} x_0 \left(\ln \frac{1}{2k_m \ell_s} + \tilde{\Upsilon} \right), \quad (4.21)$$

if $k_m \ell_s \ll 1$; at $k_m \ell_s \gg 1$, the correction is suppressed as $1/(k_m \ell_s)^2$. $\tilde{\Upsilon}$ is a number of the order of unity, evaluated numerically. In the limit $\ell_s \gg 1$ it amounts to $\tilde{\Upsilon} = -0.4806\dots$. For realistic parameters, e. g., a chain of 1000 junctions with $g = 3$ and $\ell_s = 10$, modulated with $t = 0.2$ and $m = 5$, this gives $\delta S_{\text{env}} \approx 0.2$.

Finally, to find the correction to the high-frequency asymptotics of the kernel $K(\omega)$, determined by Eq. (4.6), we directly evaluate

$$\overline{(X, X)} - \sum_\alpha \left[\overline{(X, \Psi_\alpha)} \right]^2 = \frac{\ell_{s0}}{2N} \left(1 - \frac{t \cos k_{2m} x_0}{2} \frac{1}{1 + k_m^2 \ell_{s0}^2} \right) + O(\ell_s^2/N^2). \quad (4.22)$$

For $k_m \ell_{s0} \ll 1$, this correction corresponds precisely to the local value of ℓ_s , and thus of $\ell_s^2/E_g \propto C$ at the QPS location. For $k_m \ell_{s0} \gg 1$, the correction is suppressed, as the modulation is effectively averaged out on the length ℓ_{s0} .

4.2.3 Island area modulation

For modulation (4.8b), Eq. (3.36) gives

$$X(x) = \frac{x}{N} - \frac{1}{2} - \frac{t}{k_{2m}N} \sin k_{2m}x_0. \quad (4.23)$$

The wave functions Ψ_α are found from the wave equation

$$\frac{\partial^2 \Psi_\alpha}{\partial x^2} + \kappa^2(\omega_\alpha) \mu(x) \Psi_\alpha = 0. \quad (4.24)$$

The perturbative expression for $\Psi_\alpha(x)$ is again Eq. (4.16), with coefficients obtained from Eqs. (4.2.2) by replacing $k_{\alpha\pm 2m} \rightarrow k_\alpha$ in the numerators and inverting the overall sign. The WKB wave function is given by the same expression (4.16), but the phase $s(x)$ is given by

$$s(x) = \kappa(\omega_\alpha) \int_0^x \sqrt{\mu(x')} dx'. \quad (4.25)$$

The final result for $\overline{(X, \Psi_\alpha)}$ turns out to be exactly the same as for the case of the junction area modulation, Eq. (4.14). δS_{env} is also given by Eq. (4.21).

Evaluation of Eq. (4.6) with the perturbed wave functions again gives Eq. (4.22). This time, at $k_m \ell_{s0} \ll 1$ it corresponds to taking the local value of the ground capacitance C_g .

4.2.4 SQUID area modulation

For modulation (4.8c), the profile $X(x)$ is again given by Eq. (4.9). The coefficients A_\pm, B_\pm are obtained by multiplying those from Eqs. (4.2.2) by $1 + k_\alpha^2 \ell_s^2$. All subsequent calculations are analogous; the result is the same as in Eq. (4.21) but the number $\tilde{\Upsilon}$ is different, we obtain $\tilde{\Upsilon} = -0.0695 \dots$

Evaluation of Eq. (4.6) can be simplified by noting that modulation (4.8c) does not affect the scalar product. By completeness, $\sum_\alpha \Psi_\alpha(x) \Psi_\alpha(x') \equiv \mathcal{I}(x, x')$ is the kernel of the unit operator in the space of functions with Dirichlet boundary conditions, and it does not depend on the choice of the functional basis Ψ_α in this space. Thus, Eq. (4.6) can be evaluated using the wave functions for the homogeneous chain, $\Psi_\alpha(x) = \sqrt{2/(1 + k_\alpha^2 \ell_{s0}^2)} \sin k_\alpha x$. As a result, the correction vanishes. Indeed, modulation (4.8c) does not involve the capacitances at all.

4.2.5 Combined modulation

We can also consider a case when both Josephson energies and capacitances are modulated, $E_J(x) = e_{l0} \mu_l(x)$ and $E_g(x) = E_{g0}/\mu_c(x)$, generally speaking, with two different amplitudes t_l and t_c . Then, it is easy to see that the resulting effect on $\overline{(X, \Psi_\alpha)}$ is additive. For the first-order perturbative wave functions this follows trivially, while for the WKB wave functions it follows from the steepest-descent calculation, analogous to Eq. (4.17). Its result is determined by the derivative $s'(x=0)$, which, in turn, can be calculated perturbatively.

The results obtained above may be conveniently combined if we introduce the local dimensionless admittance:

$$g(x) \equiv \pi \sqrt{\frac{E_J(x)}{8E_g(x)}} \equiv g_0 + \delta g(x). \quad (4.26)$$

For all types of modulation, discussed in Sec. 4.2.1, we have

$$\delta g(x)/g_0 = -(t/2) \cos k_{2m}(x - x_0) + O(t^2). \quad (4.27)$$

For the combined modulation with two different amplitudes t_l and t_c , the correction is

$$\delta g(x)/g_0 = -(t_l/2 + t_c/2) \cos k_{2m}(x - x_0) + O(t^2). \quad (4.28)$$

Then, up to terms $O(1)$, at $k_m \ell_s \ll 1$ we can express correction δS_{env} in terms of $\delta g(x=0)$, which is the local correction to the chain admittance at the QPS position, for all types of modulations:

$$\delta S_{\text{env}} = \delta g(x=0) \ln \frac{1}{2k_m \ell_s}, \quad (4.29)$$

4.3 Disordered chain

4.3.1 Fluctuations of the QPS action

In this section we consider two types of disorder in the chain: spatial inhomogeneities, such as random variation in the junction areas, resulting in relative modulation of the Josephson energy and junction capacitance

$$E_{c,n} = \frac{E_c}{1 + \eta_n}, \quad E_{J,n} = E_J (1 + \eta_n), \quad (4.30)$$

as well as random induced charges q_n on the islands [see Hamiltonian (3.1)], which can be caused by random gate voltages, and result in a random phase of a single QPS $\theta_n = \sum_{m=0}^n 2\pi q_m / (2e)$ (see Eq. (3.5)). We consider spatial disorder to be relatively weak, $\langle \eta_n^2 \rangle \ll 1$, which produces small relative corrections to the action S_n and the prefactor Ω_n in Eq. (3.17). While the latter results in a small relative correction to the QPS amplitude W , the correction to the action, δS_n , even though small compared to S_n , can still be large compared to unity, since S_n itself is large. As δS_n stands in the exponent, it may significantly modify W . Therefore, in the following we focus on the statistics of δS_n , calculating it to the linear order in η_n . For this we can again use the unperturbed expression (4.2) for ϑ_{cl} in Eq. (4.1), because it was derived from the condition $\delta S / \delta \vartheta = 0$. Then the correction to the action is:

$$\delta S_n = \int \left[\frac{\eta_n}{16E_c} \left(\frac{d\vartheta_{cl}}{d\tau} \right)^2 + \eta_n E_J (1 + \cos \vartheta_{cl}) \right] d\tau + \frac{1}{2} \int \delta \mathcal{K}_n(\omega) |\vartheta_{cl}(\omega)|^2 \frac{d\omega}{2\pi} \equiv \delta S_{n,loc} + \delta S_{n,env}, \quad (4.31)$$

where the kernel \mathcal{K} is

$$\mathcal{K}_n(\omega) = \frac{|\omega|}{(2e)^2 Z_n(i|\omega|)}. \quad (4.32)$$

We assume η_n to be Gaussian distributed with $\langle \eta_n \rangle = 0$, so the average correction to the action is zero. The quadratic fluctuations of the action are determined (i) by the variation of the slipping junction area, which in turn determines $\delta S_{n,loc}$, the first two terms in Eq. (4.31), and (ii) by the correlator $\langle \delta \mathcal{K}_n(\omega) \delta \mathcal{K}_n(\omega') \rangle$, corresponding to the variation in the impedance of the rest of the chain, which governs $\delta S_{n,env}$, the last term in Eq. (4.31). The latter is determined by the Mooij-Schön modes, which become localized in the presence of disorder. Calculation of the correlator is fully analogous to that of impedance fluctuations at real frequencies [81]: using the recurrence relation for the impedance as the chain length is increased by one, one arrives at a Langevin-like equation.

The basic idea of the approach is to study the change in the admittance $Y_N(i\omega) \equiv 1/Z_N(i\omega)$ of an open chain of N Josephson junctions upon addition of an extra junction $N+1$. We can write the following recurrence relation for the admittance:

$$Y_{N+1} = \omega C_g + \frac{Y_N Y_J}{Y_N + Y_J}, \quad (4.33)$$

where $Y_J = 1/(\omega L_{N+1}) + \omega C_{N+1}$ is the imaginary frequency admittance of the added junction and the Josephson inductance is defined as $1/L_{N+1} = (2e)^2 E_{J,N+1}$.

First, let us consider a homogeneous chain. Then the recurrence relation (4.33) has a stationary point Y_∞ , determined by the condition

$$Y_\infty = \omega C_g + \frac{Y_\infty Y_J}{Y_\infty + Y_J}, \quad (4.34)$$

which gives

$$Y_\infty = \frac{\omega C_g}{2} + \sqrt{\frac{\omega^2 C_g^2}{4} + \omega C_g Y_J} \approx \sqrt{\omega C_g Y_J}. \quad (4.35)$$

The latter approximation follows from $C \gg C_g$. Focusing on small deviations from the stationary point, we introduce a new variable $X_N = Y_N - Y_\infty$. The linearized recurrence relation takes a simple form:

$$X_{N+1} = \tau X_N, \quad \tau \equiv \frac{Y_J^2}{(Y_\infty + Y_J)^2}. \quad (4.36)$$

Note that $1 - \tau \ll 1$, following from $C_g \ll C$.

Now we can include fluctuations of the chain parameters,

$$C_{N+1} \rightarrow C (1 + \eta_{N+1}), \quad L_{N+1} \rightarrow \frac{L}{1 + \eta_{N+1}}, \quad (4.37)$$

and write the linearized recurrence relation as

$$X_{N+1} = \tau X_N + \frac{Y_\infty^2 Y_J}{(Y_\infty + Y_J)^2} \eta_{N+1} = \tau X_N + \delta X_{N+1}. \quad (4.38)$$

Using the condition $1 - \tau \ll 1$ we can cast this equation into a differential form:

$$\frac{dX_N}{dN} = -(1 - \tau) X_N + \frac{Y_\infty^2 Y_J}{(Y_\infty + Y_J)^2} \eta_{N+1}, \quad (4.39)$$

which is a Langevin equation.

So far we considered the admittance at a given frequency ω . We are interested in the correlator of admittances at two different frequencies ω and ω' . Then taking into account the fact that δX_{N+1} and X_N are not correlated we can average the product of equations (4.38) at different frequencies:

$$\begin{aligned} \langle X_{N+1}(\omega) X_{N+1}(\omega') \rangle &= \tau(\omega) \tau(\omega') \langle X_N(\omega) X_N(\omega') \rangle + \\ &+ \langle \delta X_{N+1}(\omega) \delta X_{N+1}(\omega') \rangle, \end{aligned} \quad (4.40)$$

which can again be rewritten as a differential equation:

$$\begin{aligned}
\frac{d}{dN} \langle X_N(\omega) X_N(\omega') \rangle &= \\
&= (\tau(\omega) \tau(\omega') - 1) \langle X_N(\omega) X_N(\omega') \rangle + \\
&+ \langle \delta X_{N+1}(\omega) \delta X_{N+1}(\omega') \rangle.
\end{aligned} \tag{4.41}$$

As we consider long chains, we can go to the limit $N \rightarrow \infty$ and look for the stationary solution:

$$\langle X(\omega) X(\omega') \rangle = \frac{\langle \delta X(\omega) \delta X(\omega') \rangle}{1 - \tau(\omega) \tau(\omega')}, \tag{4.42}$$

which is the correlator of admittance fluctuations. The correlator of the kernel fluctuations is

$$\langle \delta \mathcal{K}(\omega) \delta \mathcal{K}(\omega') \rangle = \frac{|\omega| |\omega'|}{(2e)^4} \langle X(\omega) X(\omega') \rangle. \tag{4.43}$$

Evaluating $\langle \delta X(\omega) \delta X(\omega') \rangle$ from the definition (4.38) and collecting all factors, we obtain the following behaviour in the two limiting cases. For $\omega, \omega' \gg \omega_p$ we have

$$\langle \delta \mathcal{K}(\omega) \delta \mathcal{K}(\omega') \rangle = \frac{|\omega|^2 |\omega'|^2}{2^8 E_g^{3/2} E_c^{1/2}} \langle \eta^2 \rangle. \tag{4.44}$$

At low frequencies $\omega, \omega' \ll \omega_p$, the result is

$$\langle \delta \mathcal{K}(\omega) \delta \mathcal{K}(\omega') \rangle = \frac{\sqrt{2E_J}}{32E_g^{3/2}} \frac{|\omega|^2 |\omega'|^2}{|\omega| + |\omega'|} \frac{\langle \eta^2 \rangle}{2}. \tag{4.45}$$

We are interested in the low-frequency limit of $\langle \delta \mathcal{K}(\omega) \delta \mathcal{K}(\omega') \rangle$ because the integrand in Eq. (4.31) is quickly suppressed at $\omega > \omega_p$ due to the frequency dependence of $\vartheta_{cl}(\omega)$, Eq. (4.2). From this we can estimate

$$\langle \delta S_{env}^2 \rangle \sim \langle \eta^2 \rangle \frac{\ell_s \sqrt{E_J E_c}}{E_g^2} \int_0^{\sim \sqrt{E_J E_c}} \frac{d\omega d\omega'}{\omega + \omega'} \sim \langle \eta^2 \rangle \frac{\ell_s E_J E_c}{E_g^2} \sim \langle \eta^2 \rangle \frac{g^2}{\ell_s}. \tag{4.46}$$

As typically $g^2 \lesssim \ell_s$, $\langle \delta S_{env}^2 \rangle \ll 1$. At the same time

$$\langle \delta S_{loc}^2 \rangle \sim \langle \eta^2 \rangle \frac{E_J}{E_c} \gg \langle \delta S_{env}^2 \rangle, \tag{4.47}$$

due to the condition $C_g \ll C$. Moreover, $\langle \delta S_{loc}^2 \rangle$ can be larger than 1, depending on the parameters, as $\langle \eta^2 \rangle \ll 1$, while $\frac{E_J}{E_c} \gg 1$.

As a result, the fluctuations of the QPS action are dominated by the local values of the slipping junction parameters, while the effect of Mooij-Schön modes modification by the disorder plays a minor role. This happened because the environment contribution to the QPS amplitude is determined by the impedance at imaginary frequencies, which turns out to be weakly fluctuating. This is in striking contrast to the behaviour at real frequencies, when localization of the Mooij-Schön modes by the disorder results in strong impedance fluctuations [81].

Having established the dominant character of the local contribution to the action fluctuations, we can study the statistics of the QPS amplitude W by using Eq. (3.17) with $S_n = S_{\text{hom}} + \delta S_n$, where S_{hom} is the action of the homogeneous chain, Eq. (3.53), and δS_n are independent Gaussian random variables:

$$\delta S_n = \sqrt{8 \frac{E_J}{E_c}} \eta_n, \quad \langle \delta S_n \rangle = 0, \quad \langle \delta S_n \delta S_m \rangle = 8 \frac{E_J}{E_c} \langle \eta_n^2 \rangle \delta_{nm} = \sigma^2 \delta_{nm}. \quad (4.48)$$

This problem is addressed in the following subsections.

4.3.2 QPS amplitude distribution without random induced charges

First, we consider only the junction area variation assuming no induced charges. For long chains we can use the central limit theorem resulting in the Gaussian distribution with the average amplitude and dispersion

$$\langle W \rangle = \Omega e^{-S_{\text{hom}}} N e^{\sigma^2/2}, \quad \sqrt{\langle W^2 \rangle - \langle W \rangle^2} = \Omega e^{-S_{\text{hom}}} \sqrt{N(e^{2\sigma^2} - e^{\sigma^2})}. \quad (4.49)$$

The central limit theorem is valid when the dispersion is much smaller than the average, that is

$$N \gg e^{\sigma^2} - 1. \quad (4.50)$$

However, even for small relative area fluctuations $\langle \eta_n^2 \rangle \ll 1$, it is quite possible that $\sigma^2 \gtrsim 1$. Indeed, taking the parameters of the experiment in [72], $E_J/E_c \approx 90$, and assuming $\langle \eta_n^2 \rangle = 10^{-2}$, we obtain $\sigma^2 \approx 7$. Then the central limit theorem applies only for exponentially large N .

For $\sigma > 1$ and insufficiently large N , the distribution of W can be far from Gaussian; it develops a long asymmetric tail for large W . In this case the peak of the distribution can be located at W much smaller than the average value $\langle W \rangle$ (see Fig. 4.3); the average is then determined by rare configurations contributing

to the tail. In fact, this problem is known since long ago in many different areas, such as communications [82, 83], optics [84], transport in disordered systems [85], finances [86], yet no general analytical expression for the resulting distribution is available. Sometimes the resulting distribution can be approximated by a lognormal one [84, 86, 83]. Below we revisit this problem for $\sigma^2 \gtrsim 1$ and give some analytical expressions valid in different regimes [Eqs. (4.59) and (4.62)], and compare them to the results of the direct numerical sampling and its lognormal fit (Fig. 4.3).

To derive analytical expressions, let us represent the QPS amplitude as $W = A\Omega e^{-S_{\text{hom}}}$, then the distribution function for the normalized amplitude A is defined as

$$\begin{aligned} f(A) &= \left\langle \delta \left(A - \sum_{n=1}^N \exp(-\delta S_n) \right) \right\rangle = \\ &= \int \frac{dt}{2\pi} e^{itA} \left[\int \frac{dx}{\sqrt{2\pi\sigma}} e^{-\frac{x^2}{2\sigma^2}} \exp(-ite^{-x}) \right]^N. \end{aligned} \quad (4.51)$$

The average value $\langle A \rangle = N e^{\sigma^2/2}$.

The t integral can be calculated in the saddle-point approximation similarly to Ref. [85]. Let us rotate the integration contour in Eq. (4.51) to the imaginary axis:

$$f(A) = \int_{-i\infty}^{i\infty} \exp[zA - NI(z)] \frac{dz}{2\pi i}, \quad (4.52)$$

$$I(z) \equiv -\ln \left[\int \frac{dx}{\sqrt{2\pi\sigma}} e^{-\frac{x^2}{2\sigma^2}} \exp(-ze^{-x}) \right]. \quad (4.53)$$

In the saddle-point approximation, we have

$$f(A) \approx \sqrt{\frac{1}{2\pi NI''(z_s)}} \exp[z_s A + NI(z_s)], \quad (4.54)$$

where $I'(z) = dI/dz$ and z_s is defined as the solution of the equation

$$A + NI'(z_s) = 0. \quad (4.55)$$

Because we consider $N \gg 1$, the important values of z are those for which $I(z) \ll 1$, so we can expand the logarithm and approximate

$$I(z) \approx \int \frac{dx}{\sqrt{2\pi\sigma}} e^{-\frac{x^2}{2\sigma^2}} [1 - \exp(-ze^{-x})]. \quad (4.56)$$

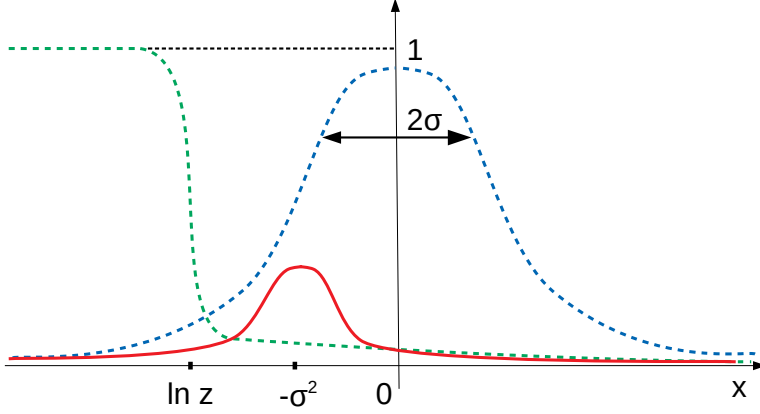


Figure 4.2: Two factors of the integrand in $I(z)$ (4.56), $\exp(-\frac{x^2}{2\sigma^2})$ (dashed blue line) and $1 - \exp(-ze^{-x})$ (dashed green line), and their product (solid red line).

In the saddle point approximation the integral (4.52) is determined by the small area near the real axis. To calculate $I(z)$ (4.56) we approximate $\exp(-ze^{-x}) \approx 1 - ze^{-x}$ for $x > \ln z$ and $\exp(-ze^{-x}) \approx 1$ for $x < \ln z$. Then if $-\ln z \gtrsim \sigma^2 + \sigma$ the integrand can be approximated as Gaussian for $x > \ln z$ and is suppressed for $x \lesssim \ln z$ [85] (see Fig. 4.2):

$$I(z) \approx - \int_{\ln z}^{\infty} ze^{\sigma^2/2} \frac{dx}{\sqrt{2\pi}\sigma} \exp\left[-\frac{(x + \sigma^2)^2}{2\sigma^2}\right] = -\frac{ze^{\sigma^2/2}}{2} \operatorname{erfc}\left(\frac{\ln z + \sigma^2}{\sqrt{2}\sigma}\right), \quad (4.57)$$

Therefore, Eq. (4.55) can be written as:

$$A - N \frac{e^{\sigma^2/2}}{2} \operatorname{erfc}\left(\frac{\ln z_s + \sigma^2}{\sqrt{2}\sigma}\right) + N \frac{e^{\sigma^2/2}}{\sqrt{2\pi}\sigma} \exp\left[-\left(\frac{\ln z_s + \sigma^2}{\sqrt{2}\sigma}\right)^2\right] \approx 0.$$

Introducing new variable $y = \frac{\ln z_s + \sigma^2}{\sqrt{2}\sigma}$ and considering $|y| \ll \sigma$ we obtain

$$y \approx \operatorname{erfc}^{-1}\left(\frac{2A}{Ne^{\sigma^2/2}}\right) - \frac{1}{\sqrt{2}\sigma}. \quad (4.58)$$

Now we calculate the second derivative of I :

$$I''(z_s) \approx \frac{e^{\sigma^2/2}}{\sqrt{2\pi\sigma z_s}} \exp \left[- \left(\frac{\ln z_s + \sigma^2}{\sqrt{2\sigma}} \right)^2 \right] - \frac{e^{\sigma^2/2}}{\sqrt{2\pi\sigma z_s}} \frac{\ln z_s + \sigma^2}{\sigma^2} \exp \left[- \left(\frac{\ln z_s + \sigma^2}{\sqrt{2\sigma}} \right)^2 \right] \approx \frac{\exp(3\sigma^2/2 - \sqrt{2\sigma}y - y^2)}{\sqrt{2\pi\sigma}}.$$

resulting in

$$f(A) \approx \frac{\sigma}{N e^{\sigma^2/2}} M^{1/2} \exp \left(-M e^{\sqrt{2\sigma}Q - Q^2} + \frac{Q^2 + \sqrt{2\sigma}Q}{2} \right), \quad (4.59)$$

where $Q = \operatorname{erfc}^{-1} \left(\frac{2A}{N e^{\sigma^2/2}} \right)$ and $M = \frac{N e^{-\sigma^2/2}}{\sqrt{2\pi\sigma e}}$.

For validity of the saddle-point approximation we need

$$\left| N I'''(z_s) \left[\frac{1}{\sqrt{N I''(z_s)}} \right]^3 \right| \ll 1, \quad (4.60)$$

where the quantity in the square brackets is the typical width of the relevant region near z_s . As a result, we obtain the condition $N \gtrsim \sigma e^{\sigma^2/2 - \sigma} \gg 1$.

Another analytically tractable regime is when the whole sum is determined by a single term, corresponding to the junction with the highest QPS amplitude (the weakest junction). The probability of having one junction with $x < \delta S_n < x + dx$ and the rest of the junctions with $\delta S_n < x$ is

$$p(x) dx = \left(\int_{-\infty}^x \frac{dx}{\sqrt{2\pi\sigma}} e^{-\frac{x^2}{2\sigma^2}} \right)^{N-1} \frac{N}{\sqrt{2\pi\sigma}} e^{-\frac{x^2}{2\sigma^2}} dx, \quad (4.61)$$

where N in the last factor corresponds to the fact that the junction with the highest amplitude can be any of the N junctions. Then for the distribution we have

$$f(A) = \int \delta(A - e^{-x}) p(x) dx = \frac{N}{\sqrt{2\pi\sigma A}} \exp \left[-\frac{(N-1)}{2} \operatorname{erfc} \left(\frac{\ln A}{\sqrt{2\sigma}} \right) - \frac{\ln^2 A}{2\sigma^2} \right]. \quad (4.62)$$

The weakest junction approximation is valid when the amplitude on the weakest junction, $\exp(-\min\{\delta S_n\})$, is sufficiently larger than the sum of the amplitudes on the rest of the junctions, which can be estimated from above as $(N-1) \exp(-\min'\{\delta S_n\})$, where $\min'\{\delta S_n\}$ denotes the second smallest of $\{\delta S_n\}$. To es-

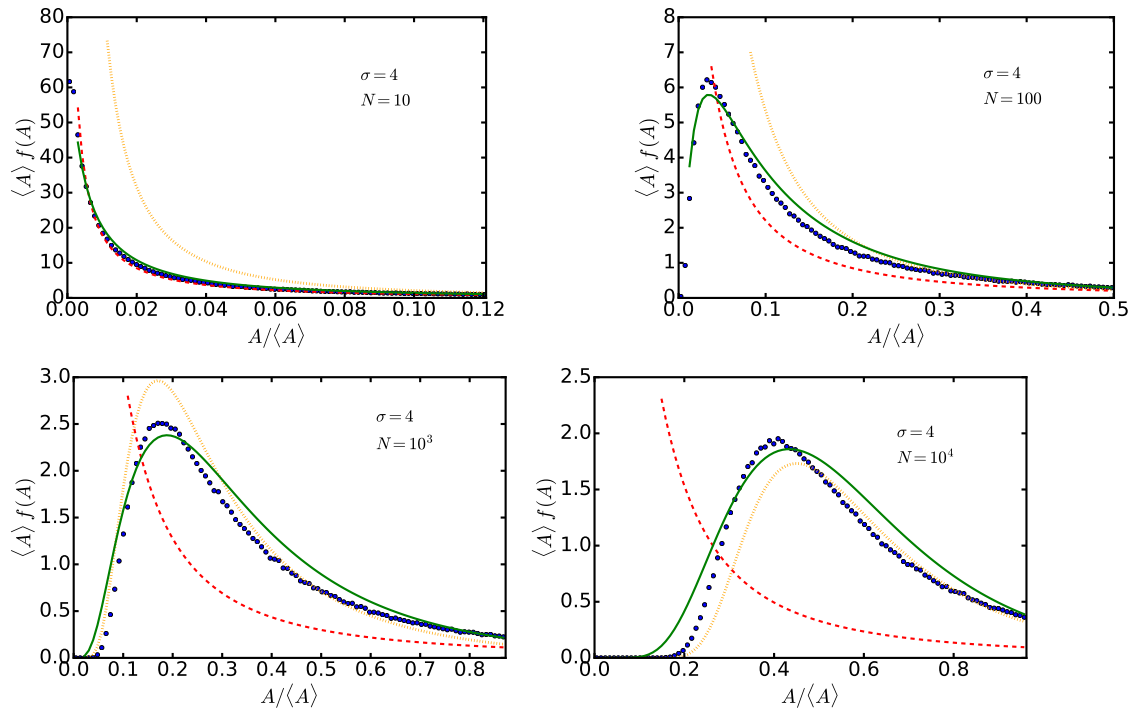


Figure 4.3: Distribution $f(A)$ in the absence of induced charges, calculated for $\sigma = 4$ and different N by the direct numerical sampling (blue dots), using the weakest junction approximation (4.62) (red dashed lines), the saddle-point approximation (4.59) (orange dotted lines), and the lognormal fit (solid green lines).

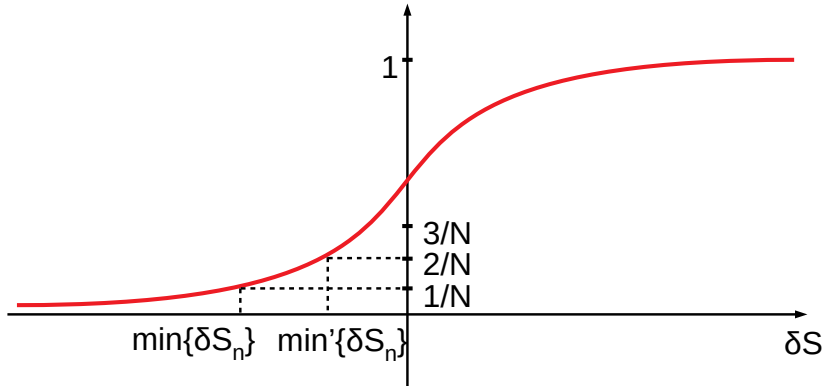


Figure 4.4: Cumulative probability distribution of δS_n and estimates of the two smallest δS_n for a typical sample.

to estimate the typical values of the two smallest δS_n , we recall the standard procedure for sampling the Gaussian distribution: from a sample of N numbers $\{x_n\}$, uniformly distributed between 0 and 1, one obtains a sample of the Gaussian $\{\delta S_n\}$ by taking the inverse of the cumulative probability distribution function (see Fig. 4.4). In a typical sample, $\min\{x_n\} \sim 1/N$ and $\min'\{x_n\} - \min\{x_n\} \sim 1/N$, so we estimate

$$\frac{1}{2} \operatorname{erfc} \left(\frac{\min\{\delta S_n\}}{\sqrt{2}\sigma} \right) = \frac{1}{N}, \quad \frac{1}{2} \operatorname{erfc} \left(\frac{\min'\{\delta S_n\}}{\sqrt{2}\sigma} \right) = \frac{2}{N}. \quad (4.63)$$

This results in the validity condition

$$N \lesssim \exp \left[(\ln^2 2/2)^{1/3} \sigma^{2/3} \right]. \quad (4.64)$$

In Fig. 4.3 we compare results derived in weakest junction approximation, the saddle-point approximation, a lognormal fit and direct numerical sampling. Lognormal fit is reasonable in all limits, however, it is not clear how to choose its parameters *a priori*, therefore, it does not seem to be useful. The weakest junction approximation works well for short chains, while the saddle-point approximation is more accurate for longer chains.

4.3.3 QPS amplitude distribution in the presence of random induced charges

If we include random induced charges q_n , we obtain a random phase in the amplitude of a single QPS centered on each junction $\theta_n = 2\pi \sum_{m=0}^n q_m / (2e)$ [32, 33], as a result instead of the coherent sum for the total QPS amplitude in Eq. (3.17) we have the

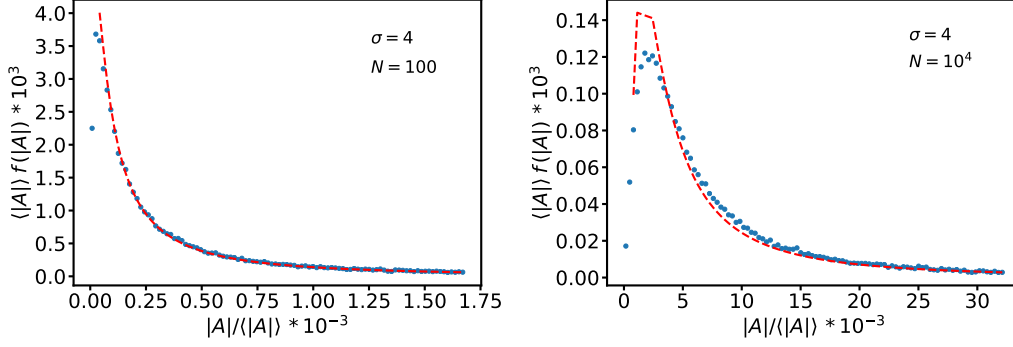


Figure 4.5: Distribution $f(|A|)$ with random induced charges, calculated for $\sigma = 4$ and different N by the direct numerical sampling (blue dots) and using the weakest junction approximation (4.62) (red dashed lines).

sum with random phases. If $\langle q_n^2 \rangle / (2e)^2 \gg 1$, the distribution of q_n is flat, so the phases θ_n are uncorrelated. This represents a universal limit of maximally strong disorder. Then the normalized QPS amplitude is given by

$$A = \sum_{n=0}^{N-1} e^{-\delta S_n - i\theta_n}. \quad (4.65)$$

Therefore, A is complex and its average is zero. The central limit theorem results in the complex Gaussian distribution with

$$\sqrt{\langle |A|^2 \rangle} = \sqrt{N} e^{\sigma^2}. \quad (4.66)$$

The criterion for the validity of the central limit theorem is the correspondence of the moments of A to the moments of the complex Gaussian distribution, for example

$$\langle |A|^4 \rangle - 2\langle |A|^2 \rangle^2 \ll \langle |A|^4 \rangle. \quad (4.67)$$

This results in the condition

$$N \gg (e^{4\sigma^2} - 1)/2, \quad (4.68)$$

even more restrictive than in the real case.

In the complex case, we were unable to derive a compact expression for the distribution function corresponding to the saddle point approximation. The weakest junction approximation works when

$$N \lesssim \exp \left[(2 \ln^2 2)^{1/3} \sigma^{2/3} \right]. \quad (4.69)$$

Then the distribution of $|A|$ is the same as the distribution of A in Eq. (4.62). The only difference is in the restriction on the chain length N : the approximation is valid for a wider range of N as seen from Eq. (4.69) and Eq. (4.64).

In Fig. 4.5 we compare the numerical sampling and the weakest junction approximation. One can see that the latter remains accurate for a longer chains than in case of no induced charges.

Chapter summary

This chapter is dedicated to effects of weak spatial inhomogeneities on the QPS amplitude in a Josephson junction chain. We started by studying the case of weak artificial periodic modulations of the chain parameters, such as Josephson energy E_J , junction capacitance C and capacitance to the ground C_g , discussing different realisations of those modulations. We derived the corrections to an environmental and a local contribution to a QPS action, showing that any of those corrections can affect the QPS amplitude. The correction to the logarithmic term has a cut-off at the modulation wave-length N/m instead of system length N .

Then we studied the effects of disorder of two types: weak random variations of the junction areas and random induced charges on superconducting islands, caused by random gate voltages. We showed that the corrections to the environmental contribution to the QPS action can be neglected, while the local part of the action can be modified strongly enough to change the QPS amplitude dramatically. As a result, for short chains a junction with the smallest area can be seen as a weak link, where all the phase slips occur. We studied the statistics of the QPS amplitude and derived a criterion, determining chain behaviour in both limits of zero, Eq. (4.50), and large random induced charges, Eq. (4.68). For small $\sigma \ll 1$ this criterion is trivial, in all the chains with length $N \gg 1$ a QPS amplitude is very close to the one in a homogeneous chain. However, for large $\sigma \gg 1$ the criterion defines, whether the total QPS amplitude is averaged over several weak junctions, resulting in all the chains behaving similarly, with the QPS amplitude given by the average value, $\langle W \rangle = N\Omega e^{-S_{hom} + \sigma^2/2}$ in case of zero induced charges and $\sqrt{\langle |W|^2 \rangle} = \sqrt{N}\Omega e^{-S_{hom} + \sigma^2}$ in the presence of large induced charges, or whether the chains, produced with the same average parameters but different disorder realizations, behave differently, as the total QPS amplitude has a wide distribution over different realizations.

Chapter 5

QPS in superconducting nanowires

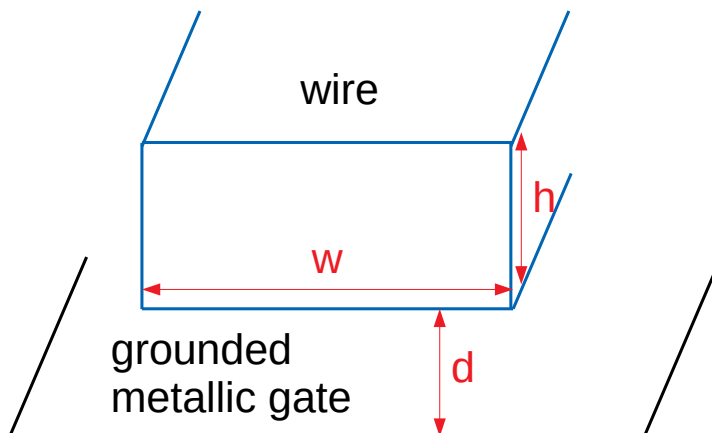


Figure 5.1: Schematic representation of a superconducting nanowire of width w and thickness h at a distance d from the metallic gate

The results obtained in the previous section for JJ chains can be applied to superconducting wires. We consider a superconducting nanowire of rectangular cross-section, whose width is smaller than the superconducting coherence length: $\lambda_F \ll h \lesssim w \ll \xi$, here λ_F is the Fermi wavelength, h and w are the thickness and the width of the wire respectively, ξ is the superconducting coherence length in the bulk metal. The wire is placed at a distance d from a grounded metallic gate. We consider the wire to be in the dirty limit, assuming that the electron mean free path is much smaller than superconducting coherence length $\ell \ll \xi$. Therefore, there are three possible diffusive regimes in the system. First, if the electron mean free path is shorter than the width $\ell \ll h$, the wire is in the three-dimensional diffusive limit with the diffusion coefficient $D = v_F \ell / 3$. If $h \ll \ell \ll w$, then the system is in the two-dimensional diffusive regime $D = v_F \ell / 2$. And finally, for $w \ll \ell$ we

have one-dimensional diffusive regime with $D \sim wv_F$ due to sensitivity of electronic motion to the surface roughness. We also consider the distance d between the wire and the grounded metallic gate to be much larger than the wire width, $d \gg w$ (see Fig. 5.1). Here are some typical values of superconducting coherence length and the electron mean free path in experimental setups: for rhenium $\xi = 100 - 150$ nm and ℓ ranging from 60 nm to $2 \mu\text{m}$ [87], for aluminium $\xi_0 = 1.7 \mu\text{m}$ and $\ell \approx 10$ nm [88].

Following [89] we can write the phase action for the superconducting wire as a gradient expansion on the scales $k \ll 1/\xi$ (for wires k has the dimension of inverse length, while for the JJ chains it was dimensionless, as we were measuring length in Josephson junctions). As the coordinate and time derivatives of the phase contribute to the action in the same form as gauge fields V and \mathbf{A} , the scalar and the vector potential, upon integrating out electron degrees of freedom the action takes the form

$$S = \frac{1}{8} \int \frac{dk d\omega}{(2\pi)^2} [\omega^2 \chi_{\rho\rho}(k, \omega) + \omega k \chi_{\rho j}(k, \omega) + k\omega \chi_{j\rho}(k, \omega) + k^2 \chi_{jj}(k, \omega)] |\phi|^2, \quad (5.1)$$

where the coefficients are defined as components of the response matrix $\hat{\chi}$:

$$\begin{pmatrix} \rho \\ j \end{pmatrix} = \begin{pmatrix} \chi_{\rho\rho} & \chi_{\rho j} \\ \chi_{j\rho} & \chi_{jj} \end{pmatrix} \begin{pmatrix} eV \\ -\frac{e}{c}A \end{pmatrix} = \hat{\chi}(k, \omega) \begin{pmatrix} eV \\ -\frac{e}{c}A \end{pmatrix}, \quad (5.2)$$

which determines the response of the electron density ρ and current j to the scalar

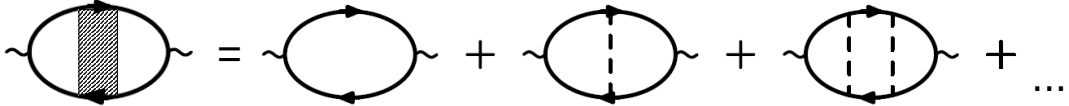


Figure 5.2: Ladder diagrams series for the components of the response matrix $\chi_{\rho\rho}$, χ_{jj} , $\chi_{j\rho}$ and $\chi_{\rho j}$. Solid lines correspond to electron Green's functions averaged over disorder, the dashed lines correspond to impurity potential. Each wavy line corresponds either to 1 or current operator j , depending on the indices of χ .

and vector potentials. The components of the response matrix can be calculated in Feynman diagrammatic formalism as loops with two vertices, each of them can be either scalar (corresponding to the scalar field V) or vector (corresponding to the vector field \mathbf{A}). In case of intrinsic disorder (as we consider diffusive regime) the averaging over impurities is done by summing over the series of all ladder diagrams (diagrams with noncrossing impurity lines, see Fig. 5.2). As a result, in low-frequency and low-momentum limit $\omega \ll \Delta$, $k \ll \xi^{-1}$ without interactions we

have [90]

$$\chi_{\rho\rho}^0 \approx \nu, \quad \chi_{\rho j}^0 = \chi_{j\rho}^0 \approx \frac{\pi\nu D}{16\Delta} k\omega, \quad \chi_{jj}^0 \approx \pi\nu D\Delta. \quad (5.3)$$

Here Δ is the superconducting gap, ν and D are the density of states per unit length and the diffusion coefficient for the wire in the normal state. They can be related to the bulk density of states ν_{3D} and the superconducting coherence length of the wire material, as well as to the wire cross-section $s = wh$, $\nu = s\nu_{3D}$, $\xi = \sqrt{D/\Delta}$. However, we need to take into account Coulomb interaction in the system. There are contributions both from the electrons in the wire itself and in the metallic gate at distance d :

$$U(x-x') = \int_0^w \frac{dy}{w} \frac{dy'}{w} \left(\frac{e^2/\epsilon}{\sqrt{(x-x')^2 + (y-y')^2}} - \frac{e^2/\epsilon}{\sqrt{(x-x')^2 + 4d^2}} \right). \quad (5.4)$$

Then in the random-phase approximation (see Fig 5.3) we obtain the χ -matrix as

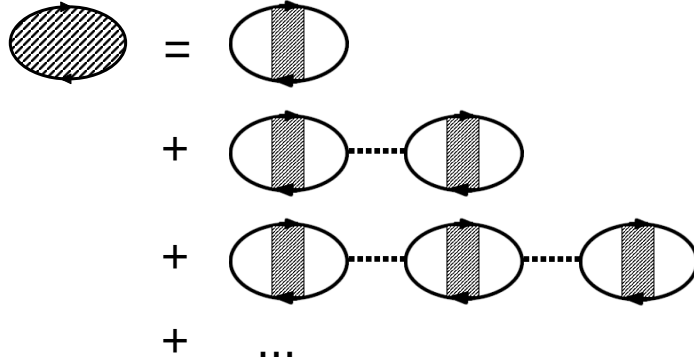


Figure 5.3: Random-phase approximation. Dotted lines correspond to Coulomb interaction.

$$\hat{\chi}(k, \omega) = \hat{\chi}^0(k, \omega) \left[1 + \begin{pmatrix} U(k) & 0 \\ 0 & 0 \end{pmatrix} \hat{\chi}^0(k, \omega) \right]^{-1}. \quad (5.5)$$

Here $\hat{\chi}^0$ is the response matrix defined without Coulomb interactions in the system,

$U(k)$ is the Fourier transform of the Coulomb interaction. Then

$$\hat{\chi} = \frac{1}{1 + U(k)\chi_{\rho\rho}^0} \begin{pmatrix} \chi_{\rho\rho}^0 & \chi_{\rho j}^0 \\ \chi_{j\rho}^0 & \chi_{jj}^0 [1 + U(k)\chi_{\rho\rho}^0] - U(k)\chi_{\rho j}^0\chi_{j\rho}^0 \end{pmatrix} \quad (5.6)$$

One can see that the first term in Eq. (5.1) is suppressed by

$$\chi_{\rho\rho}^0 U(k) \approx \frac{2e^2\nu}{\epsilon} \left[\ln \frac{2d}{we^{-3/2}} - k^2 d^2 \ln \frac{e^{1-\gamma}}{|k|d} + O(k^4 d^4) \right], \quad (5.7)$$

due to the fact that $\chi_{\rho\rho}^0 \approx \nu$, where ν is the one-dimensional density of states for electrons in the wire, and in metallic wires $\nu e^2 \gg 1$ (even for a small cross-section $s = 100 \text{ nm}^2$, for rhenium $\nu e^2 = 3,6 \times 10^3$ [87], for aluminium $\nu e^2 = 5 \times 10^3$ [88]). As a result, even for relatively low $k < \xi^{-1}$ we have to consider high frequencies ($\omega > 2\Delta$) and the quasiparticles should be taken into consideration.

As $U(k) \approx U(0) = \frac{2e^2}{\epsilon} \ln \frac{2d}{we^{-3/2}}$ for $k \ll 1/d$ is very strong, many terms are suppressed, the action can be written as [53]

$$S \approx \frac{1}{8} \int dk d\omega (2\pi)^2 |\phi(k, \omega)|^2 \left(\frac{\omega^2}{U(0)} + \chi_{jj}(\omega) k^2 \right), \quad (5.8)$$

where $\chi_{jj}(\omega)$ is proportional to the optical conductivity on imaginary frequencies, $\chi_{jj}(\omega) = |\omega| \sigma(-i|\omega|)$ [91]. For low frequencies, $\omega \ll \Delta$, $\chi_{jj} \approx \chi_{jj}^0$, we can determine the plasma (Mooij-Schön) mode velocity as $v_{pl} = \sqrt{U(0)\chi_{jj}^0}$ and low-frequency admittance as $g = \frac{\pi}{4} \sqrt{\frac{\pi\nu}{U(0)}} \xi \Delta$.

As a result, the low-energy excitations (the Mooij-Schön modes) are similar to the ones in JJ chains up to the frequencies $\omega \lesssim 2\Delta$. The difference is that while in the JJ chain model there are no excitations above the cutoff frequency ω_p , in a wire the role of the cutoff frequency is played by the superconducting gap 2Δ , above which quasiparticle excitations are present and can be virtually excited during the phase tunnelling process. Therefore, slow phase readjustment in a superconducting wire is completely analogous to a JJ chain, while in the core of the QPS the order parameter is suppressed and the phase action is invalid. Thus, for the Ohmic (environment) part of the action one can use the expressions derived for JJ chains, if ℓ_s is defined as the inverse cut-off wave vector for the Mooij-Schön modes:

$$\ell_s \sim v_{pl}/\Delta = \sqrt{U(0)\nu\pi} \xi = \sqrt{\frac{2\pi\nu e^2}{\epsilon} \ln \frac{2d}{we^{-3/2}}} \xi \gg \xi. \quad (5.9)$$

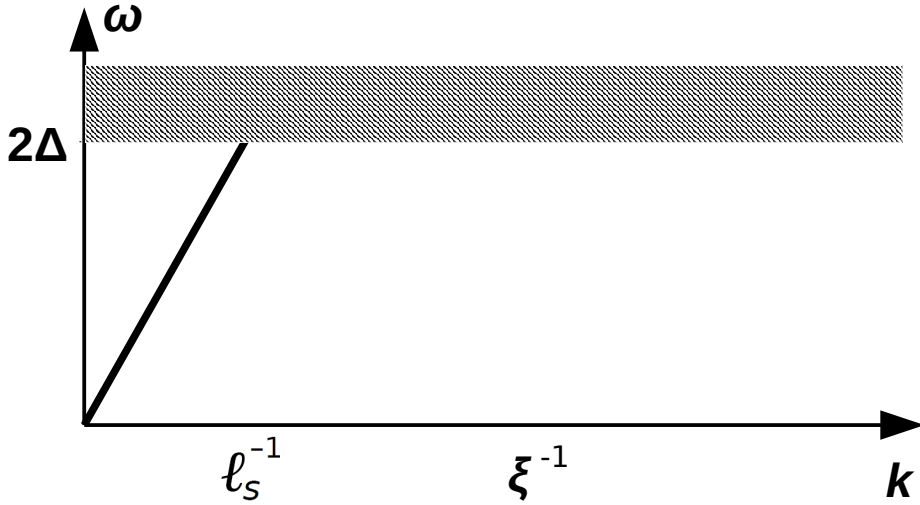


Figure 5.4: The dispersion curve of the phase oscillations (Mooij-Schön modes) up to 2Δ

The non-Ohmic (local) contribution to the action is significantly different for wires and JJ chains. A quantitative theory for the non-Ohmic contribution to the action S_{loc} in superconducting wires does not exist, as the absolute value of the order parameter should be taken into consideration along with quasiparticles excitations. Still, some qualitative understanding can be reached. The key fact is that for wires, the instanton duration is of the order of Δ^{-1} [53]. Then, the contribution to the action from the integral of $K(\omega)$ is parametrically smaller than that from the Josephson E_J term (for wires the Josephson term has a more complicated form, non-local in time, but the corresponding contributions can still be identified and estimated [53]).

The low energy properties of a superconducting wire are determined by the inductance per unit length, $\mathcal{L} = (e^2\pi\nu\xi^2\Delta^2)^{-1}$, and ground capacitance per unit length, $\mathcal{C} = e^2/U(0)$. We can represent a superconducting wire as a Josephson junction chain with parameters E_J , C_g and junction size a by matching the Mooij-Schön mode velocity and the low frequency wire admittance:

$$\frac{1}{\sqrt{\mathcal{L}\mathcal{C}}} = a\sqrt{8E_JE_g}, \quad \sqrt{\frac{\mathcal{C}}{\mathcal{L}}} = (2e)^2\sqrt{\frac{E_J}{8E_g}}. \quad (5.10)$$

While for Josephson junction chains the frequency cut-off is $\sqrt{8E_JE_c}$, for wires it is given by the superconducting gap 2Δ . The analog of the random spatial variation $E_{J,n} = E_J(1+\eta_n)$ would be the spatial variation $\mathcal{L}(x) = \mathcal{L}/[1+\eta(x)]$, which can result

from, e.g., spatial fluctuations in the wire thickness on the spatial scale exceeding the thickness itself and the superconducting coherence length ξ . The parameters $\mathcal{L}(x)$ and $\mathcal{C}(x)$ are already averaged over the microscopic disorder due to impurities, acting on the length scale shorter than ξ . Then instead of $\langle \eta_n \eta_m \rangle = G \delta_{nm}$ with $G \ll 1$ we have $\langle \eta(x) \eta(x') \rangle = \mathcal{G} \delta(x - x')$, where \mathcal{G} has the dimensionality of length and $\delta(x - x')$ is peaked on the length $\sim \xi$. If we represent a segment of the wire of length $a \gtrsim \xi$ by a Josephson junction with $E_J = 1/[(2e)^2 a \mathcal{L}]$, then $G = \mathcal{G}/a$. Thus, the weak-disorder condition is $\mathcal{G} \ll \xi$.

Similarly to the Josephson junction chains, the QPS action in superconducting wires can be represented as a sum of two contributions: $S_{\text{QPS}} = S_{\text{loc}} + S_{\text{env}}$. The environment part of the action is also determined by the Mooij-Schön modes. This enables us to use the Eq. (4.45) for the low-frequency admittance fluctuations:

$$\langle \delta \mathcal{K}(\omega) \delta \mathcal{K}(\omega') \rangle = \frac{\mathcal{C}^{3/2} \mathcal{L}^{-1/2} |\omega|^2 |\omega'|^2}{2(2e)^4 (|\omega| + |\omega'|)} \mathcal{G}. \quad (5.11)$$

Using the estimate Δ^{-1} for the instanton duration [53], from Eq. (4.31) we obtain an estimate

$$\langle \delta S_{\text{env}}^2 \rangle \sim \frac{\mathcal{C} \sqrt{\mathcal{C}/\mathcal{L}} \Delta \mathcal{G}}{(2e)^4}. \quad (5.12)$$

The local part of the QPS action can not be calculated precisely for superconducting wires [90, 53]. However, it can be estimated as $S_{\text{loc}} \sim \frac{1}{(2e)^2 \mathcal{L} \xi \Delta}$ [53], which gives

$$\langle \delta S_{\text{loc}}^2 \rangle \sim \frac{\mathcal{G}/\xi}{(2e)^4 \mathcal{L}^2 \xi^2 \Delta^2}. \quad (5.13)$$

As a result, we have $\langle \delta S_{\text{loc}}^2 \rangle \gg \langle \delta S_{\text{env}}^2 \rangle$ if

$$\xi \ll \frac{1}{\Delta \sqrt{\mathcal{L} \mathcal{C}}}. \quad (5.14)$$

In fact, this relation usually holds for superconducting wires because the mode velocity $1/\sqrt{\mathcal{L} \mathcal{C}}$ is sufficiently high. Indeed, $1/\mathcal{C}$ has two contributions: one from the quantum capacitance of the Fermi sea, and the electrostatic contribution due to Coulomb interaction. In the absence of Coulomb interaction the mode velocity would be such that both sides of Eq. (5.14) would be of the same order. However, the Coulomb contribution is usually much stronger, so the velocity is high enough to ensure the strong inequality (5.14). The right-hand side of this inequality can be seen as an analogue of ℓ_s for the superconducting wires, and inequality (5.14) is an

analogue of $\ell_s \gg 1$. Moreover, condition (5.14) results in

$$\langle \delta S_{\text{env}}^2 \rangle \ll \frac{\sqrt{\pi} (\nu \Delta \xi)^2}{32 \nu^{3/2} U^{3/2}(0)}. \quad (5.15)$$

Depending on the cross section of the wire, it can be significant or negligible, $\langle \delta S_{\text{env}}^2 \rangle > 1$ or $\langle \delta S_{\text{env}}^2 \rangle < 1$. For example, for small cross section, $s = 100 \text{ nm}^2$, $\nu \Delta \xi \sim 10^2$ for rhenium and aluminium, while $e^2 U(0) \sim 10^3$, resulting in $\langle \delta S_{\text{env}}^2 \rangle < 1$. However, it grows with the cross section.

As a result, analogously to the JJ chains, the fluctuations of the QPS action are mostly determined by the local values of the wire parameters in the phase-slip core of the size ξ , which coincides with the predictions of [53]. The contribution to the environmental part of the action is parametrically smaller. However, it still can be significant, depending on the wire cross section and disorder.

Chapter summary

In the last chapter we applied the results, obtained in the previous chapters for Josephson junction chains, to superconducting nanowires. The results for the hydrodynamic part of the QPS action, S_{env} , due to Mooij-Schön modes are analogous for both the chains and the wires, provided parameters are correctly identified. The results for the core action cannot be used for the wires.

Chapter 6

Conclusions and Outlook

In this thesis we have studied quantum phase slips (QPS). After a brief general introduction we started with studying phase slips in a single dissipative Josephson junction. The dissipation was modelled as an external resistance, while the induced current tilts the potential, resulting in possibility of tunneling from a ground state in one minimum of the potential to an excited state in the neighboring lower minimum. This process is an incoherent QPS. We derived the form of voltage peaks at resonant values of induced current.

In the next chapter we reproduced the known results for coherent QPS in close and open Josephson junction chains. We discussed the relation of coherent QPS amplitude scaling with system length to Kosterlitz-Thouless renormalization group. We also found the numerical correction to the logarithmic term in QPS action.

The fourth chapter is dedicated to effects of disorder on QPS. First, we studied coherent QPSs in chains with artificially periodically modulated parameters, such as capacitances and Josephson energies of the junctions. We derived the corrections to an environmental δS_{env} and a local δS_{loc} parts of QPS action, which can both be significant. Then we considered two types of disorder: random variations of the junctions' areas and random charges, induced by gate voltages. The former result in negligible correction to the environmental part of QPS action $\delta S_{env} \ll 1$, however, the correction to the local part can be significant, $\delta S_{loc} > 1$. Random induced charges gives random phases for QPS on different junctions. As a result average QPS amplitude is zero. Then we studied the QPS amplitude statistics and found the criterion for chain homogeneity.

In the end we applied the results obtained in the previous chapters to superconducting nanowires. We discussed the problems of derivation the QPS amplitude for the wire, as the phase action is not valid on the length scales smaller than the su-

perconducting coherence length ξ , which is the typical size of the QPS core, where the phase tunneling occurs due to suppression of absolute value of the order parameter. However, low-frequency properties of the system are again determined by gapless Mooij-Schön modes. Therefore, the environment part of the action can be calculated, while for the local part only estimations are available. We showed that disorder effect on the QPS amplitude is similar to the one in Josephson junction chains. As a result, for the majority of experimentally realistic wires, the QPS amplitude is determined by a short region of the wire with the smallest cross-section, that can be seen as a weak link, which agrees with predictions of [53].

There are several perspective directions for further development of the present work. One effect, which can be studied, is the relaxation from an excited state of a closed Josephson junction chain. The problem is non-trivial, as in case of zero external dissipation the only possibility to decrease the system energy is through exciting Mooij-Schön modes, which are discrete in a finite system. As a result, the energy can be decreased only by some discrete amounts, which can possibly prevent the system from relaxation. Another interesting phenomenon is the analogue of a resonant Zener breakdown for an open Josephson junction chain with dissipation through external resistance. And finally, it would be interesting to study how quantum fluctuations influence switching from zero voltage state to finite voltage, corresponding to the running state, in an underdamped Josephson junction.

Appendix A

WKB calculation of the tunneling matrix element in the tilted washboard potential

To find the tunneling matrix element between the classical ground state in one minimum of the tilted cosine potential and the m -th excited state in the neighboring lower minimum (from now on we call them left and right, respectively), we put the system exactly at resonance, $I = m\omega_0 e/\pi$, and calculate the tunnel splitting in the WKB approximation. We have to write the solutions in the neighboring minima and connect them to the WKB solutions under the barrier. It is important to mention that tunneling shifts the level energies from their harmonic values. As a result, one has to deal with parabolic cylinder functions, which can be seen as generalization of Hermite polynomials on the case of non-integer index n , such that the energy of the state inside each minimum is $E = (n + 1/2)\omega_0$. It is important to remember, that the energy here is counted from the bottom of each minimum, therefore, the same energy level corresponds to different n in different minima. As we consider the tunneling to be exponentially weak. Then on the left side we have $n = \epsilon \ll 1$, while on the right $n = m + \epsilon$. That gives us two solutions in each minimum, which allows us to connect them to both WKB exponents under the barrier.

The asymptotics for the wave functions in the parabolic potential of the left minimum are

$$\psi_n(\phi \rightarrow -\infty) = C_L \frac{1}{\Gamma(n+1)} \left(\sqrt{\frac{\omega_0}{8E_c}} |\phi - \phi_{min}^0| \right)^n \exp\left(-\frac{\omega_0}{16E_c} (\phi - \phi_{min}^0)^2\right), \quad (\text{A.1})$$

and

$$\begin{aligned} \psi_n(\phi \rightarrow \infty) = & -C_L \frac{\sin \pi n}{2^n \sqrt{\pi}} \frac{e^{\frac{\omega_0}{16E_c}(\phi - \phi_{min}^0)^2}}{\left| \sqrt{\frac{\omega_0}{8E_c}}(\phi - \phi_{min}^0) \right|^{n+1}} \\ & + C_L \frac{e^{-i\pi n}}{\Gamma(n+1)} \left| \sqrt{\frac{\omega_0}{8E_c}}(\phi - \phi_{min}^0) \right|^n e^{-\frac{\omega_0}{16E_c}(\phi - \phi_{min}^0)^2}, \end{aligned} \quad (\text{A.2})$$

where the position of each minimum is $\phi_{min}^l = \arcsin \frac{I}{2eE_J} + 2\pi l$, and for the left minimum we put $l = 0$. It is convenient to introduce a new variable $x = \sqrt{\frac{\omega_0}{8E_c}} |\phi - \phi_{min}^0|$. For the WKB solutions in the part of the classically forbidden region, where WKB works but the potential can still be considered parabolic, we have:

$$\psi_{WKB} = \frac{A_L}{\sqrt{|p|}} e^{-S(x)} + \frac{B_L}{\sqrt{|p|}} e^{S(x)}, \quad (\text{A.3})$$

where $S(x)$ is the WKB action

$$S = \int_a^\phi |p(\phi)| d\phi = \int_{x_0}^x \sqrt{x^2 - x_0^2} dx \approx \frac{x^2}{2} + \frac{x_0^2}{2} \ln \frac{x_0}{2\sqrt{ex}}. \quad (\text{A.4})$$

Here a is the turning point, corresponding to $x_0 = \sqrt{\frac{\omega_0}{8E_c}}(a - \phi_{min}^0) = \sqrt{2n+1}$ in the new variable. Substituting this into Eq. (A.3), we obtain

$$\psi_{WKB} \approx A_L \left(\frac{2\sqrt{e}}{\sqrt{2n+1}} \right)^{n+1/2} x^n e^{-x^2/2} + B_L x^{-n-1} \left(\frac{\sqrt{2n+1}}{2\sqrt{e}} \right)^{(n+1/2)} e^{x^2/2}. \quad (\text{A.5})$$

We can connect the solutions

$$\frac{e^{-i\pi n}}{\Gamma(n+1)} x^n C_L = A_L \left(\frac{2\sqrt{e}}{\sqrt{2n+1}} \right)^{n+1/2} x^n, \quad (\text{A.6})$$

resulting in

$$A_L = \frac{e^{-i\pi n}}{\Gamma(n+1)} \left(\frac{2\sqrt{e}}{\sqrt{2n+1}} \right)^{-n-1/2} C_L, \quad (\text{A.7})$$

and

$$-\frac{\sin \pi n}{2^n \sqrt{\pi}} \frac{C_L}{x^{n+1}} = B_L x^{-n-1} \left(\frac{\sqrt{2n+1}}{2\sqrt{e}} \right)^{(n+1/2)}, \quad (\text{A.8})$$

resulting in

$$B_L = -\sqrt{2} \frac{\sin \pi n}{\sqrt{\pi}} \left(\frac{\sqrt{2n+1}}{\sqrt{e}} \right)^{-(n+1/2)} C_L. \quad (\text{A.9})$$

The function on the left corresponds to $n = \epsilon \ll 1$. Then

$$A_L \approx (2\sqrt{e})^{-1/2} C_L, \quad B_L \approx -\sqrt{2\pi\epsilon} e^{1/4} C_L. \quad (\text{A.10})$$

On the right side of the barrier the solution can be found exactly the same way, just by exchanging $-\infty \leftrightarrow +\infty$ asymptotics, and introducing $y = \sqrt{\frac{\omega_0}{8E_c}} |\phi - \phi_{min}^1|$. The WKB solution under the right side of the barrier can be written in the form

$$\psi_{WKB} = \frac{A_R}{\sqrt{|p|}} e^{-S(y)} + \frac{B_R}{\sqrt{|p|}} e^{S(y)}, \quad (\text{A.11})$$

where the WKB action is calculated from the left turning point y_0 . We connect solutions under the barrier and in the classical region on the right exactly the same way as we have done it for the left side:

$$A_R = \frac{e^{-i\pi n}}{\Gamma(n+1)} \left(\frac{2\sqrt{e}}{\sqrt{2n+1}} \right)^{-n-1/2} C_R, \quad (\text{A.12})$$

$$B_R = -\sqrt{2} \frac{\sin \pi n}{\sqrt{\pi}} \left(\frac{\sqrt{2n+1}}{\sqrt{e}} \right)^{-(n+1/2)} C_R. \quad (\text{A.13})$$

Now we can use the fact, that on the right side we have $n = m + \epsilon$, where m is integer and $\epsilon \ll 1$:

$$A_R \approx \frac{(-1)^m}{m!} \left(\frac{2\sqrt{e}}{\sqrt{2m+1}} \right)^{-m-1/2} C_R, \quad (\text{A.14})$$

$$B_R \approx -\sqrt{2\pi} (-1)^m \epsilon \left(\frac{\sqrt{2m+1}}{\sqrt{e}} \right)^{-(m+1/2)} C_R. \quad (\text{A.15})$$

Connecting WKB solution under the barrier is simple, as the actions in the exponents are calculated from the turning points, therefore

$$B_R = A_L e^{-S_m}, \quad A_R = B_L e^{S_m}, \quad (\text{A.16})$$

where S_m is the tunneling action between the turning points. As a result, we finally

get

$$-\sqrt{2\pi}(-1)^m \epsilon \left(\frac{\sqrt{2m+1}}{\sqrt{e}} \right)^{-(m+1/2)} C_R = (2\sqrt{e})^{-1/2} C_L e^{-S_m}, \quad (\text{A.17})$$

$$-\sqrt{2\pi} \epsilon e^{1/4} C_L = \frac{(-1)^m}{m!} \left(\frac{2\sqrt{e}}{\sqrt{2m+1}} \right)^{-m-1/2} C_R e^{-S_m}. \quad (\text{A.18})$$

Then we have

$$C_R/C_L = 2^{m/2} \sqrt{m!},$$

and

$$\epsilon = \pm \frac{\left(\sqrt{m+1/2} \right)^{m+1/2} e^{-S_m}}{\sqrt{2\pi m!} 2^{1/4}} e^{-\frac{m+1}{2}}.$$

This corresponds to the tunneling matrix element

$$X = \frac{\omega_0 \left(\sqrt{m+1/2} \right)^{m+1/2} e^{-S_m}}{\sqrt{2\pi m!} 2^{1/4}} e^{-\frac{m+1}{2}}. \quad (\text{A.19})$$

Now it only remains to calculate the tunneling action S_m :

$$S_m = \frac{1}{2} \sqrt{\frac{E_J}{E_c}} \int_a^b \sqrt{-\left(\cos \phi - \cos \phi_{min}^0 \right) - \frac{I}{2eE_J} (\phi - \phi_{min}^0) - \frac{1}{2} \frac{\omega_0}{E_J}} d\phi, \quad (\text{A.20})$$

where a and b are the turning points (see Fig.2.4). We can determine a as

$$\frac{1}{2} \omega_0 - E_J \cos(\phi_{min}^0) - \frac{I}{2e} \phi_{min}^0 = -E_J \cos a - \frac{I}{2e} a. \quad (\text{A.21})$$

As we assume it to be low enough for the harmonic oscillator approximation to be valid, we can write

$$a \approx \sqrt{\frac{8E_c}{\omega_0}} + \phi_{min}^0. \quad (\text{A.22})$$

For b we have

$$b \approx \phi_{min}^1 - \sqrt{\frac{8E_c(m+1/2)}{\omega_0}}. \quad (\text{A.23})$$

Therefore, the action is

$$S_m \approx \sqrt{\frac{8E_J}{E_c}} - \left(m+1 + \ln \frac{E_J/E_c}{(2m+1)^{1/4}} \right) + O\left((E_c/E_J)^{1/4} \right). \quad (\text{A.24})$$

Bibliography

- [1] H. Kamerlingh Onnes. Further experiments with liquid helium. d. on the change of electrical resistance of pure metals at very low temperatures, etc. v. the disappearance of the resistance of mercury. *Akad. van Wetenschappen*, 14:818, 1911.
- [2] H. Fröhlich. On the theory of superconductivity: The one-dimensional case. *Proceedings of the Royal Society of London A*, 223:1154, 1954.
- [3] R. A. Ferrell. Possibility of one-dimensional superconductivity. *Phys. Rev. Lett.*, 13:330–332, Sep 1964.
- [4] W. A. Little. Possibility of synthesizing an organic superconductor. *Phys. Rev.*, 134:A1416–A1424, Jun 1964.
- [5] T. M. Rice. Superconductivity in one and two dimensions. *Phys. Rev.*, 140:A1889–A1891, Dec 1965.
- [6] Yu. A. Bychkov, L. P. Gor'kov, and I. E. Dzyaloshinskiĭ. Possibility of superconductivity type phenomena in a one-dimensional system. *Sov. Phys. JETP*, 23:489, 1966.
- [7] R. Fazio and H. van der Zant. Quantum phase transitions and vortex dynamics in superconducting networks. *Physics Reports*, 355(4):235 – 334, 2001.
- [8] K. Yu. Arutyunov, D. S. Golubev, and A. D. Zaikin. Superconductivity in one dimension. *Physics Reports*, 464(1):1 – 70, 2008.
- [9] S. Doyle, P. Mauskopf, J. Zhang, A. Monfardini, L. Swenson, J. Baselmans, S. Yates, and M. Roesch. A review of the lumped element kinetic inductance detector. *Proc. SPIE*, 7741:1908–1911, 2010.
- [10] J. Flowers. The route to atomic and quantum standards. *Science*, 306:1324–1330, 2004.

- [11] J. E. Mooij and Yu. V. Nazarov. Superconducting nanowires as quantum phase-slip junctions. *Nature Phys.*, 2:169, 2006.
- [12] W. Guichard and F. W. J. Hekking. Phase-charge duality in josephson junction circuits: Role of inertia and effect of microwave irradiation. *Phys. Rev. B*, 81:064508, Feb 2010.
- [13] R. M. Bradley and S. Doniach. Quantum fluctuations in chains of josephson junctions. *Phys. Rev. B*, 30:1138–1147, Aug 1984.
- [14] J. E. Mooij and G. Schön. Propagating plasma mode in thin superconducting filaments. *Phys. Rev. Lett.*, 55:114–117, Jul 1985.
- [15] B. D. Josephson. Possible new effects in superconductive tunnelling. *Phys. Lett.*, 1:251–253, 1962.
- [16] P. W. Anderson and J. M. Rowell. Probable observation of the josephson superconducting tunneling effect. *Phys. Rev. Lett.*, 10:230, 1963.
- [17] Ph. Jung, A. V. Ustinov, and S. M. Anlage. Progress in superconducting metamaterials. *Superconductor Science and Technology*, 27, 2014.
- [18] S. Corlevi, W. Guichard, F. W. J. Hekking, and D. B. Haviland. Phase-charge duality of a josephson junction in a fluctuating electromagnetic environment. *Phys. Rev. Lett.*, 97:096802, 2006.
- [19] V. E. Manucharyan, J. Koch, L. I. Glazman, and M. H. Devoret. Fluxonium: Single cooper-pair circuit free of charge offsets. *Science*, 326(5949):113–116, 2009.
- [20] J. Koch, V. E. Manucharyan, M. H. Devoret, and L. I. Glazman. Charging effects in the inductively shunted josephson junction. *Phys. Rev. Lett.*, 103:217004, Nov 2009.
- [21] I. M. Pop, K. Hasselbach, O. Buisson, W. Guichard, B. Pannetier, and I. Protopopov. Measurement of the current-phase relation in josephson junction rhombi chains. *Phys. Rev. B*, 78:104504, 2008.
- [22] S. Gladchenko, D. Olaya, E. Dupont-Ferrier, B. Douçot, L.B. Ioffe, and M.E. Gershenson. Superconducting nanocircuits for topologically protected qubits. *Nature Phys.*, 5:48–53, 2009.

- [23] R. L. Kautz. Noise, chaos, and the josephson voltage standard. *Reports on Progress in Physics*, 59, 1996.
- [24] W. A. Little. Decay of persistent currents in small superconductors. *Phys. Rev.*, 156:396–403, Apr 1967.
- [25] J. S. Langer and V. Ambegaokar. Intrinsic resistive transition in narrow superconducting channels. *Phys. Rev.*, 164:498, Dec 1967.
- [26] D. E. McCumber and B. I. Halperin. Time scale of intrinsic resistive fluctuations in thin superconducting wires. *Phys. Rev. B*, 1:1054, Feb 1970.
- [27] N. Giordano. Evidence for macroscopic quantum tunneling in one-dimensional superconductors. *Phys. Rev. Lett.*, 61:2137–2140, Oct 1988.
- [28] A. Bezryadin, C. N. Lau, and M. Tinkham. Quantum suppression of superconductivity in ultrathin nanowires. *Nature*, 404:971, 2000.
- [29] C. N. Lau, N. Markovic, M. Bockrath, A. Bezryadin, and M. Tinkham. Quantum phase slips in superconducting nanowires. *Phys. Rev. Lett.*, 87:217003, Nov 2001.
- [30] F. Altomare, A. M. Chang, M. R. Melloch, Yu. Hong, and C. W. Tu. Evidence for macroscopic quantum tunneling of phase slips in long one-dimensional superconducting al wires. *Phys. Rev. Lett.*, 97:017001, Jul 2006.
- [31] M. Zgirski, K.-P. Riikonen, V. Touboltsev, and K. Yu. Arutyunov. Quantum fluctuations in ultranarrow superconducting aluminum nanowires. *Phys. Rev. B*, 77:054508, Feb 2008.
- [32] D. A. Ivanov, L. B. Ioffe, V. B. Geshkenbein, and G. Blatter. Interference effects in isolated josephson junction arrays with geometric symmetries. *Phys. Rev. B*, 65:024509, Dec 2001.
- [33] K. A. Matveev, A. I. Larkin, and L. I. Glazman. Persistent current in superconducting nanorings. *Phys. Rev. Lett.*, 89:096802, Aug 2002.
- [34] A. M. Hriscu and Yu. V. Nazarov. Coulomb blockade due to quantum phase slips illustrated with devices. *Phys. Rev. B*, 83:174511, May 2011.
- [35] V. E. Manucharyan, N. A. Masluk, A. Kamal, J. Koch, L. I. Glazman, and M. H. Devoret. Evidence for coherent quantum phase slips across a josephson junction array. *Phys. Rev. B*, 85:024521, Jan 2012.

- [36] I. M. Pop, B. Douçot, L. Ioffe, I. Protopopov, F. Lecocq, I. Matei, O. Buisson, and W. Guichard. Experimental demonstration of aharonov-casher interference in a josephson junction circuit. *Phys. Rev. B*, 85:094503, Mar 2012.
- [37] S. E. Korshunov. Zero-phonon friction mechanism for linear defects in quantum crystals. *Sov. Phys. JETP*, 63:1242, 1986. [*Zh. Eksp. Teor. Fiz.* **90**, 2118 (1986)].
- [38] S. E. Korshunov. Effect of dissipation on the low-temperature properties of a tunnel-junction chain. *Sov. Phys. JETP*, 68:609, 1989. [*Zh. Eksp. Teor. Fiz.* **95**, 1058 (1989)].
- [39] D. Meidan, Y. Oreg, and G. Refael. Sharp superconductor-insulator transition in short wires. *Phys. Rev. Lett.*, 98:187001, May 2007.
- [40] M. Sahu, M.-H. Bae, A. Rogachev, D. Pekker, T.-C. Wei, N. Shah, P. M. Goldbart, and A. Bezryadin. Individual topological tunnelling events of a quantum field probed through their macroscopic consequences. *Nature Phys.*, 5:503, 2009.
- [41] I. M. Pop, I. Protopopov, F. Lecocq, Z. Peng, B. Pannetier, O. Buisson, and W. Guichard. Measurement of the effect of quantum phase slips in a josephson junction chain. *Nature Phys.*, 6:589, 2010.
- [42] T. T. Hongisto and A. B. Zorin. Single-charge transistor based on the charge-phase duality of a superconducting nanowire circuit. *Phys. Rev. Lett.*, 108:097001, Feb 2012.
- [43] K. Yu. Arutyunov, T. T. Hongisto, J. S. Lehtinen, L. I. Leino, and A. L. Vasiliev. Quantum phase slip phenomenon in ultra-narrow superconducting nanorings. *Scientific Reports*, 2:293, 2012.
- [44] O. V. Astafiev, L. B. Ioffe, S. Kafanov, Yu. A. Pashkin, K. Yu. Arutyunov, D. Shahar, O. Cohen, and J. S. Tsai. Coherent quantum phase slip. *Nature*, 484:355, 2012.
- [45] J. T. Peltonen, O. V. Astafiev, Yu. P. Korneeva, B. M. Voronov, A. A. Korneev, I. M. Charaev, A. V. Semenov, G. N. Golt'sman, L. B. Ioffe, T. M. Klapwijk, and J. S. Tsai. Coherent flux tunneling through nbn nanowires. *Phys. Rev. B*, 88:220506, Dec 2013.
- [46] A. J. Dahm, A. Denenstien, T. F. Finnegan, D. N. Langenberg, and D. J. Scalapino. Study of the josephson plasma resonance. *Phys. Rev. Lett.*, 20:859–863, Apr 1968.

- [47] I. O. Kulik. Surface-charge oscillations in superconductors. *Sov. Phys. JETP*, 38:1008, 1974. [Zh. Eksp. Teor. Fiz. **65**, 201 (1973)].
- [48] B. Camarota, F. Parage, F. Balestro, P. Delsing, and O. Buisson. Experimental evidence of one-dimensional plasma modes in superconducting thin wires. *Phys. Rev. Lett.*, 86:480–483, Jan 2001.
- [49] I. M. Pop. *Quantum Phase-Slips in Josephson Junction Chains*. PhD thesis, Université de Grenoble, 2011.
- [50] N. A. Masluk, I. M. Pop, A. Kamal, Z. K. Mineev, and M. H. Devoret. Microwave characterization of josephson junction arrays: Implementing a low loss superinductance. *Phys. Rev. Lett.*, 109:137002, Sep 2012.
- [51] G. Rastelli, I. M. Pop, and F. W. J. Hekking. Quantum phase slips in josephson junction rings. *Phys. Rev. B*, 87:174513, May 2013.
- [52] F. W. J. Hekking and L. I. Glazman. Quantum fluctuations in the equilibrium state of a thin superconducting loop. *Phys. Rev. B*, 55:6551–6558, Mar 1997.
- [53] M. Vanević and Yu. V. Nazarov. Quantum phase slips in superconducting wires with weak inhomogeneities. *Phys. Rev. Lett.*, 108:187002, May 2012.
- [54] J. M. Kosterlitz and D. J. Thouless. Ordering, metastability and phase transitions in two-dimensional systems. *J. Phys. C: Solid State Phys.*, 6, 1973.
- [55] H. P. Büchler, V. B. Geshkenbein, and G. Blatter. Quantum fluctuations in thin superconducting wires of finite length. *Phys. Rev. Lett.*, 92:067007, Feb 2004.
- [56] A. E. Svetogorov, M. Taguchi, Y. Tokura, D. M. Basko, and F. W. J. Hekking. Theory of coherent quantum phase slips in josephson junction chains with periodic spatial modulations. *Phys. Rev. B*, 97:104514, 2018.
- [57] A. E. Svetogorov and D. M. Basko. Effect of disorder on coherent quantum phase slips in josephson junction chains. *Phys. Rev. B*, 98:054513, 2018.
- [58] K. K. Likharev and A. B. Zorin. Theory of the bloch-wave oscillations in small josephson junctions. *Journal of Low Temperature Physics*, 59:347–382, 1985.
- [59] B. Douçot and L. B. Ioffe. Voltage-current curves for small josephson junction arrays. *Phys. Rev. B*, 76:214507, 2007.

- [60] A. Zazunov, N. Didier, and F. W. J. Hekking. Quantum charge diffusion in underdamped josephson junctions and superconducting nanowires. *EPL*, 83, 2008.
- [61] G. L. Ingold and H. Grabert. Effect of zero point phase fluctuations on josephson tunneling. *Phys. Rev. Lett.*, 83, 1999.
- [62] A. Murani, N. Bourlet, H. le Sueur, F. Portier, C. Altimiras, D. Esteve, H. Grabert, J. Stockburger, and P. Joyez. Absence of a dissipative quantum phase transition in josephson junctions. *arxiv*, 2019.
- [63] D. V. Averin, A. B. Zorin, and K. K. Likharev. Bloch oscillations in small josephson junctions. *JETP*, 61:4007, 1985.
- [64] R. L. Kautz and J. M. Martinis. Noise-affected $i - v$ curves in small hysteretic josephson junctions. *Phys. Rev. B*, 49, 1990.
- [65] M. Žonda, W. Belzig, and T. Novotný. Voltage noise, multiple phase-slips, and switching rates in moderately damped josephson junctions. *Phys. Rev. B*, 91:134305, 2015.
- [66] C. Zener. A theory of the electrical breakdown of solid dielectrics. *Proc. of the Royal Society. Series A*, 145, 1934.
- [67] H. T. Schneider, H. andGrah, K. v. Klitzing, and K. Ploog. Resonance-induced delocalization of electrons in gaas-alas superlattices. *Phys. Rev. Lett.*, 65:2720, 1990.
- [68] A. Sibille, J. F. Palmier, and F. Laruelle. Zener interminiband resonant breakdown in superlattices. *Phys. Rev. Lett.*, 80:4506, 1998.
- [69] M. M. Helm, W. W. Hilber, G. G. Strasser, R. R. De Meester, F. M. Peeters, and A. Wacke. Continuum wannier-stark ladders strongly coupled by zener resonances in semiconductor superlattices. *Phys. Rev. Lett.*, 82:3120, 1999.
- [70] L. S. Kuzmin, Yu. V. Nazarov, D. B. Haviland, P. Delsing, and T. Claeson. Coulomb blockade and incoherent tunneling of cooper pairs in ultrasmall junctions affected by strong quantum fluctuations. *Phys. Rev. Lett.*, 67:1161, 1991.
- [71] M. Watanabe and D. B. Haviland. Coulomb blockade and coherent single-cooper-pair tunneling in single josephson junctions. *Phys. Rev. Lett.*, 86:5120, 2001.

- [72] A. Ergül, J. Lidmar, J. Johansson, Ya. Azizoğlu, D. Schaeffer, and D. B. Haviland. Localizing quantum phase slips in one-dimensional josephson junction chains. *New Journal of Physics*, 15(9):095014, 2013.
- [73] T. Weißl, G. Rastelli, I. Matei, I. M. Pop, O. Buisson, F. W. J. Hekking, and W. Guichard. Bloch band dynamics of a josephson junction in an inductive environment. *Phys. Rev. B*, 91:014507, Jan 2015.
- [74] S. Coleman. The uses of instantons. In *Lectures delivered at the International School of Subnuclear Physics*. Erice, 1977.
- [75] A. I. Vainshtein, V. I. Zakharov, V. A. Novikov, and M. A. Shifman. Abc of instantons. *Sov. Phys. Uspekhi*, 25:195, 1982. [*Usp. Fiz. Nauk.* **136**, 553 (1982)].
- [76] L. D. Landau and E. M. Lifshitz. *Quantum Mechanics*. Butterworth-Heinemann, Oxford, 1977.
- [77] G. Rastelli, M. Vanević, and W. Belzig. Coherent dynamics in long fluxonium qubits. *New Journal of Physics*, 17:053026, 2015.
- [78] A. Ergül, T. Weißl, J. Johansson, J. Lidmar, and D. B. Haviland. Spatial and temporal distribution of phase slips in josephson junction chains. *Scientific Reports*, 17:11447, 2017.
- [79] D. V. Nguyen and D. M. Basko. Inhomogeneous josephson junction chains: a superconducting meta-material for superinductance optimization. *Eur. Phys. J. Special Topics*, 226:1499, 2017.
- [80] M. Taguchi, D. M. Basko, and F. W. J. Hekking. Mode engineering with a one-dimensional superconducting metamaterial. *Phys. Rev. B*, 92:024507, Jul 2015.
- [81] D. M. Basko and F. W. J. Hekking. Disordered josephson junction chains: Anderson localization of normal modes and impedance fluctuations. *Phys. Rev. B*, 88:094507, Sep 2013.
- [82] N. A. Marlow. A normal limit theorem for power sums of independent random variables. *The Bell System Technical Journal*, 46:2081 – 2089, Nov 1967.
- [83] N. C. Beaulieu, A. A. Abu-Dayya, and P. J. McLane. Estimating the distribution of a sum of independent lognormal random variables. *IEEE Transactions on Communications*, 42:2869, 1995.

- [84] R. L. Mitchell. Permanence of the log-normal distribution. *Journal of the Optical Society of America*, 58:1267–1272, 1968.
- [85] M. E. Raikh and I. M. Ruzin. Transparency fluctuations in randomly inhomogeneous barriers of finite area. *JETP*, 65:1273, 1987.
- [86] P. Collin-Dufresne, R. Goldstein, and J. Hugonnier. A general formula for valuing defaultable securities. *Adv. Appl. Prob.*, 36:747, 2004.
- [87] N. A. Tulina. Influence of purity on the magnetic properties of rhenium in superconductive state. *Phys. Met. Metall.*, 50:62–68, 1980.
- [88] A. Anthore, H. Pothier, and D. Esteve. Density of states in a superconductor carrying a supercurrent. *Phys. Rev. Lett.*, 90:127001, Mar 2003.
- [89] N. Nagaosa. *Quantum Field Theory in Condensed Matter Physics*. Springer, 1999.
- [90] D. S. Golubev and A. D. Zaikin. Quantum tunneling of the order parameter in superconducting nanowires. *Phys. Rev. B*, 64:014504, Jun 2001.
- [91] D. C. Mattis and J. Bardeen. Theory of the anomalous skin effect in normal and superconducting metals. *Phys. Rev.*, 111:412–417, Jul 1958.